RECORD #
AAB3193

CONFIDENTIAL
CLASSIFICATION cancelled
SEP 1 1959

Copy
RM L57E10

110

NACA RM L57E10

AERONAUTICS LIBRARY
California Institute of Technology

NACA

# RESEARCH MEMORANDUM

## EXPERIMENTAL INVESTIGATION OF EFFECTS OF MODERATE SIDESLIP ON THE FLOW FIELDS NEAR A 45° SWEPT-WING—FUSELAGE COMBINATION AT LOW SPEED

By William J. Alford, Jr., and Thomas J. King, Jr.

Langley Aeronautical Laboratory
Langley Field, Va.

CLASSIFIED DOCUMENT

This material contains information affecting the National Defense of the United States within the meaning of the espionage laws, Title 18, U.S.C., Secs. 793 and 794, the transmission or revelation of which in any manner to an unauthorized person is prohibited by law.

NATIONAL ADVISORY COMMITTEE
FOR AERONAUTICS

WASHINGTON

July 12, 1957

CONFIDENTIAL
CLASSIFICATION cancelled

NATIONAL ADVISORY COMMITTEE FOR AERONAUTICS

RESEARCH MEMORANDUM

# EXPERIMENTAL INVESTIGATION OF EFFECTS OF MODERATE SIDESLIP ON THE FLOW FIELDS NEAR A 45° SWEPT-WING—FUSELAGE COMBINATION AT LOW SPEED

By William J. Alford, Jr., and Thomas J. King, Jr.

## SUMMARY

The flow fields near a 45° swept-wing—fuselage combination at moderate angles of sideslip (±8°), as determined experimentally at low speed, are presented as variations with chordwise distance for various spanwise and vertical locations and angles of attack.

The results indicated that for positions close to the fuselage (on and near the plane of symmetry) changes in the angle of sideslip caused large changes in the flow-field characteristics and particularly in the local angles of sideslip, which in some cases were nearly double the static angle of sideslip. In general, the effects of changing the angle of sideslip on the flow-field characteristics for all of the outboard underwing locations were qualitatively similar, although conditions at the more inboard and outboard locations were somewhat more severe for lifting conditions than at the one-half semispan location. The chordwise gradients in the flow parameters for the underwing locations were more severe than for the fuselage locations although the effect of changing the angle of sideslip was less severe, in that the incremental changes in the local angles of sideslip were approximately equal to the static angle of sideslip. Flow conditions near the wing tip were found to be critically dependent on vertical location, with the largest sideslip-induced variations occurring at the nearest vertical locations. The results also indicated that for the outboard underwing locations the wing was the predominant factor in disturbing the field of flow for the conditions investigated.

## INTRODUCTION

In order to estimate the aerodynamic loadings on external stores such as fuel tanks, bombs, or missiles and on their pylons which, of practical necessity, are located in close proximity to the airplane wing or fuselage, it is necessary to consider in detail the flow fields in which these stores are immersed.

An experimental investigation has, therefore, been made at low speed to determine in detail the flow-field characteristics near a swept-wing—fuselage combination. A previous paper (ref. 1) has presented the flow-field characteristics around a model consisting of a fuselage and either a sweptback or an unswept wing for the condition of zero sideslip.

The purpose of the present paper is to extend the results of reference 1 by presenting the results of an experimental investigation made to determine the effects of moderate sideslip angles ($\pm 8^{\circ}$) on the flow-field characteristics near a swept-wing—fuselage combination at low speed. Some of the data presented in reference 1 for the zero-sideslip condition are repeated for comparison.

## SYMBOLS

The directions of positive distances and angles for the body-axis system employed are presented in figure 1.

| | |
|---|---|
| $A$ | aspect ratio |
| $b$ | wing span, ft |
| $c$ | local wing chord, ft |
| $\bar{c}$ | mean aerodynamic chord, ft |
| $C_L$ | lift coefficient, $\frac{\text{Lift}}{q_o S}$ |
| $C_D$ | drag coefficient, $\frac{\text{Drag}}{q_o S}$ |
| $C_m$ | pitching-moment coefficient referred to $0.25\bar{c}$, $\frac{\text{Pitching moment}}{q_o S \bar{c}}$ |
| $V_o$ | free-stream velocity, ft/sec |
| $V_c$ | crossflow velocity, ft/sec |
| $V_l$ | local velocity, ft/sec |

| | |
|---|---|
| $w$ | downwash velocity, ft/sec |
| $v$ | sidewash velocity, ft/sec |
| $q_o$ | free-stream dynamic pressure, lb/sq ft |
| $q_l$ | local dynamic pressure, lb/sq ft |
| $r$ | fuselage radius, ft |
| $S$ | wing area, sq ft |
| $l$ | fuselage length, 7.61 ft |
| $d_{max}$ | maximum fuselage diameter, 0.70 ft |
| $\lambda$ | taper ratio |
| $\Lambda_{c/4}$ | sweep angle of quarter-chord line, deg |
| $\alpha$ | angle of attack, deg |
| $\beta$ | angle of sideslip, deg |
| $\alpha_l$ | resultant flow angularity induced by wing-fuselage combination, measured in XZ-plane, between local-flow direction and airplane axis of symmetry (fig. 1), $\alpha - \epsilon$, deg |
| $\beta_l$ | resultant flow angularity induced by wing-fuselage combination, measured in XY-plane, between local-flow direction and airplane axis of symmetry (fig. 1), $\beta + \sigma$, deg |
| $\epsilon$ | downwash angle induced by wing-fuselage combination, measured in XZ-plane, between free-stream-flow direction and local-flow direction, positive when local flow is inclined downward relative to free stream (fig. 1), deg |
| $\sigma$ | sidewash angle induced by wing-fuselage combination, measured in XY-plane, between free-stream-flow direction and local-flow direction; for region on left side of airplane-model plane of symmetry, positive sidewash corresponds to outward inclination of local flow relative to free stream (fig. 1), deg |
| X,Y,Z | right-hand Cartesian coordinate system (fig. 1) |
| $x$ | distance in direction of X-axis with origin at leading edge of local wing chord, positive rearward, ft |

y distance in direction of Y-axis with origin at plane of symmetry of airplane model, positive to right when viewed from rear, ft

z distance in direction of Z-axis with origin at wing-chord plane, positive up, ft

## MODEL AND APPARATUS

The model about which the flow surveys were made consisted of a fuselage equipped with a sweptback wing. A drawing of the model is presented in figure 2. The wing had a sweep of 45° of the quarter-chord line, an aspect ratio of 4.0, a taper ratio of 0.30, and NACA 65A006 airfoil sections parallel to the plane of symmetry. The fuselage had an ogival nose section, a cylindrical center section, and a truncated tail cone. The fuselage ordinates are presented in table I.

The flow-field characteristics were measured by the use of a rake of hemispherically headed probes which had both angle-of-attack and angle-of-sideslip orifices and pitot-static orifices for measuring dynamic pressure in conjunction with a multitube manometer. A drawing of the flow-survey rake and a photograph showing the rake installed on the model are presented in figure 3. The locations at which the surveys were made are shown in figure 4.

## TESTS, CORRECTIONS, AND ACCURACY

The tests were made in the Langley 300 MPH 7- by 10-foot tunnel at a velocity of 146.6 feet per second. Surveys of the flow angularity in both the longitudinal and lateral planes were included in the tests as well as dynamic pressures at numerous chordwise and six vertical locations at the lateral locations of $\frac{y}{b/2}$ of 0, -0.098, -0.25, -0.50, -0.75, and -1.01. Flow surveys were also made at values of $\frac{y}{b/2}$ of -0.25, -0.50, and -0.75 for the fuselage alone. The sideslip angles were 0° and ±8° for angles of attack of -0.2°, 3.8°, 8.2°, and 16.4°. The surveys were made under the model center line and under the left wing.

Jet-boundary corrections were calculated by the method of reference 2. Blockage corrections calculated by the method of reference 3 were applied to the free-stream dynamic pressure.

The small variations in jet-boundary and blockage corrections throughout the flow fields have been neglected because they were well within the estimated accuracy limits of the experimental data.

Some relaxation of rigorous calibration procedures was found necessary in order to expedite the data reduction. The calibrations of the survey rake were linearized, and the local dynamic pressures were considered to be the difference between free-stream total pressure and local static pressure; therefore, the effects of local losses in total pressure were not included. Inasmuch as the majority of the survey locations were outside of the wing wake and boundary layer, the regions to which the local losses in total pressure are confined, the error introduced because of neglecting the local total pressure was found to be negligible.

Additional possible sources of error were incurred by the local misalinement angles existing in the clear wind tunnel and by the adjustment accuracy in the model and rake supports. The consideration of all known sources of error indicated that the local angles of attack were accurate to $\pm 1.0^\circ$ below a local angle of $16^\circ$ in either plane and could possibly be in error by as much as $\pm 2.0^\circ$ in regions where the local angle was $24^\circ$ or more. The local angles of sideslip are believed to be accurate to within $\pm 1.5^\circ$ below a local angle of $16^\circ$ in either plane and could possibly be in error $\pm 2.5^\circ$ at a local angle of $24^\circ$. The local-dynamic-pressure ratios are believed to be accurate to within $\pm 0.025$ below a local angle of $16^\circ$ in either plane and could possibly be in error by $\pm 0.04$ at a local angle of $24^\circ$.

## PRESENTATION OF RESULTS

In analyzing the flow-field characteristics it is often desirable to have as a reference the force and moment characteristics of the model. These data for the model used in the present investigation are presented in figure 5.

The flow-field characteristics of the swept-wing—fuselage combination are presented for lateral locations of $\frac{y}{b/2}$ of 0, -0.098, -0.25, -0.50, -0.75, and -1.01 in figures 6, 7, 8, 9, 10, and 11, respectively. Comparisons of the flow fields of the fuselage alone and the wing-fuselage combination as a function of angle of sideslip, for three angles of attack and spanwise locations, and two chordwise locations are presented in figures 12 to 14. A summary plot of the effects of variation in sideslip angle on the local angularities for the fuselage locations is presented in figure 15.

The flow angularities are presented in terms of the local conditions $\alpha_l$ and $\beta_l$. For the sign convention adopted (fig. 1), positions where the local angle of attack $\alpha_l$ is more positive than the geometric angle of attack $\alpha$ are regions of upflow, and positions where $\alpha_l$ is less positive than $\alpha$ are regions of downflow. Positions where the

local angle of sideslip $\beta_l$ is more positive than the geometric angle of sideslip $\beta$ are regions of flow to the left when viewed from the rear. Inasmuch as the flow surveys were made under the model center line and under the left wing, the aforementioned conditions $(|\beta_l| > |\beta|)$ indicate a flow inclination toward the wing tip. Conversely, positions where $(|\beta_l| < |\beta|)$ are regions of flow to the right or toward the airplane-model plane of symmetry. Values of the local-dynamic-pressure ratio $q_l/q_o$ greater than unity indicate regions of supervelocity relative to free-stream conditions.

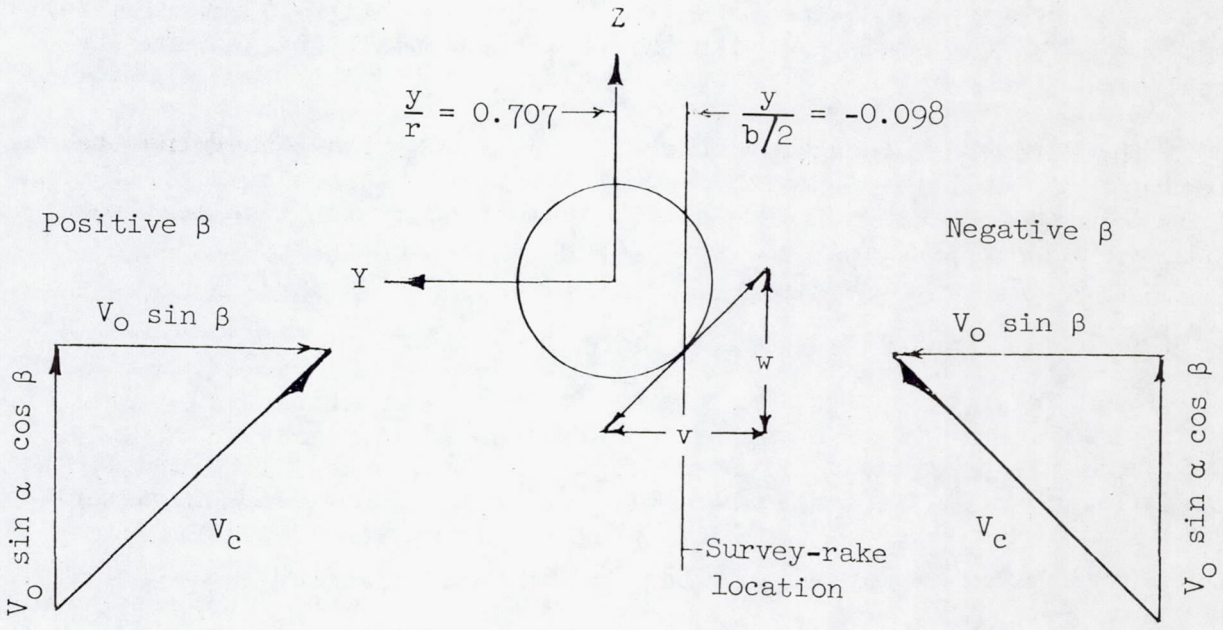
The results are, in general, presented for constant angles of attack and sideslip for six vertical locations as variations of the local-flow parameters $\alpha_l$, $\beta_l$, and $q_l/q_o$ with nondimensional chordwise distance $x/c$. The origin of measurements of $x/c$ is the leading edge of the local wing chord, with positive values in the downstream direction.

## DISCUSSION

Consideration of the flow-field characteristics beneath the plane of symmetry $\left(\frac{y}{b/2} = 0\right)$ of the wing-fuselage combination (fig. 6) indicates that the local angles of attack and dynamic pressures are only slightly affected by varying the angles of sideslip, even for the highest angle of attack investigated ($\alpha = 8.2^\circ$, figs. 6(g) to 6(i) and fig. 15(b)). For an angle of sideslip of $0^\circ$ the local angles of sideslip are essentially $0^\circ$ as would be expected from simple vortex considerations. An increase in the angle of sideslip in either direction causes large changes in the local angles of sideslip, with the largest changes being nearly double the geometric angle of sideslip and occurring for the vertical locations nearest the fuselage surface (fig. 15). These large changes can be explained by consideration of the flow conditions existing in the crossflow plane where, with the circular cross section employed, the crossflow velocity generates twice the geometric angle of sideslip on the fuselage surface at the plane of symmetry, for an angle of attack of $0^\circ$ (ref. 4). The local angles of sideslip decrease as the distance from the fuselage is increased and approach the geometric angle of sideslip. The effect of increasing the angle of attack on the local angles of sideslip is small compared to the effects of changing the angle of sideslip (fig. 15).

The results of flow surveys made at a lateral distance of 9.8 percent of the wing semispan (70.7 percent of the body radius) indicate that increases in angle of attack for the unsideslipped condition (figs. 7(a), (d), and (g)) cause increases in the local angles of attack and also substantial increases in the local angles of sideslip in contrast to

conditions at the plane of symmetry where the local angles of sideslip were unaffected by angle-of-attack variations. These changes in local angles of sideslip are due to the boundary condition of tangential surface flow which induces lateral as well as vertical angularities. The effect of angle of attack for the unsideslipped condition has been reported previously in reference 1. Variation of the angle of sideslip (figs. 7 and 15) caused large changes in the local angles of attack and sideslip although the local angles of sideslip are smaller than those at the plane of symmetry. These changes are evidenced as increases in the local angles (in both planes) for positive sideslip and, in general, as slightly larger decreases in the local angles for negative sideslip with these incremental changes varying only slightly with increasing angle of attack. A qualitative explanation of the effects of changing the lateral distance (from the plane of symmetry) and the asymmetry in the local angles with opposite sideslip may be facilitated by consideration of the two-dimensional analogy offered by the crossflow plane, illustrated in the following sketch (front view). For positive sideslip the downwash velocity w is in an upward direction and the sidewash velocity v is in the direction of the negative Y-axis.




With the axis system and sign convention of figure 1 employed, the location of present interest $\left(\frac{y}{b/2} = -0.098\right)$ is on the leeward side of the fuselage for positive sideslip and on the windward side for negative sideslip. Consideration of this fact in conjunction with the boundary condition of tangential flow at the fuselage surface indicates that for vertical locations near the fuselage surface the local angles of attack and sideslip increase for positive sideslip and decrease for negative

sideslip for this lateral location; whereas, only the local angles of sideslip changed appreciably at the plane of symmetry. As mentioned previously, the increments in the local angles are, in general, somewhat larger for negative sideslip than for positive sideslip. As seen in the sketch, the survey location is on the windward side for negative sideslip, and the body curvature produces very large flow accelerations and hence large local velocity components and angles. For positive sideslip, however, the location of interest is on the leeward side of the body, and experience has shown that the flow field in the vicinity of the surface does not complete its recovery because of adverse gradients and, consequently, lower velocities and angles result (p. 31 of ref. 4).

In general, the most noteworthy changes in the dynamic pressure are caused by changes in angle of attack, in that near an angle of attack of $0^\circ$ the flow is accelerated because of the body thickness distribution and at positive angles of attack the flow is decelerated by the wing-fuselage lift-induced velocities. A change of the sideslip angle does, however, produce some changes, even though small, in the local dynamic pressures. These changes, for the positive angles of attack, are evidenced as larger reductions relative to free-stream conditions for negative sideslip (windward side) than for positive sideslip (leeward side). These results are consistent with the foregoing simplified angularity analysis.

The foregoing discussion offers a word of caution concerning the location of objects in the immediate vicinity of the fuselage. Although the chordwise gradients in the flow characteristics might be less severe than for other spanwise locations, changes in sideslip produce large changes in the magnitude of the local angles of attack and sideslip.

For more outboard spanwise locations of $\frac{y}{b/2}$ of -0.25, -0.50, and -0.75 (figs. 8, 9, and 10), the flow-field characteristics have larger gradients with both chordwise and vertical distances when compared with the previously discussed fuselage locations. In general, the effects of changing the angle of sideslip on the flow-field characteristics for all of the outboard underwing locations are qualitatively similar, although conditions at the more inboard location $\left(\frac{y}{b/2} = -0.25, \text{ fig. } 8\right)$ and outboard location $\left(\frac{y}{b/2} = -0.75, \text{ fig. } 10\right)$ are somewhat more affected (for lifting conditions) than conditions at the one-half semispan location because of the additional effects of the fuselage for the inboard location and the proximity of the wing-tip vortex for the outboard location. In contrast to the fuselage locations where the local angles of sideslip were nearly doubled, the incremental changes for the underwing locations are approximately the same order of magnitude as the angle of sideslip, with some localized chordwise asymmetries depending on the

direction of sideslip. These asymmetries are most noticeable near the leading edge of the local wing chord for lifting conditions where, for positive sideslip angles, the incremental changes in the local angles of sideslip are decreased. This decrease is presumed to be due to the decreased gradients in spanwise loading on the trailing wing. The local angles of attack and dynamic pressures show only small changes with changes in sideslip angle. These changes are, however, as would be expected since for positive angles of sideslip (survey locations under trailing wing) the local angles of attack are slightly higher (downwash angle less) and the local dynamic pressures are slightly lower (resultant velocity less) than those for the zero-sideslip condition. The converse condition is true for the negative sideslip angles.

The flow conditions existing slightly outboard of the wing tip $\left(\frac{y}{b/2} = -1.01, \text{ fig. } 11\right)$ are seen to be critically dependent on vertical position, with the largest deviations occurring for the closest vertical locations. For the nonlifting condition, (figs. 11(a) to 11(c)) the incremental changes in the local angle of sideslip are approximately equal to the sideslip angle over most of the chordwise and vertical locations investigated. For lifting conditions (figs. 11(d) to 11(l)) changing the angle of sideslip produces marked changes in all the flow parameters for the nearest vertical location ($z/c = 0.015$) which is slightly above the wing chord. The largest chordwise variations in the flow parameters for this vertical location (particularly in the local angles of sideslip) occur for the positive sideslip angle. This large variation is presumed due to the survey locations being on the leeward side of the wing tip. For the negative sideslip angle the survey locations were on the windward side of the wing tip, and hence the incremental flow deviations are more nearly equal to the static angle of sideslip. As the vertical distance from the wing-chord plane was increased, the changes in the local-flow parameters also decreased, and the changes in the local angles of sideslip were approximately equal to the static angle of sideslip.

Comparisons of the effects of the fuselage alone with the effects of the swept-wing—fuselage combination on the flow-field characteristics as functions of sideslip angle are presented for the one-quarter, one-half, and three-quarter semispan locations in figures 12, 13, and 14, respectively. Examination of these data for these spanwise locations indicates that the effects of the fuselage alone are small in comparison with the predominant effects of the wing. The flow deviations generated by the fuselage are the largest at the one-quarter semispan location and decrease rapidly with spanwise distance.

## CONCLUDING REMARKS

The results of an experimental investigation made to determine the effects of moderate sideslip on the flow fields near a 45° swept-wing—fuselage combination at low speed indicated that for positions close to the fuselage (on and near the plane of symmetry) changes in the angle of sideslip caused large changes in the flow parameters, particularly in the local angles of sideslip, which in some cases were nearly double the static angle of sideslip. In general, the effects of changing the angle of sideslip on the flow-field characteristics for all the outboard underwing locations were qualitatively similar, although conditions at the more inboard and outboard locations were somewhat more severe for lifting conditions than conditions at the one-half semispan location. The chordwise gradients in the flow parameters for the underwing locations were more severe than those for the underfuselage locations, although the effect of changing the angle of sideslip was less severe in that the incremental changes in the local angles of sideslip were approximately equal to the static angle of sideslip. Flow conditions near the wing tip were found to be critically dependent on vertical location, with the largest sideslip-induced deviations occurring at the nearest vertical positions. The results also indicated that for the outboard underwing locations, the wing was the predominant factor in disturbing the field of flow for the conditions investigated.

Langley Aeronautical Laboratory,
National Advisory Committee for Aeronautics,
Langley Field, Va., April 24, 1957.

## REFERENCES

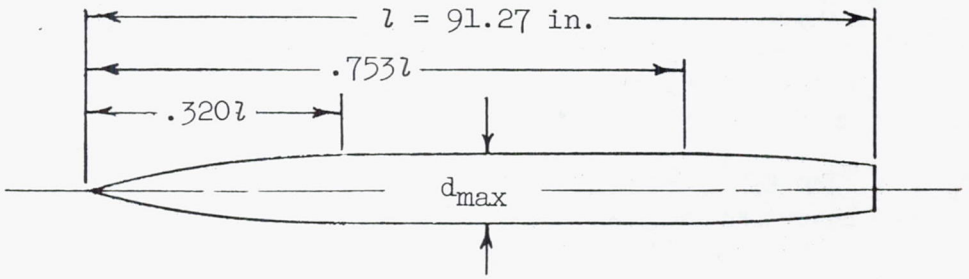
1. Alford, William J., Jr., and King, Thomas J., Jr.: Experimental Investigation of Flow Fields at Zero Sideslip Near Swept- and Unswept-Wing—Fuselage Combinations at Low Speed. NACA RM L56J19, 1957.

2. Gillis, Clarence L., Polhamus, Edward C., and Gray, Joseph L., Jr.: Charts for Determining Jet-Boundary Corrections for Complete Models in 7- by 10-Foot Closed Rectangular Wind Tunnels. NACA WR L-123, 1945. (Formerly NACA ARR L5G31.)

3. Herriot, John G.: Blockage Corrections for Three-Dimensional-Flow Closed-Throat Wind Tunnels, With Consideration of the Effect of Compressibility. NACA Rep. 995, 1950. (Supersedes NACA RM A7B28.)

4. Glauert, H.: The Elements of Aerofoil and Airscrew Theory. Second ed., Cambridge Univ. Press, 1947, pp. 31-32. (Reprinted 1948.)

TABLE I.- FUSELAGE ORDINATES




| Ordinates, percent length | |
|---|---|
| Station | Radius |
| 0 | 0 |
| 3.28 | .91 |
| 6.57 | 1.71 |
| 9.86 | 2.41 |
| 13.15 | 3.00 |
| 16.43 | 3.50 |
| 19.72 | 3.90 |
| 23.01 | 4.21 |
| 26.29 | 4.43 |
| 29.58 | 4.53 |
| 32.00 | 4.57 |
| 75.34 | 4.57 |
| 76.69 | 4.54 |
| 79.98 | 4.38 |
| 83.26 | 4.18 |
| 86.55 | 3.95 |
| 89.84 | 3.72 |
| 93.13 | 3.49 |
| 96.41 | 3.26 |
| 100.00 | 3.02 |

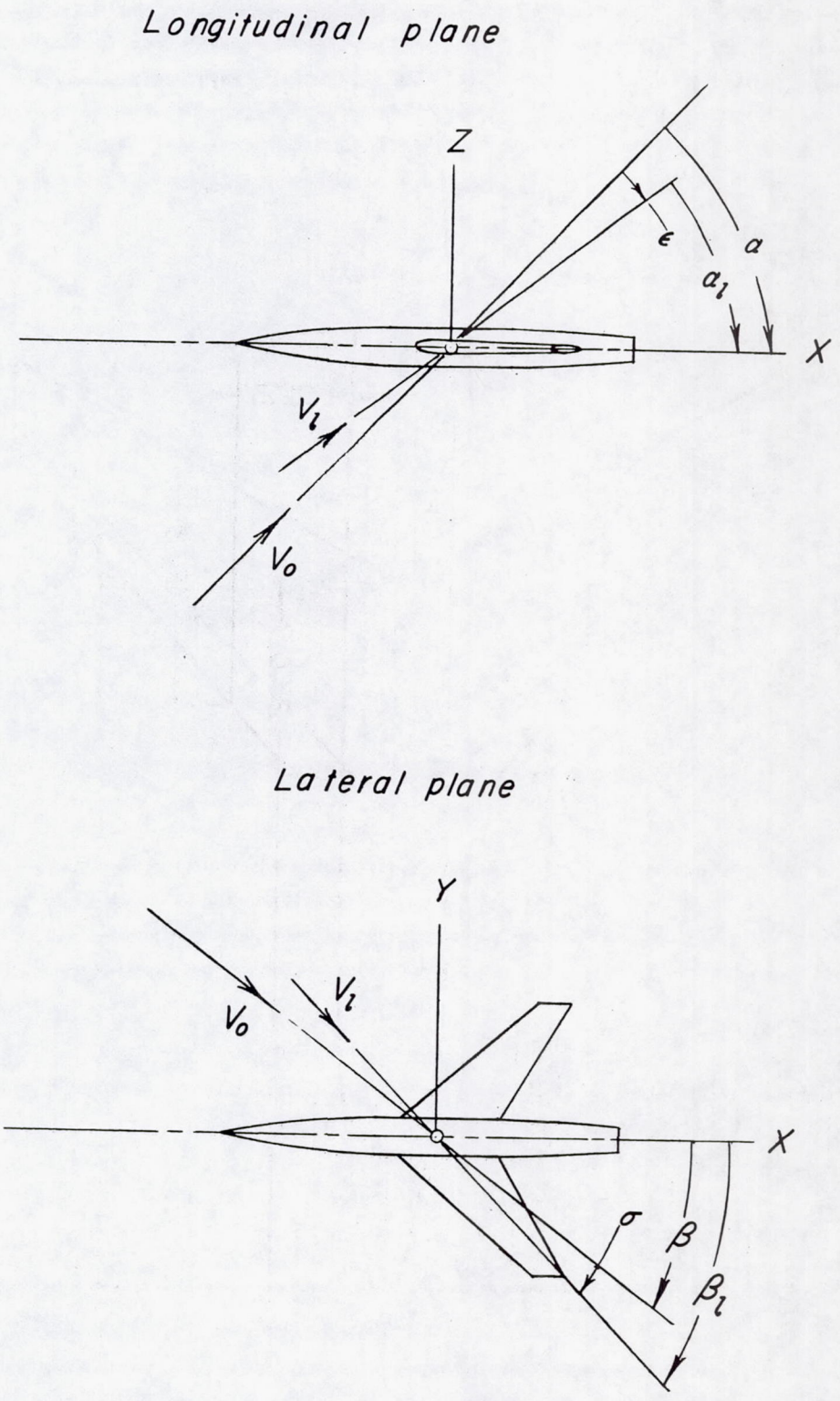
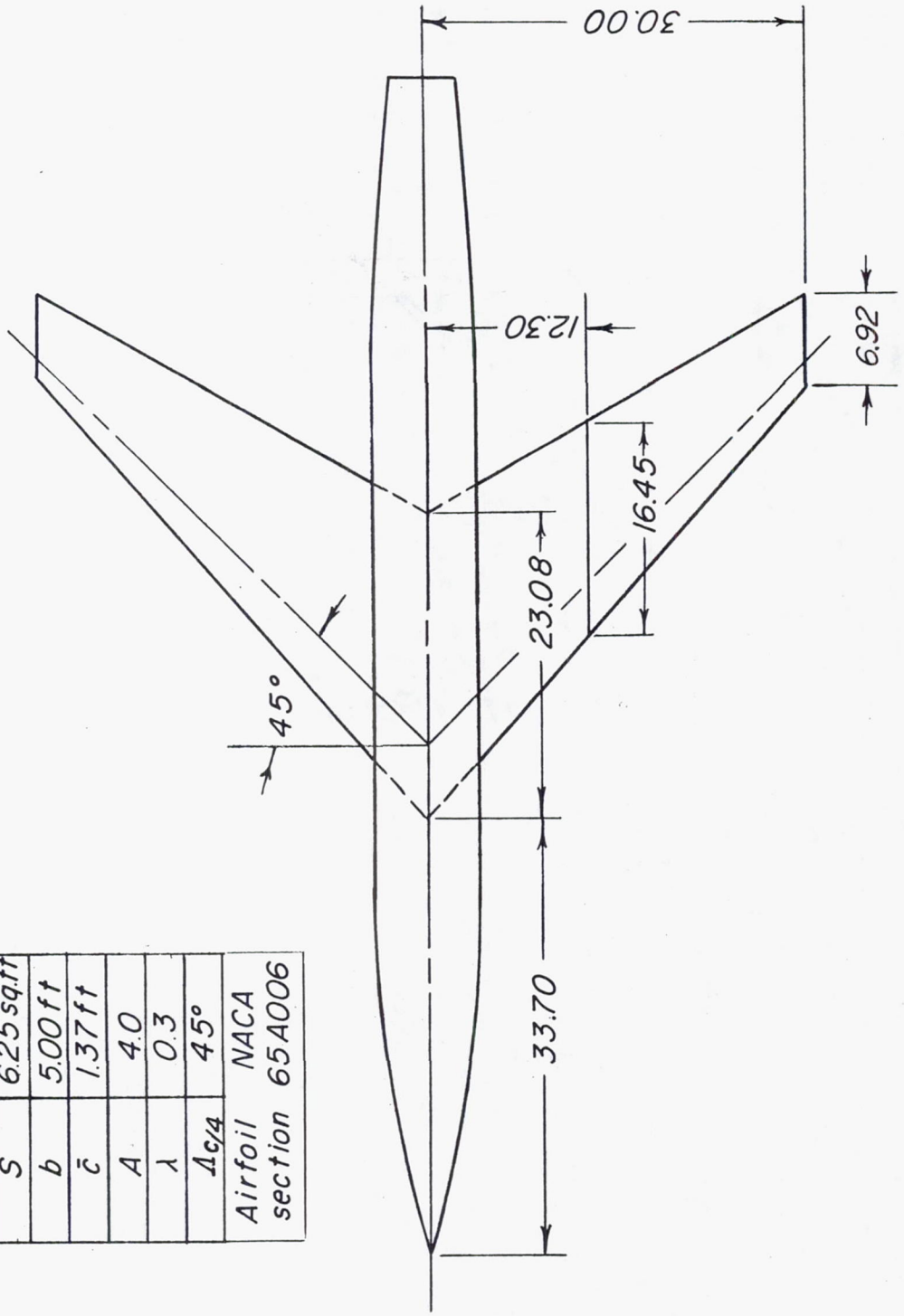
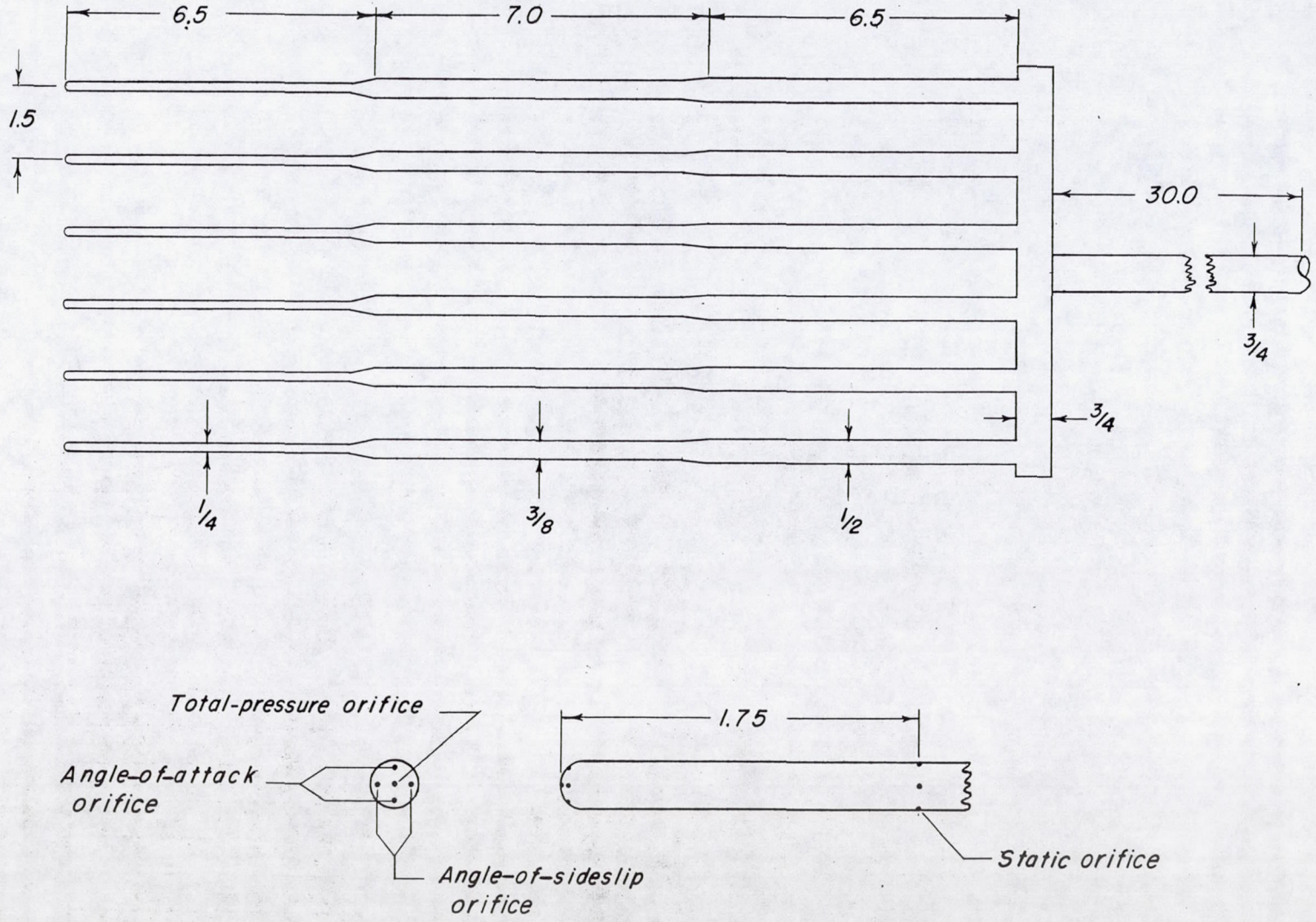



Figure 1.- Positive directions of distances and angles for body-axis system.



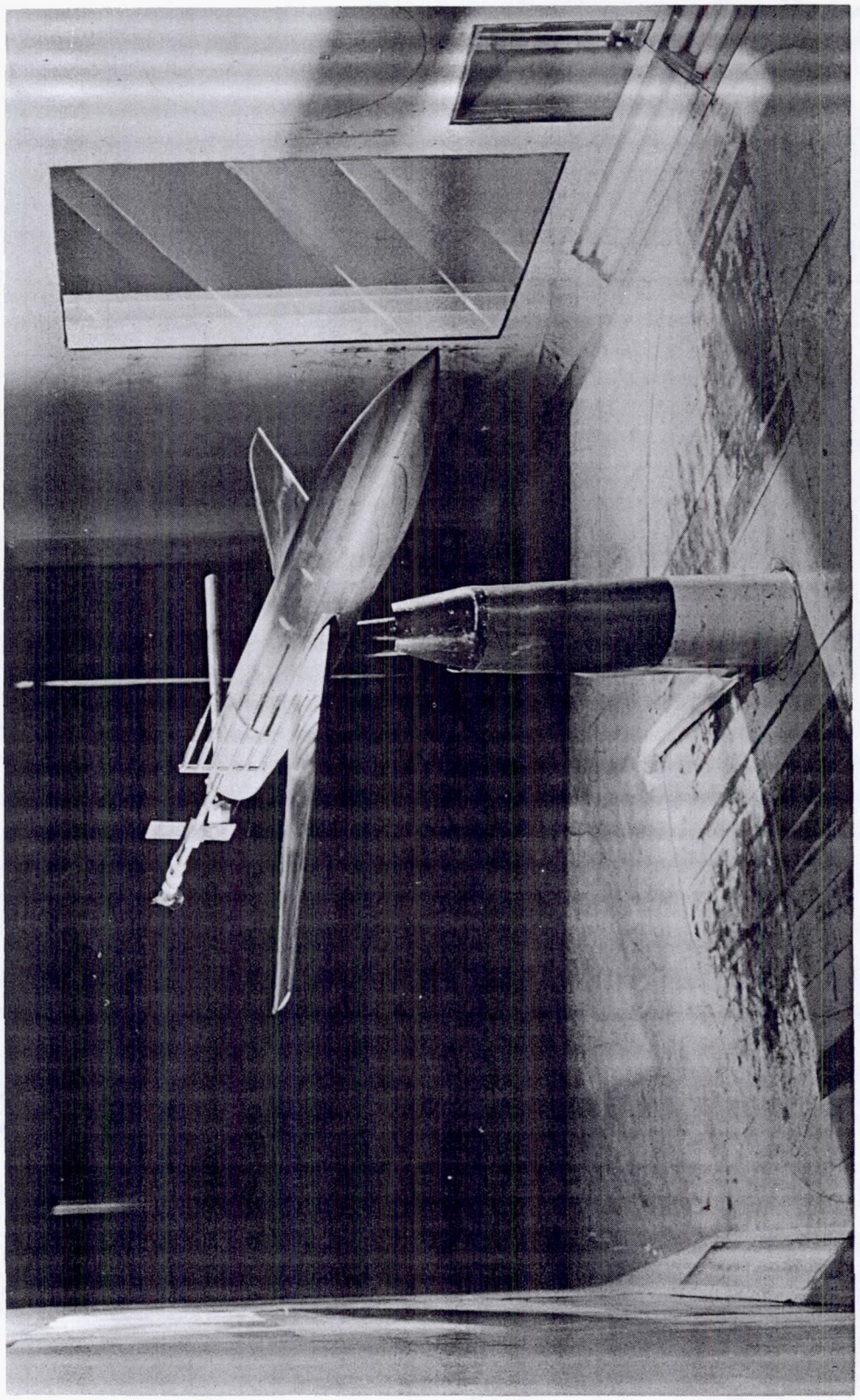

| Wing Geometry | |
|---|---|
| Symbol | Swept |
| $S$ | 6.25 sq.ft |
| $b$ | 5.00 ft |
| $\bar{c}$ | 1.37 ft |
| $A$ | 4.0 |
| $\lambda$ | 0.3 |
| $\Lambda_{c/4}$ | 45° |
| Airfoil section | NACA 65A006 |

Figure 2.- Geometric characteristics of test model. All linear dimensions are in inches except where noted.




(a) General proportions. All linear dimensions are in inches.

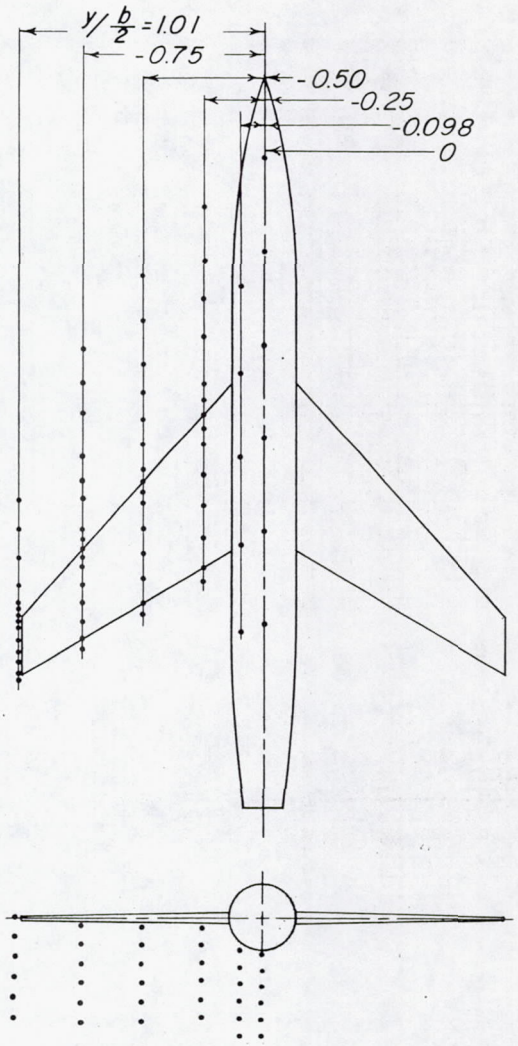
Figure 3.- Flow-survey rake.



L-80760.1

(b) Photograph of rake mounted on swept-wing—fuselage combination. (Model shown is inverted as tested.)

Figure 3.- Concluded.




Swept wing - fuselage

| $y/\frac{b}{2}$ = 0 | | $y/\frac{b}{2}$ = -0.098 | | $y/\frac{b}{2}$ = -0.25 | | $y/\frac{b}{2}$ = -0.50 | | $y/\frac{b}{2}$ = -0.75 | | $y/\frac{b}{2}$ = -1.01 | |
|---|---|---|---|---|---|---|---|---|---|---|---|
| $x/c$ | $z/c$ | $x/c$ | $z/c$ | $x/c$ | $z/c$ | $x/c$ | $z/c$ | $x/c$ | $z/c$ | $x/c$ | $z/c$ |
| 1.50 | -0.21 | 1.50 | -0.17 | 1.10 | -0.06 | 1.10 | -0.07 | 1.10 | -0.09 | 1.05 | 0.015 |
| 1.00 | -0.28 | 1.00 | -0.24 | 1.00 | -0.14 | 1.00 | -0.17 | 1.00 | -0.23 | 0.95 | -0.20 |
| 0.50 | -0.34 | 0.50 | -0.31 | 0.80 | -0.22 | 0.80 | -0.27 | 0.80 | -0.37 | 0.75 | -0.42 |
| 0 | -0.40 | 0 | -0.38 | 0.60 | -0.30 | 0.60 | -0.37 | 0.60 | -0.51 | 0.60 | -0.64 |
| -0.50 | -0.47 | -0.50 | -0.45 | 0.40 | -0.38 | 0.40 | -0.47 | 0.40 | -0.65 | 0.40 | -0.86 |
| -1.00 | -0.53 | | -0.51 | 0.20 | -0.46 | 0.20 | -0.57 | 0.20 | -0.79 | 0.20 | -1.08 |
| | | | | 0.10 | | 0.10 | | 0.10 | | 0.10 | |
| | | | | 0 | | 0 | | 0 | | 0 | |
| | | | | -0.10 | | -0.10 | | -0.10 | | -0.10 | |
| | | | | -0.20 | | -0.30 | | -0.20 | | -0.20 | |
| | | | | -0.50 | | -0.50 | | -0.55 | | -0.50 | |
| | | | | -0.75 | | -0.75 | | -0.75 | | -1.00 | |
| | | | | -1.00 | | -1.00 | | -1.00 | | -1.50 | |
| | | | | -1.35 | | -1.35 | | -1.50 | | -2.00 | |
| | | | | | | -1.70 | | -1.85 | | | |
| | | | | | | | | -2.20 | | | |

Figure 4.- Locations at which flow surveys were made.

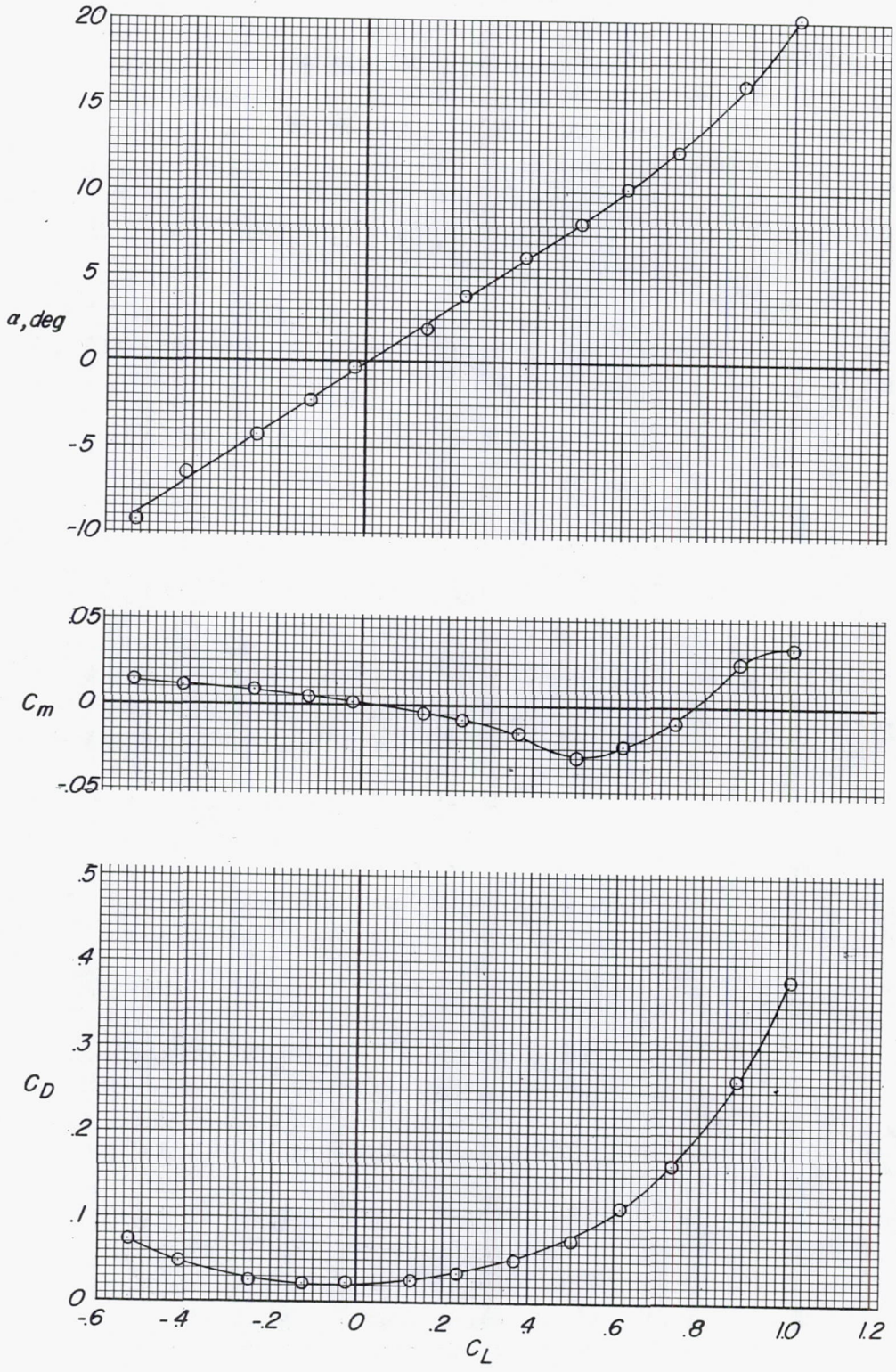
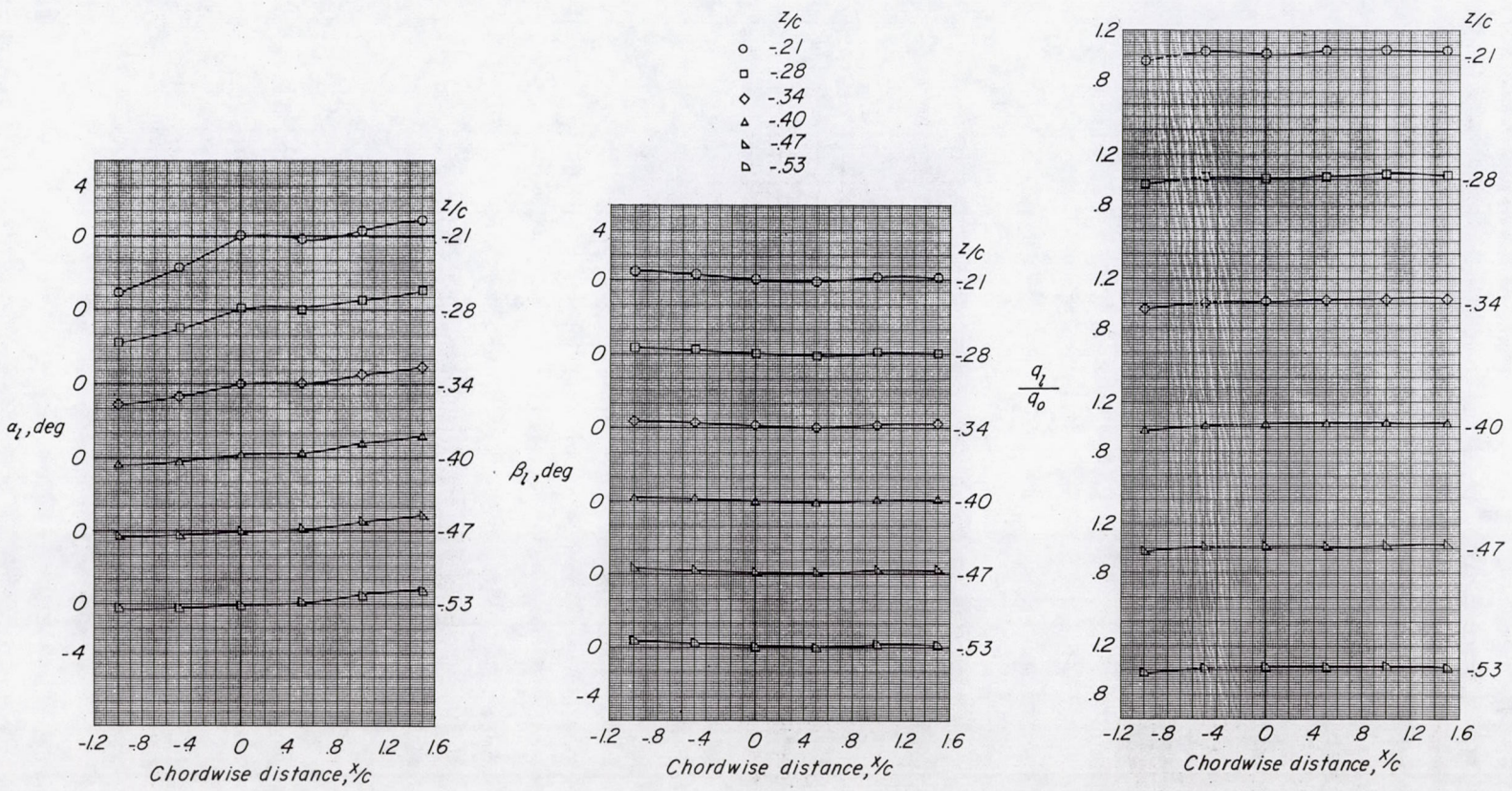


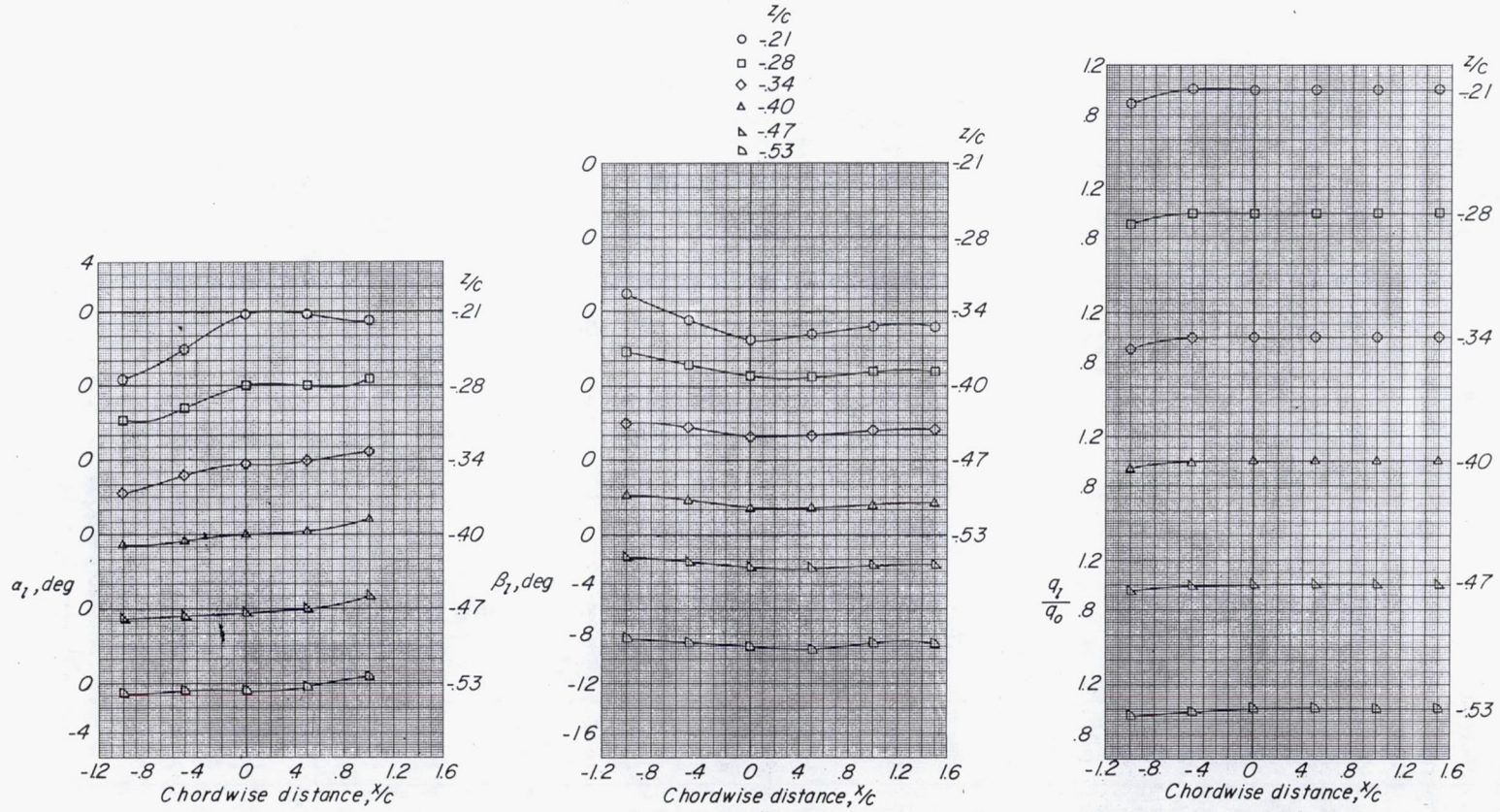

Figure 5.- Lift, drag, and pitching-moment characteristics of the test model.




(a) $\alpha = -0.2^{\circ}$; $\beta = 0^{\circ}$.

Figure 6.- Flow-field characteristics of swept-wing—fuselage combination at $y/\frac{b}{2} = 0$.

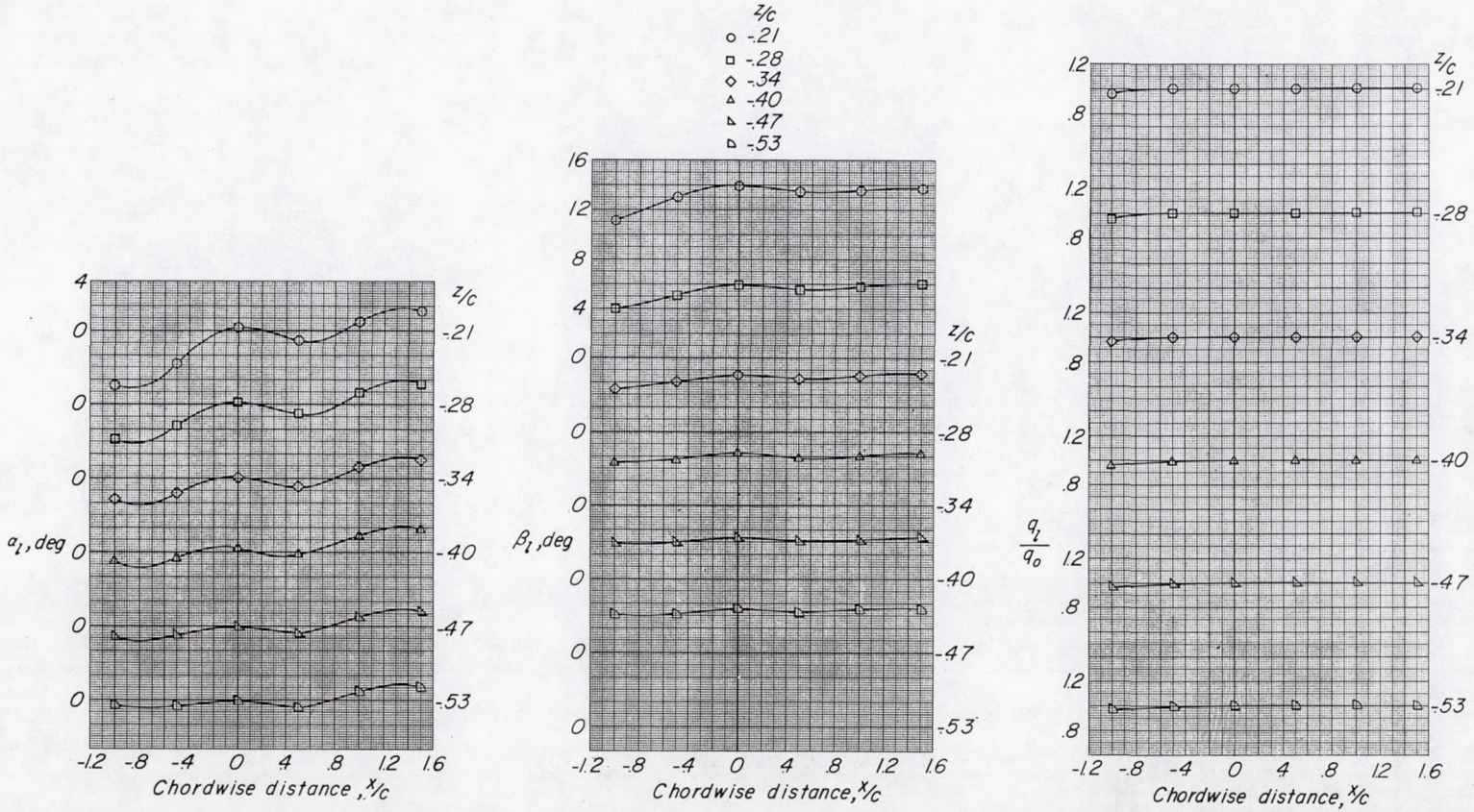
CONFIDENTIAL




(b) $\alpha = -0.2^{\circ}$; $\beta = -8^{\circ}$.

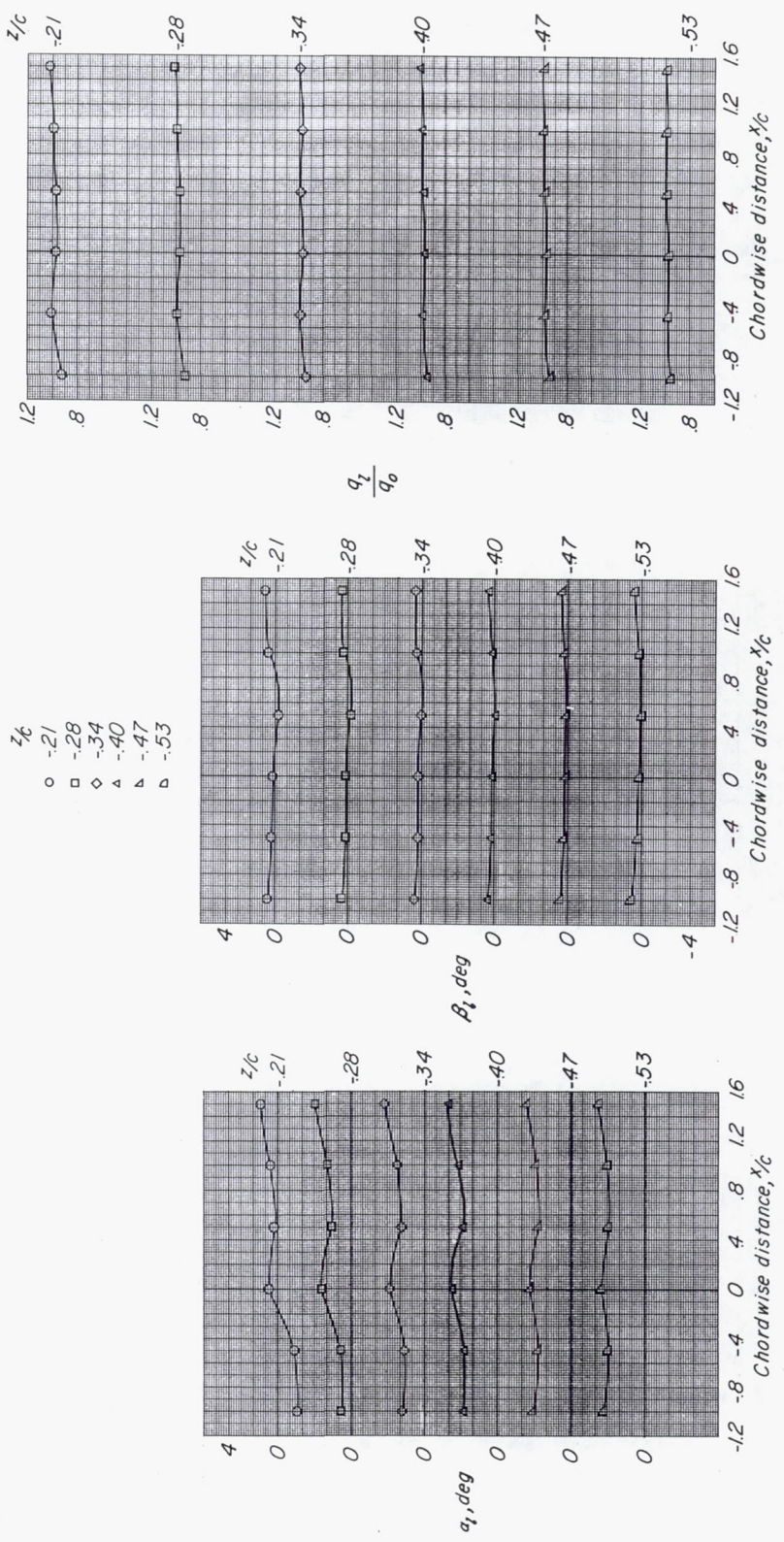
Figure 6.- Continued.

CONFIDENTIAL



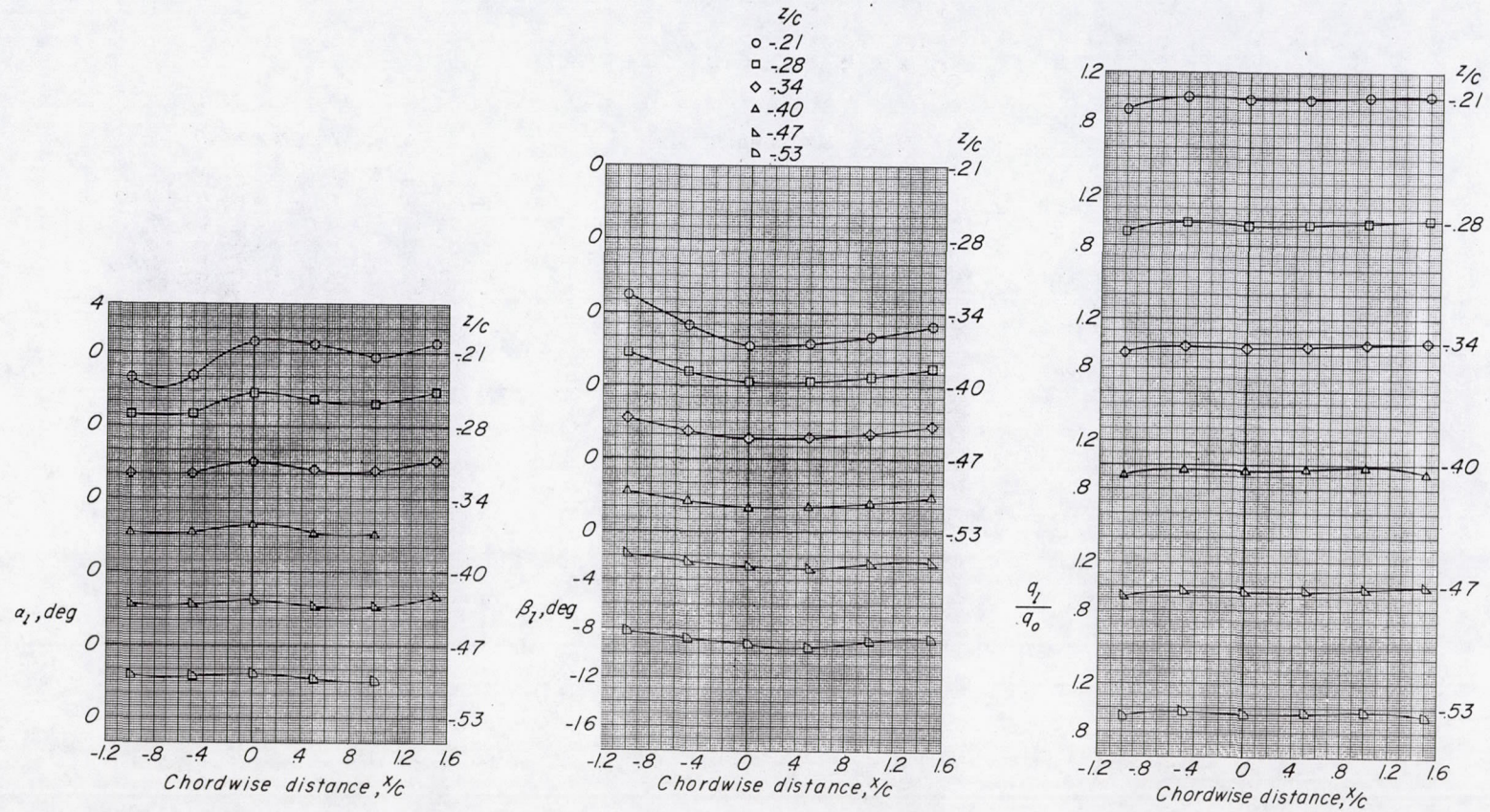

(c) $\alpha = -0.2^{\circ}$; $\beta = 8^{\circ}$.

Figure 6.- Continued.



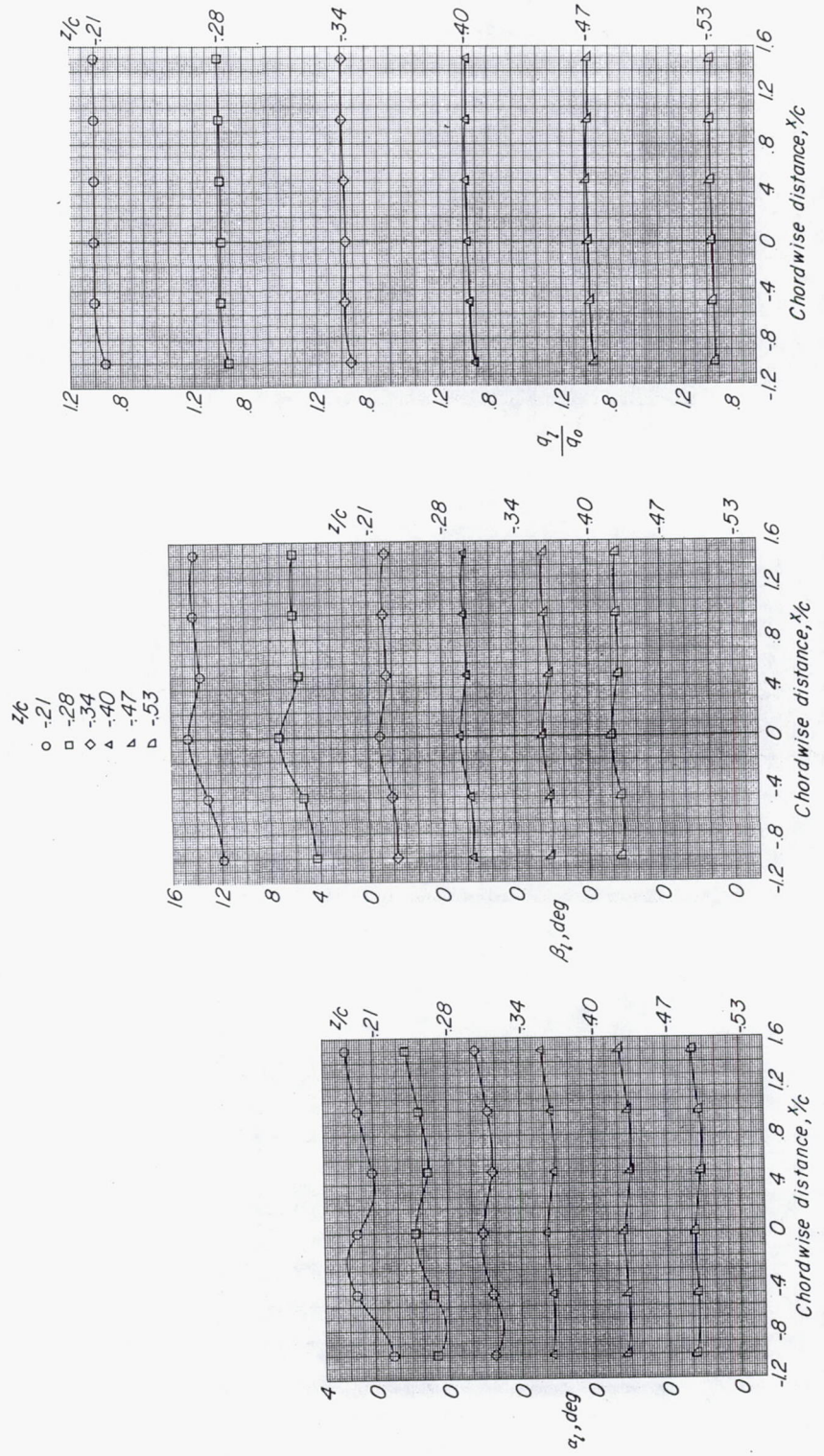

(d) $\alpha = 3.8^{\circ}$; $\beta = 0^{\circ}$.

Figure 6.- Continued.



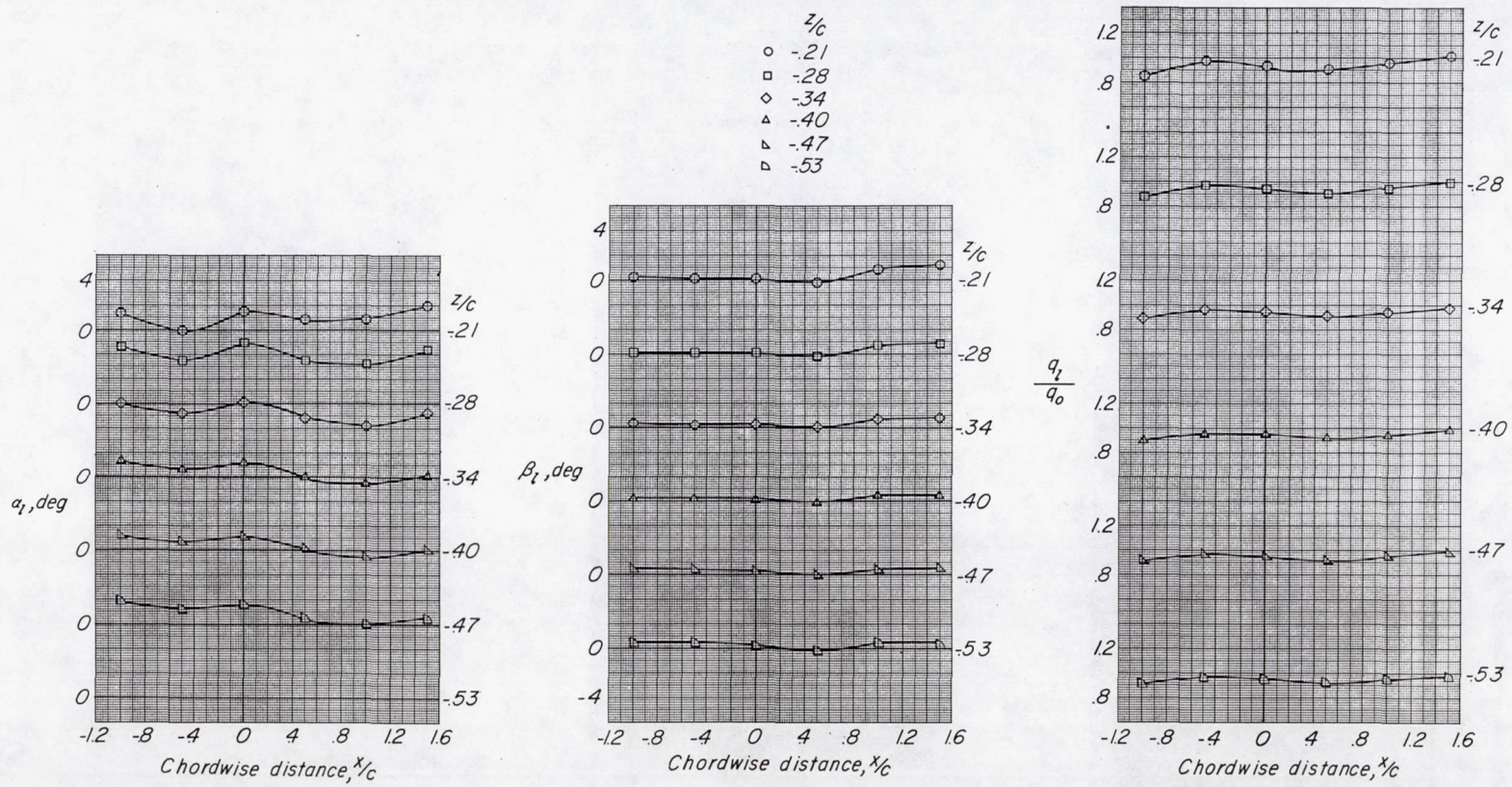

(e) $\alpha = 3.8^{\circ}$; $\beta = -8^{\circ}$.

Figure 6.- Continued.



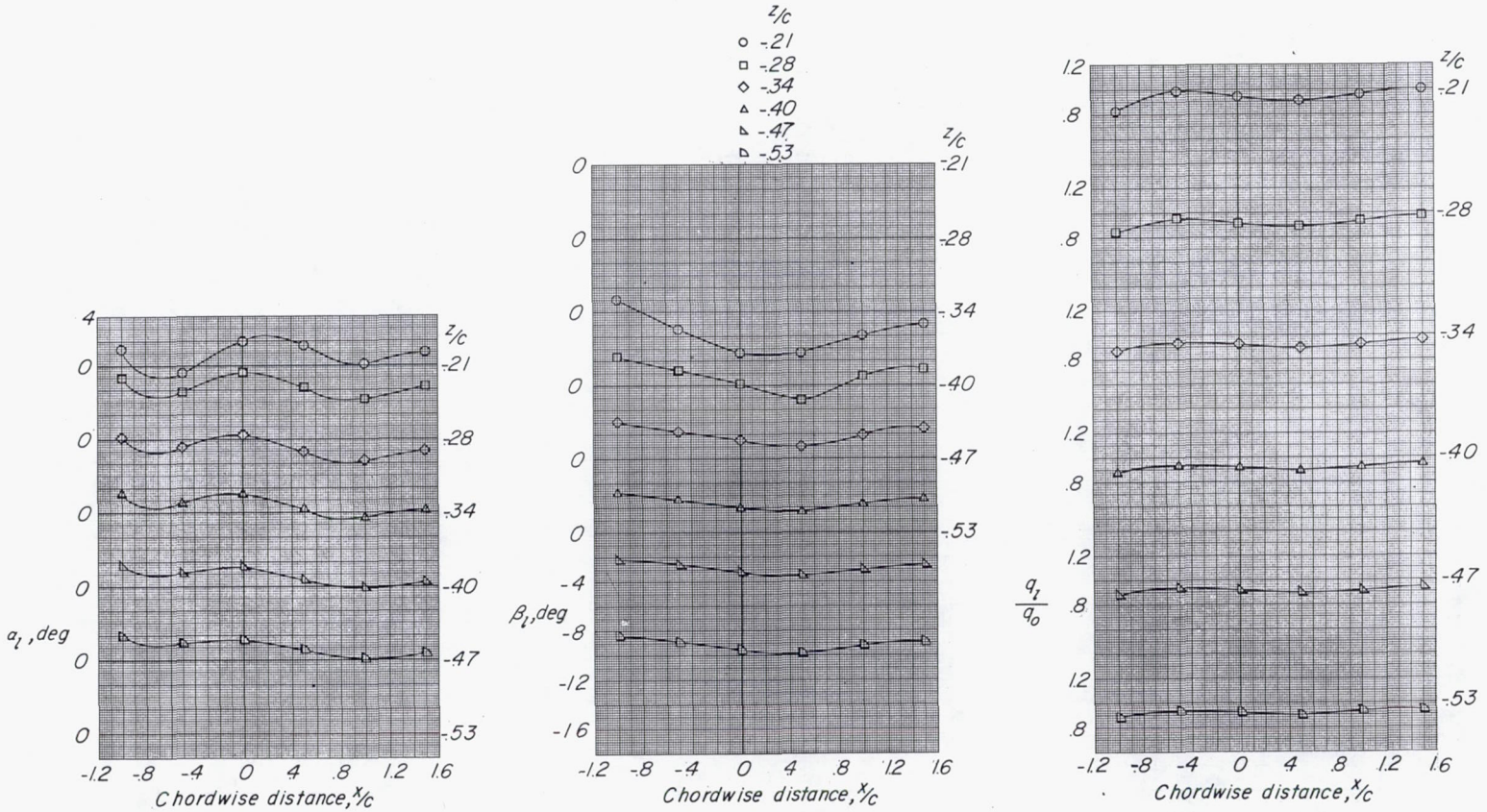

(f) $\alpha = 3.8^{\circ}$; $\beta = 8^{\circ}$.

Figure 6.- Continued.




(g) $\alpha = 8.2^{\circ}$; $\beta = 0^{\circ}$.

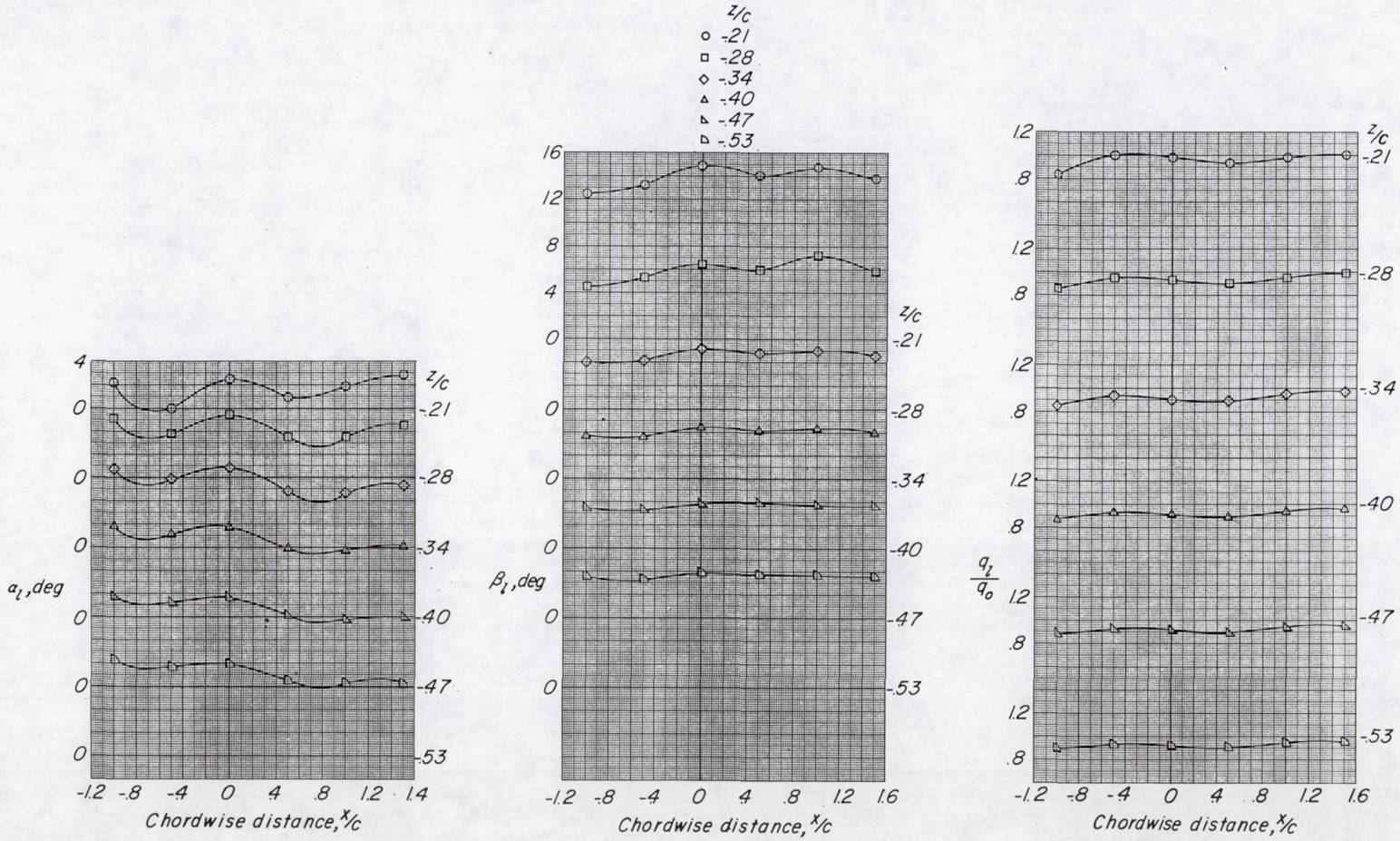
Figure 6.- Continued.




(h) $\alpha = 8.2^{\circ}$; $\beta = -8^{\circ}$.

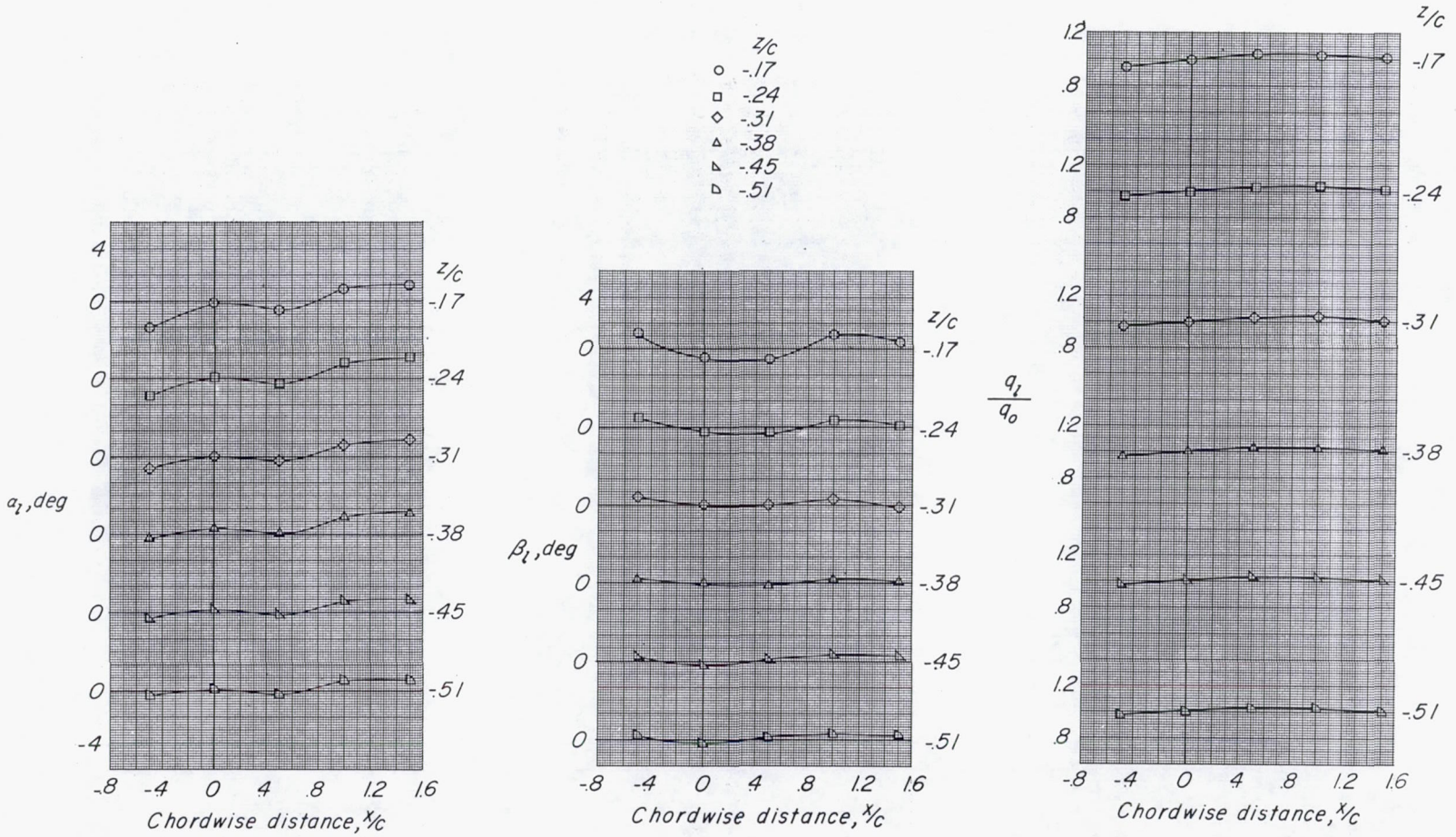
Figure 6.- Continued.

CONFIDENTIAL



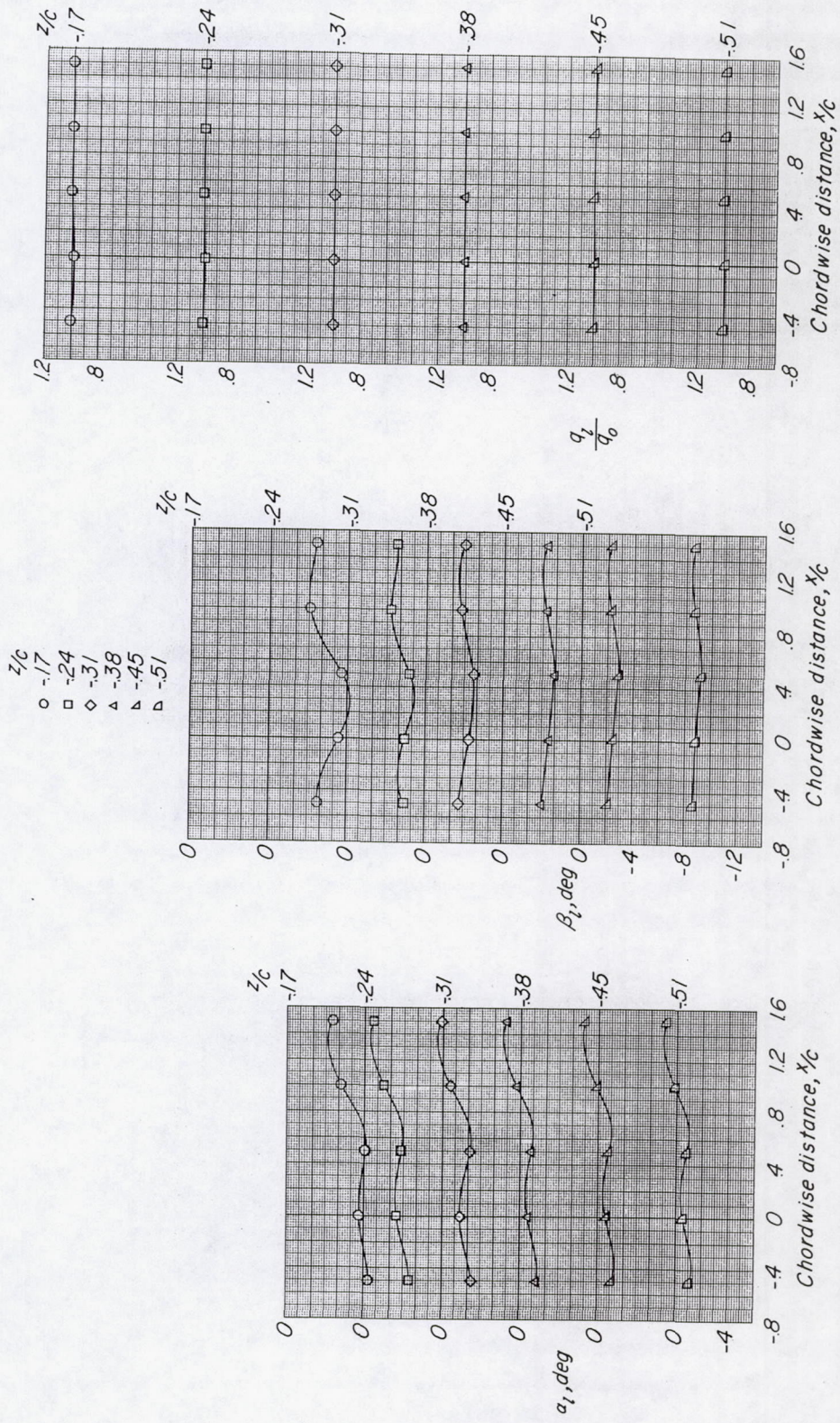

(i) $\alpha = 8.2^{\circ}$; $\beta = 8^{\circ}$.

Figure 6.- Concluded.



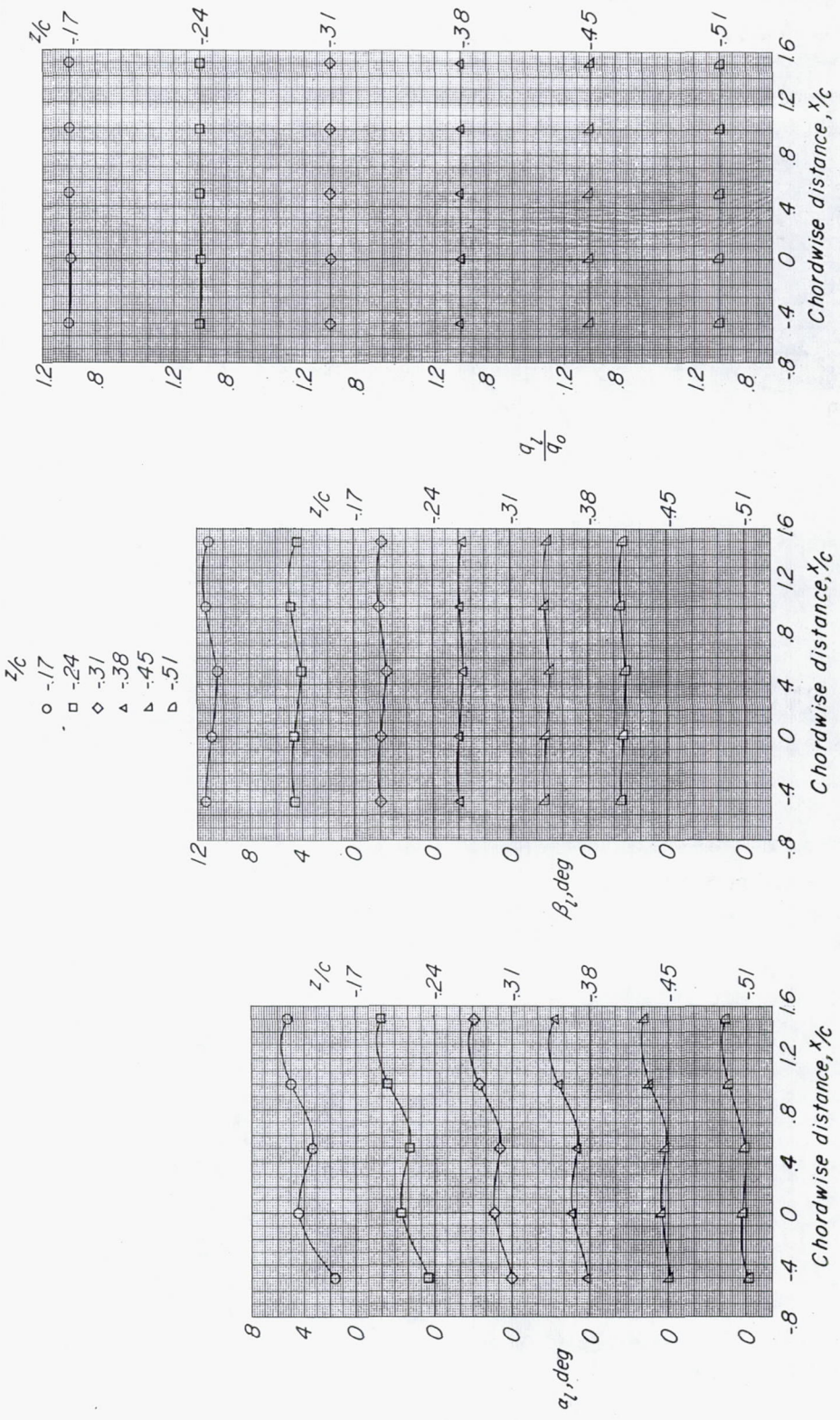

(a) $\alpha = -0.2^{\circ}$; $\beta = 0^{\circ}$.

Figure 7.- Flow-field characteristics of swept-wing—fuselage combination at $y/\frac{b}{2} = -0.098$.



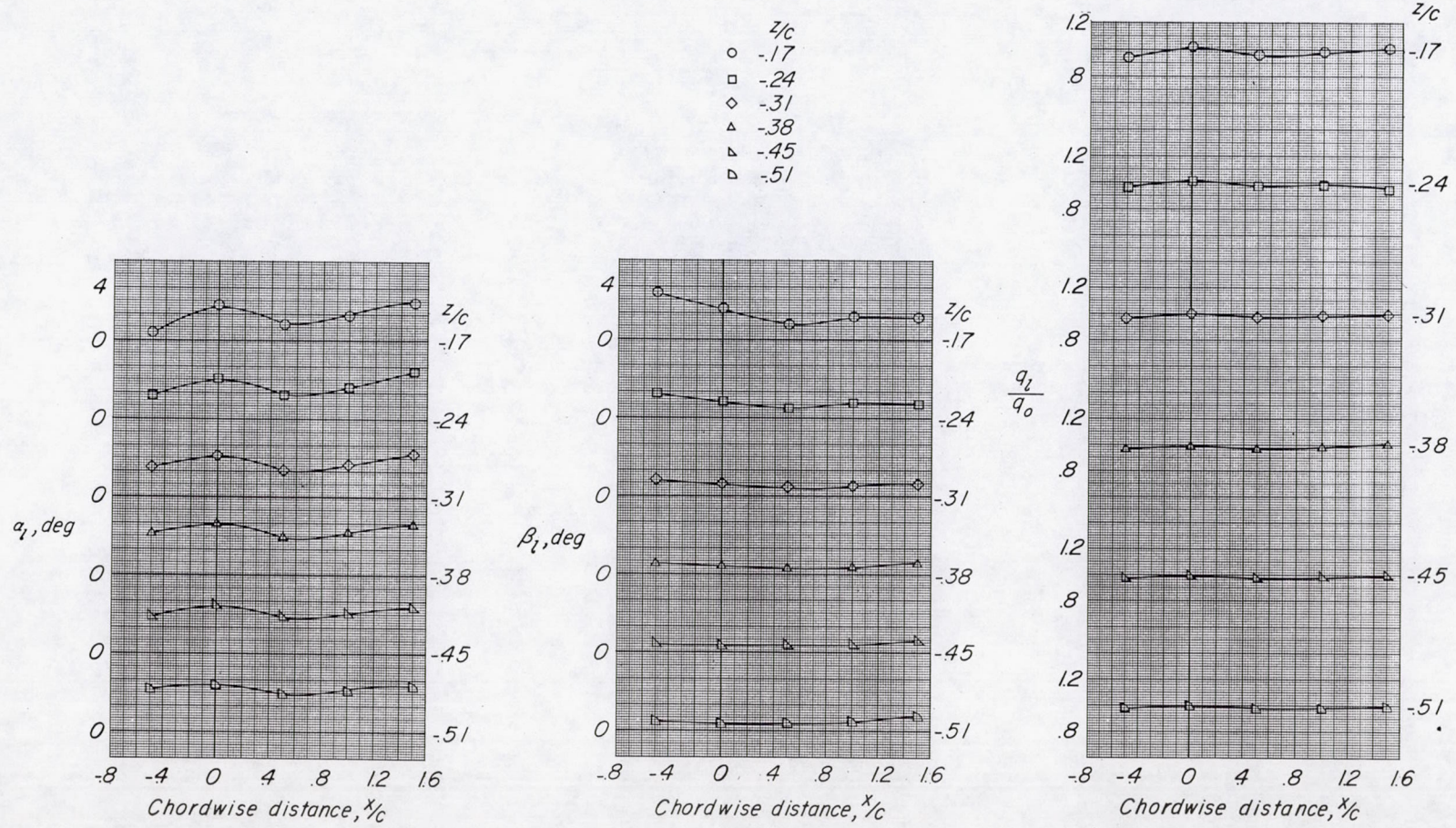

(b) $\alpha = -0.2^{\circ}$; $\beta = -8^{\circ}$.

Figure 7.- Continued.



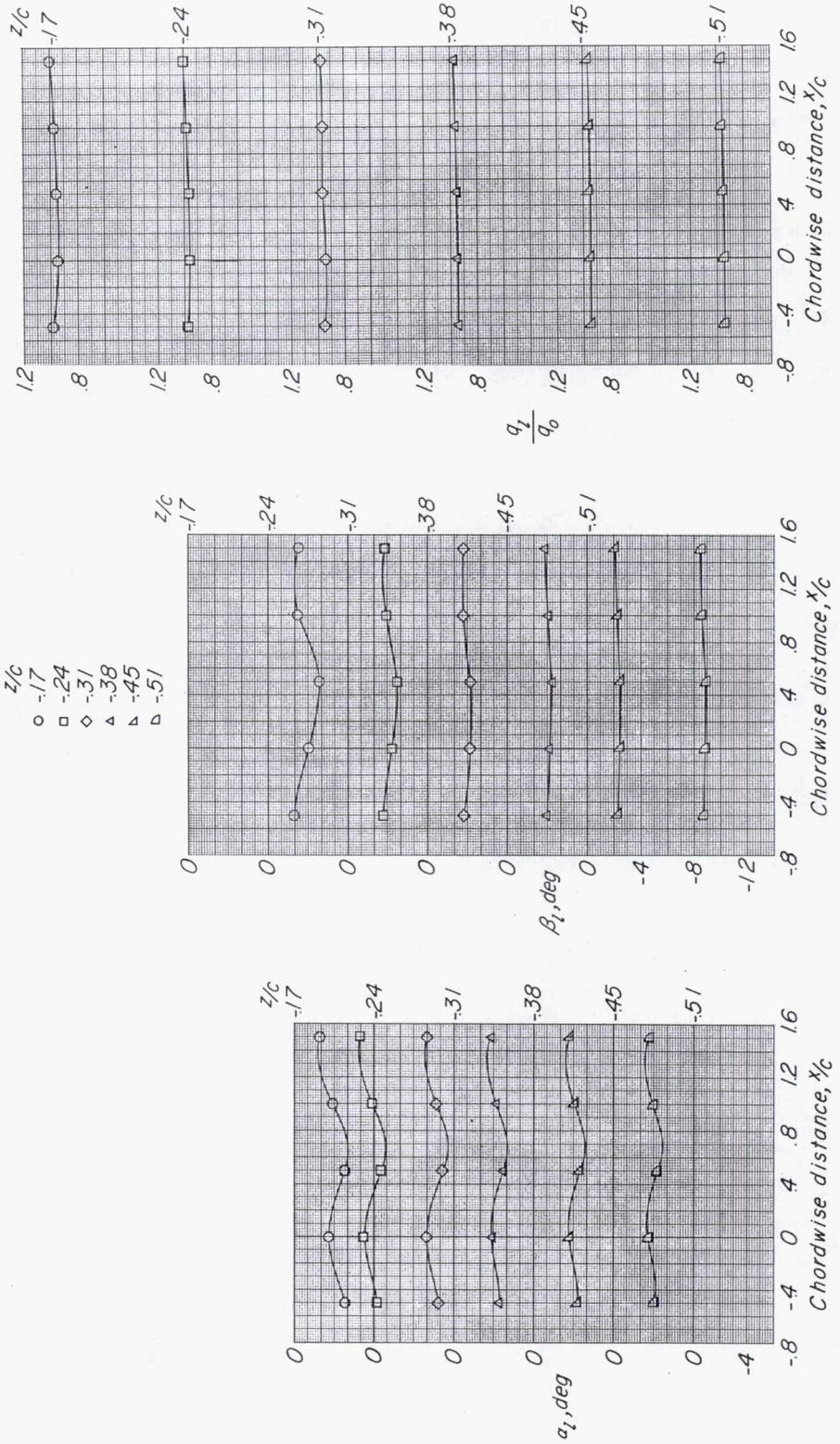

(c) $\alpha = -0.2^{\circ}$; $\beta = 8^{\circ}$.

Figure 7.- Continued.



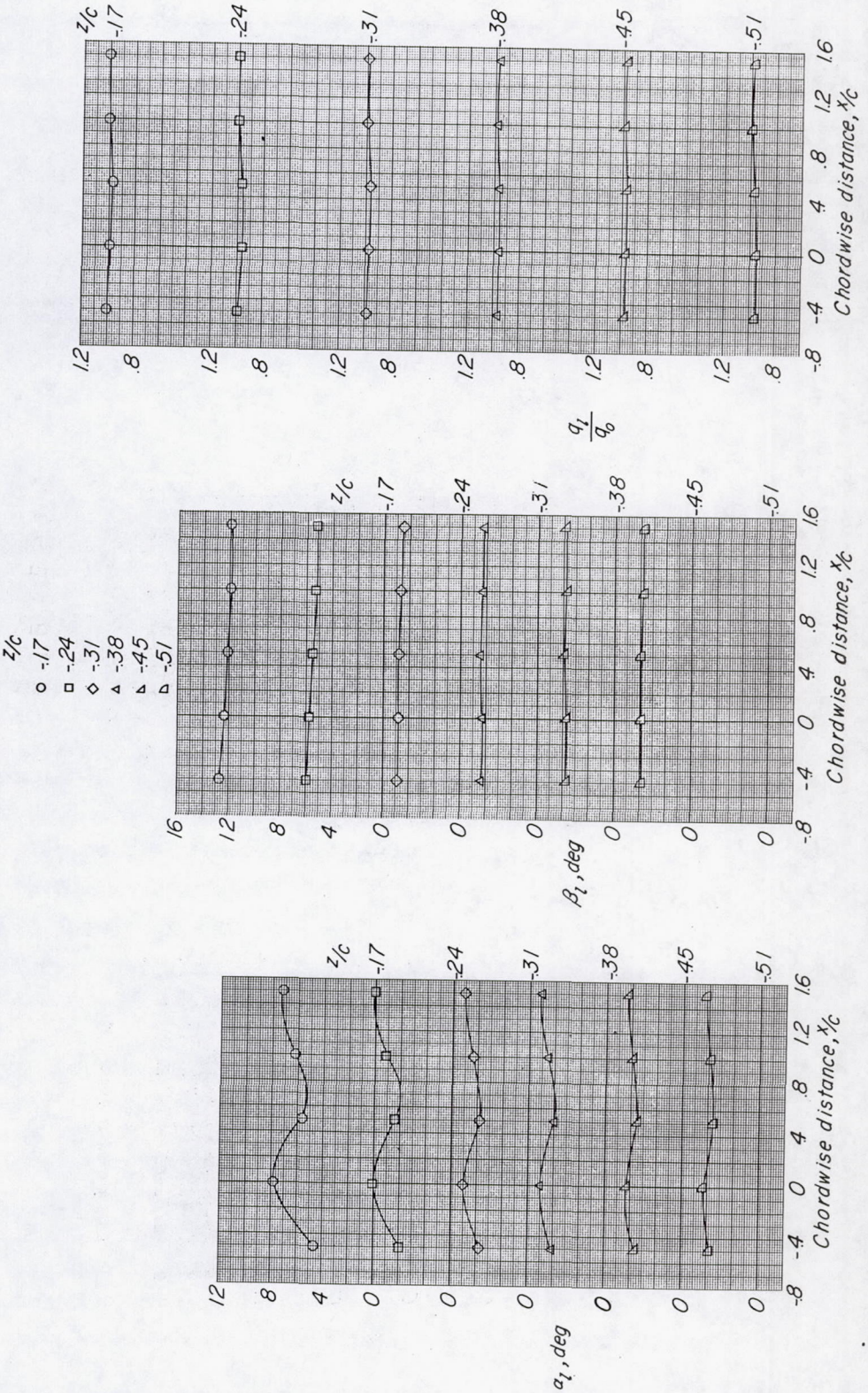

(d) $\alpha = 3.8^{\circ}$; $\beta = 0^{\circ}$.

Figure 7.- Continued.



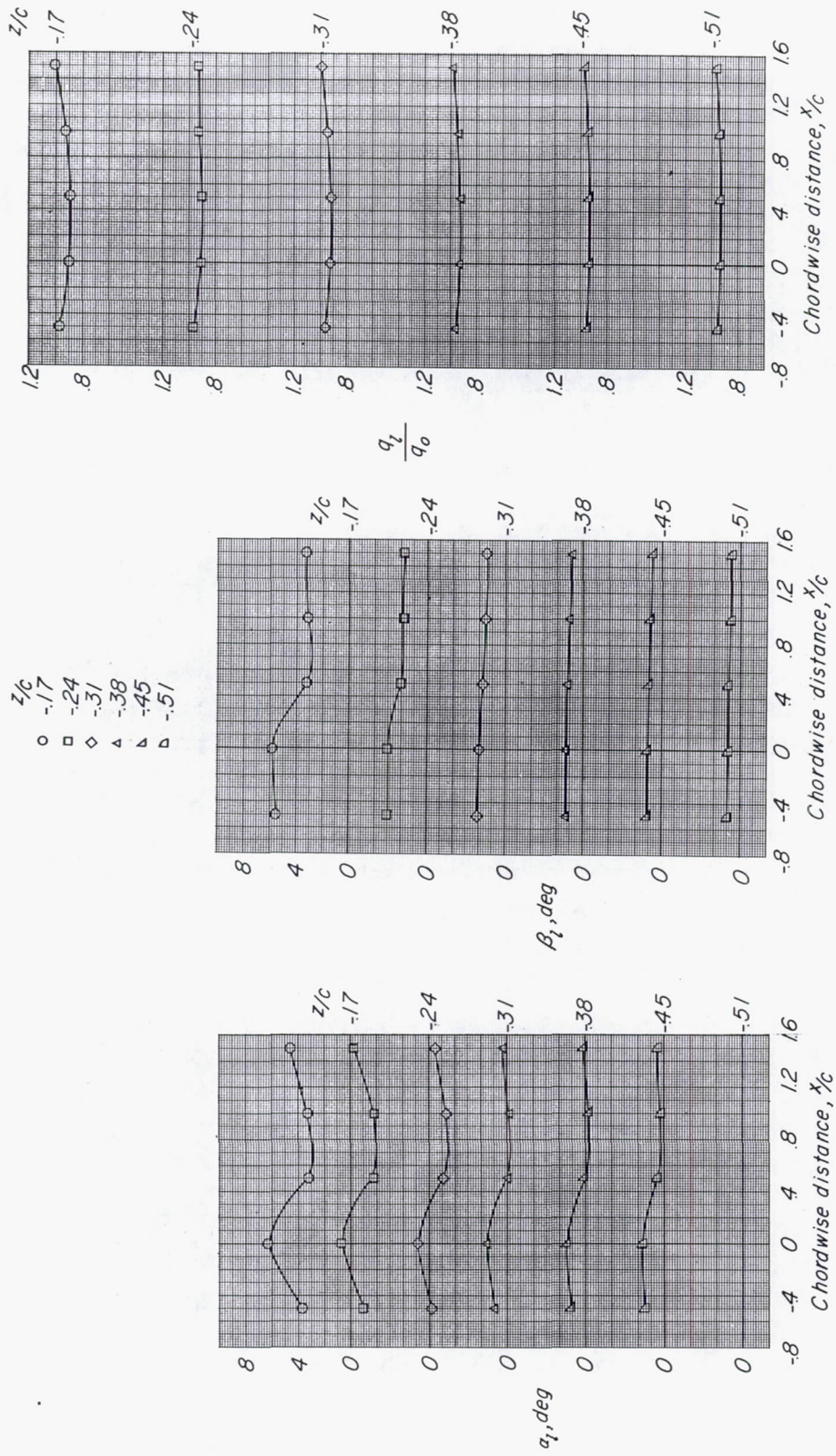

(e) $\alpha = 3.8^{\circ}$; $\beta = -8^{\circ}$.

Figure 7.- Continued.



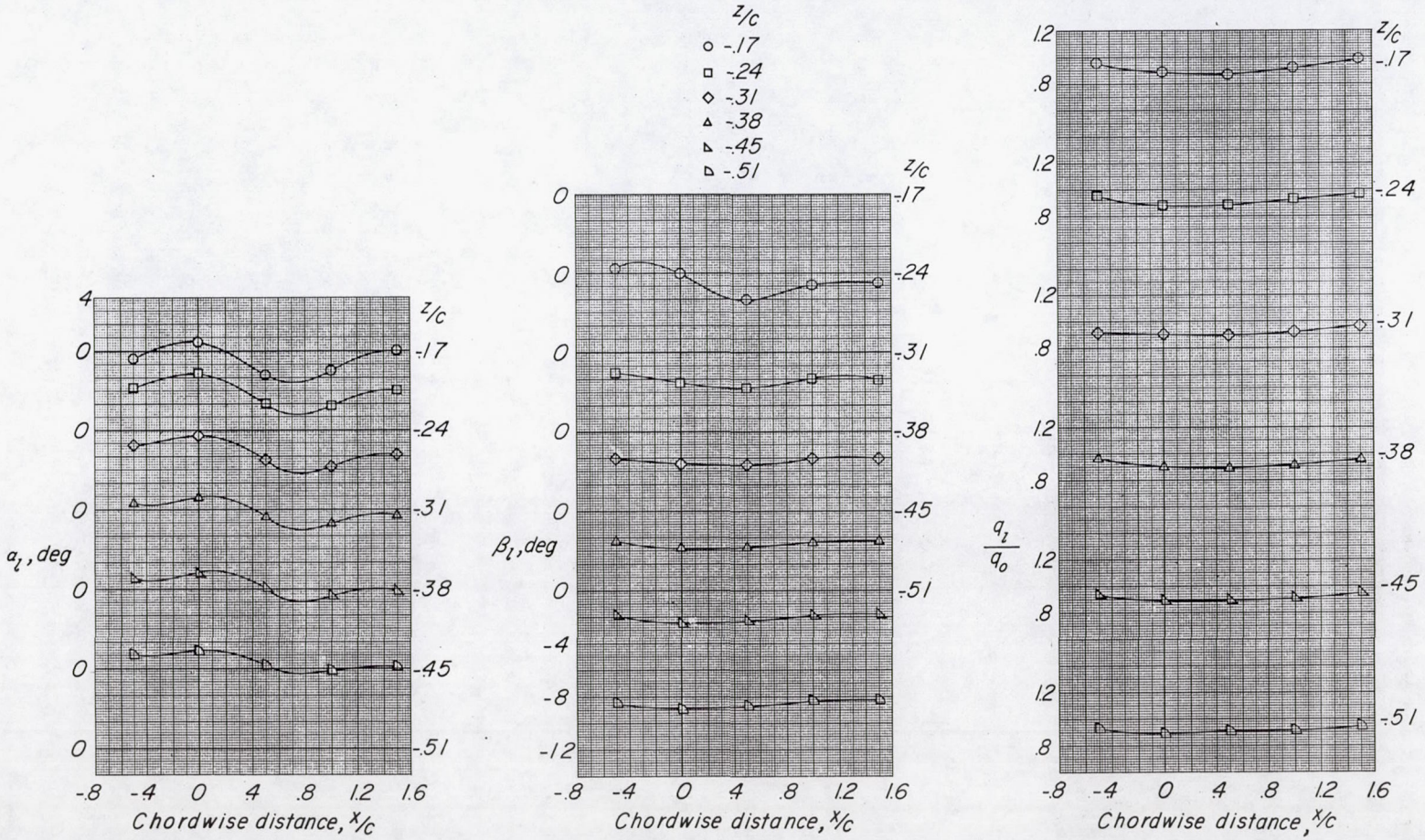

(f) $\alpha = 3.8^{\circ}$; $\beta = 8^{\circ}$.

Figure 7.- Continued.



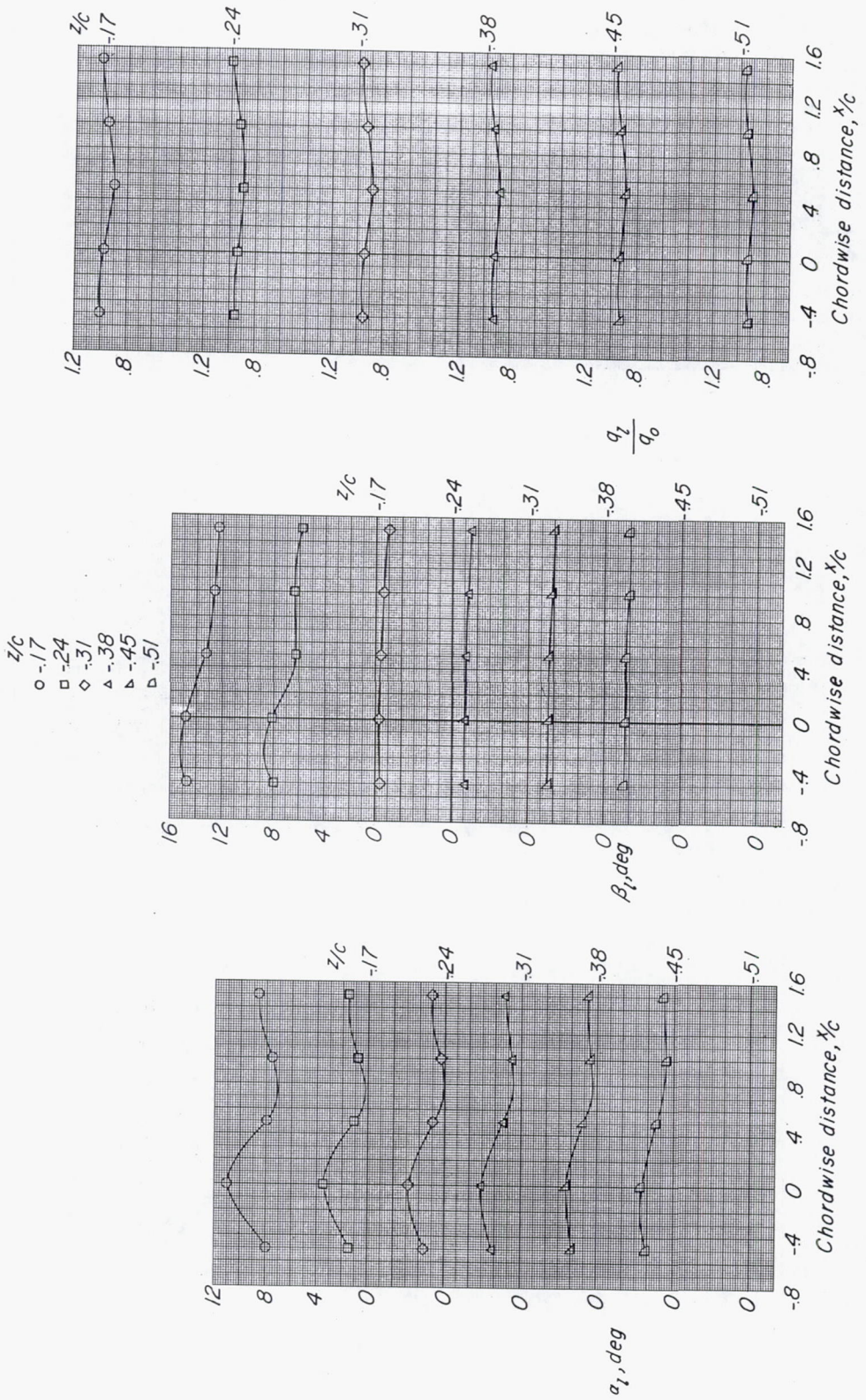

(g) $\alpha = 8.2^{\circ}$; $\beta = 0^{\circ}$.

Figure 7.- Continued.



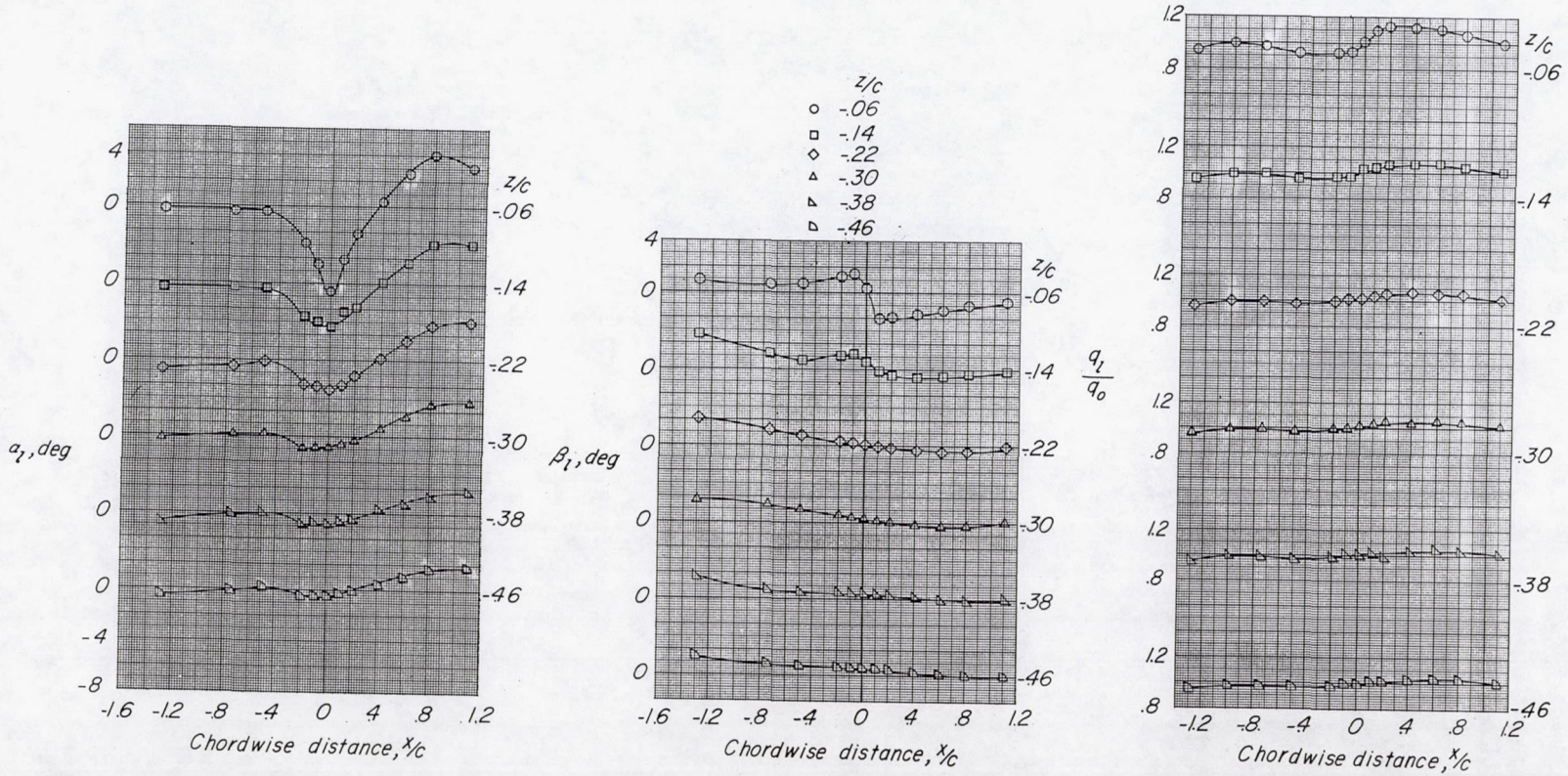

(h) $\alpha = 8.2^{\circ}$; $\beta = -8^{\circ}$.

Figure 7.- Continued.



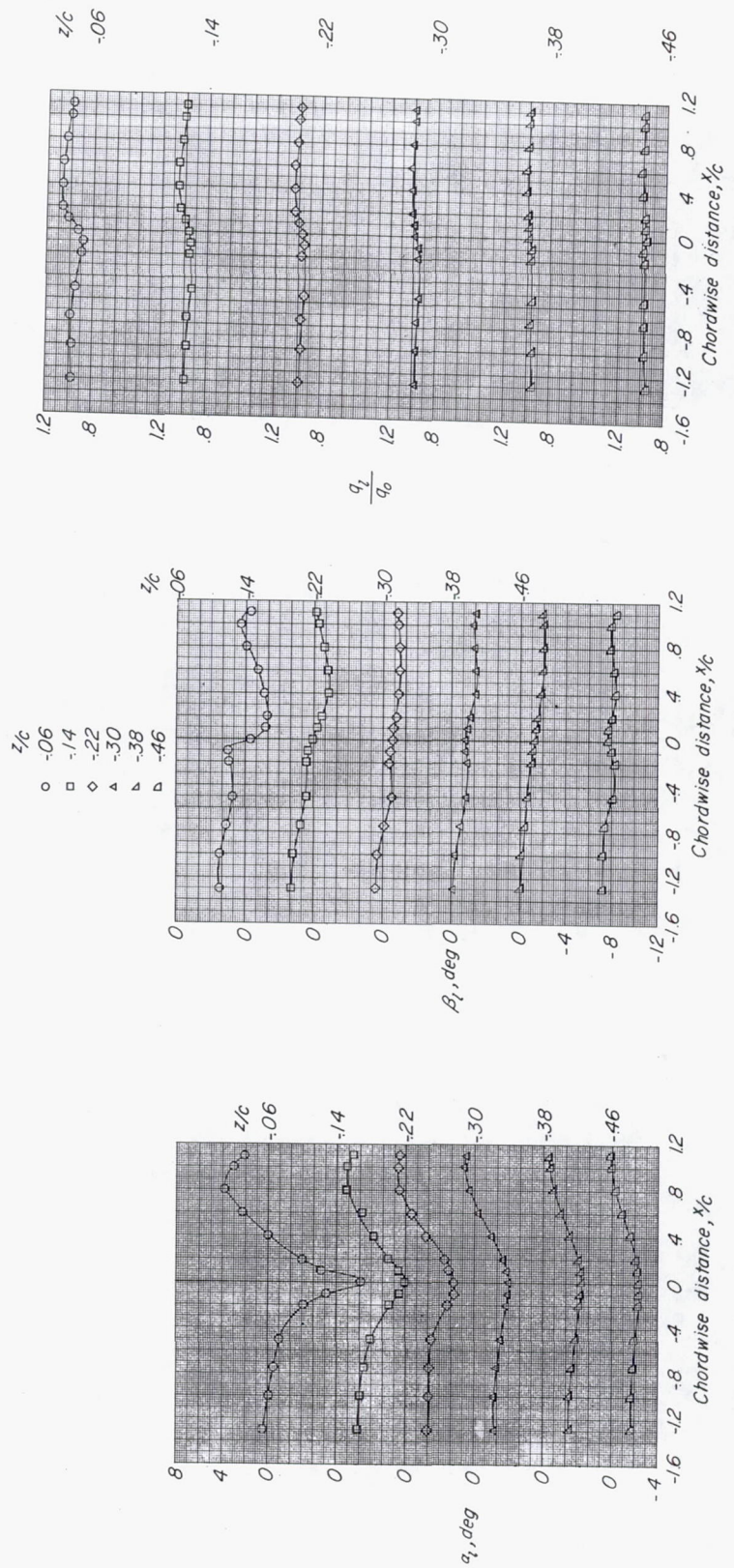

(i) $\alpha = 8.2^{\circ}$; $\beta = 8^{\circ}$.

Figure 7.- Concluded.



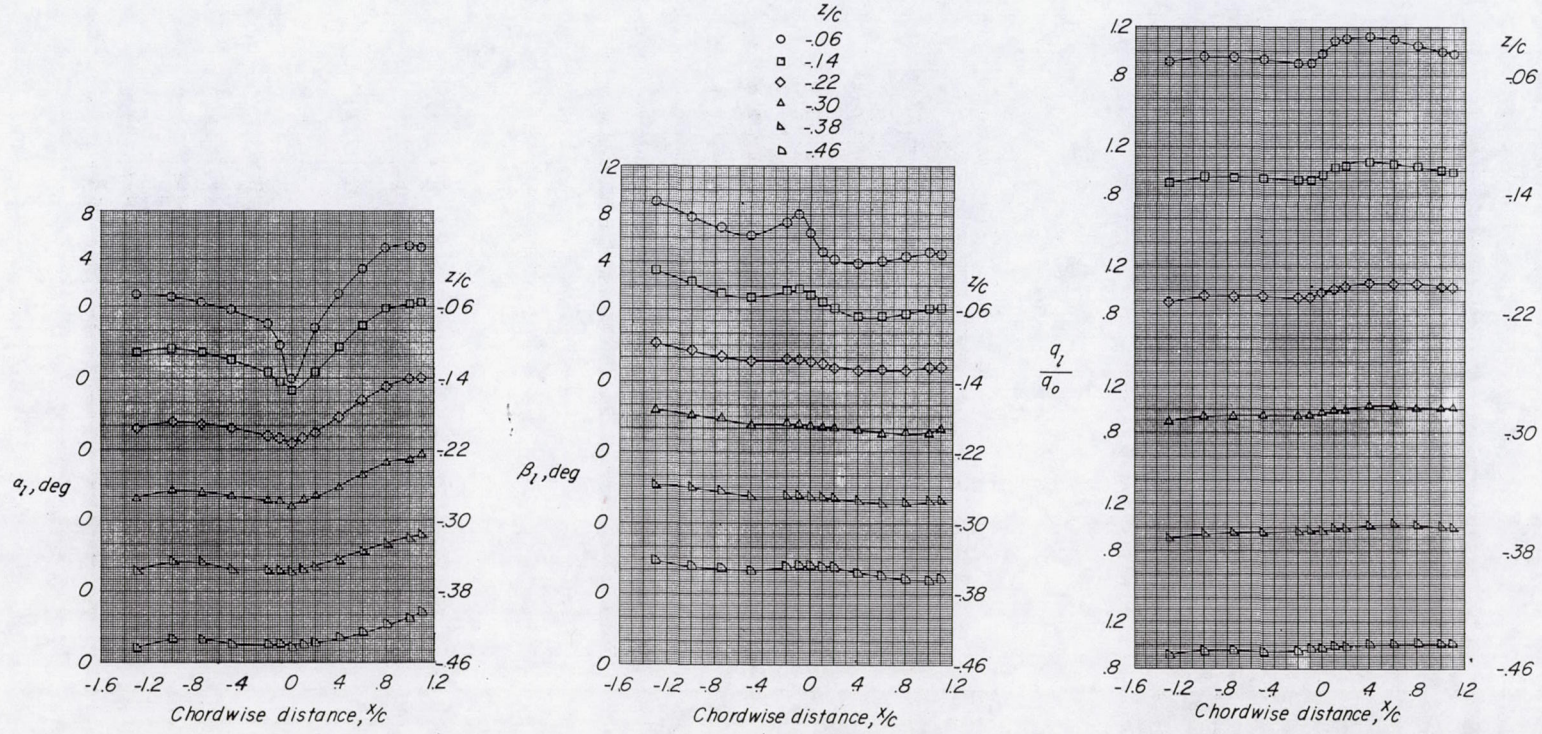

(a) $\alpha = -0.2^\circ$; $\beta = 0^\circ$.

Figure 8.- Flow-field characteristics of swept-wing—fuselage combination at $y/\frac{b}{2} = -0.25$.



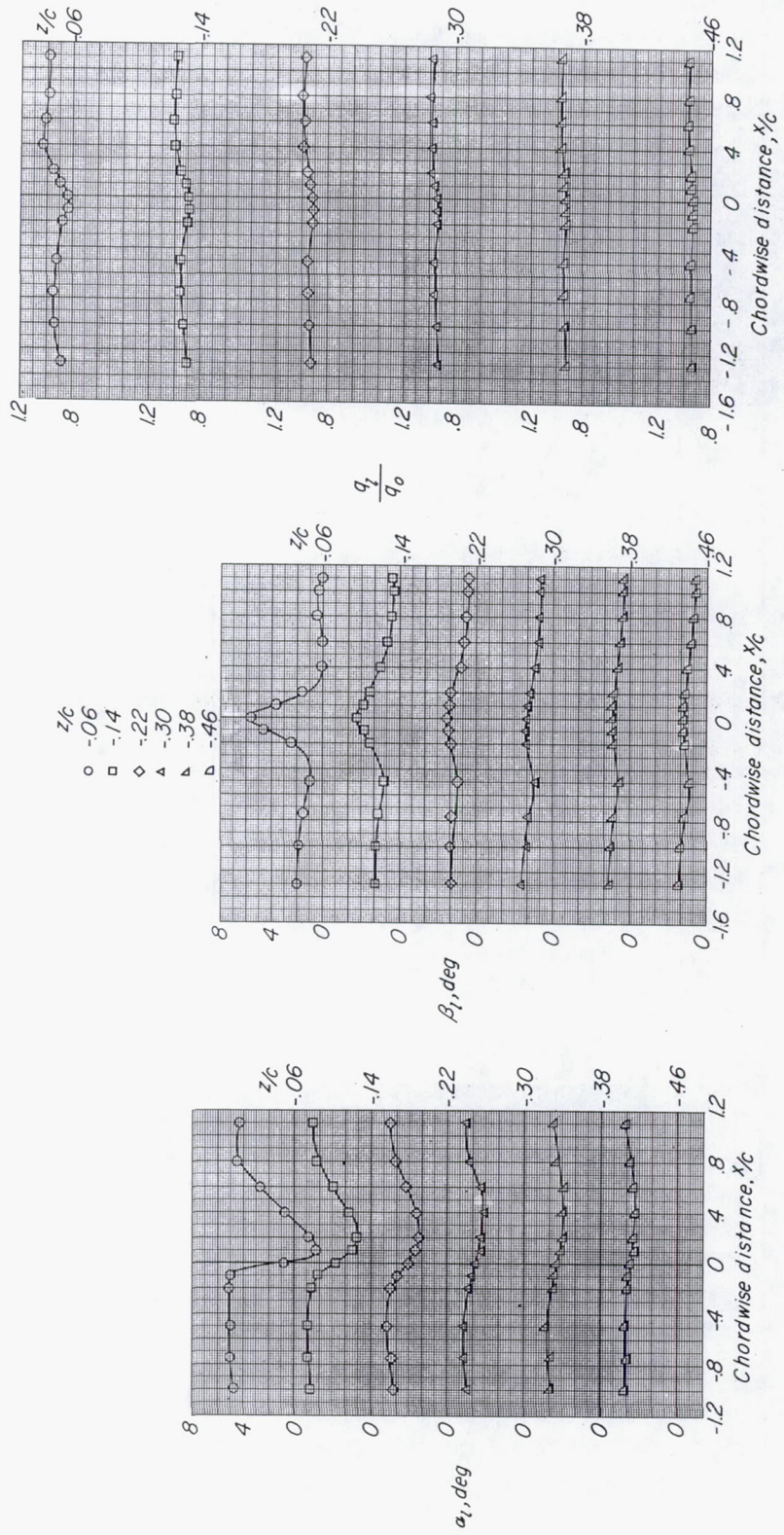

(b) $\alpha = -0.2^{\circ}$; $\beta = -8^{\circ}$.

Figure 8.- Continued.



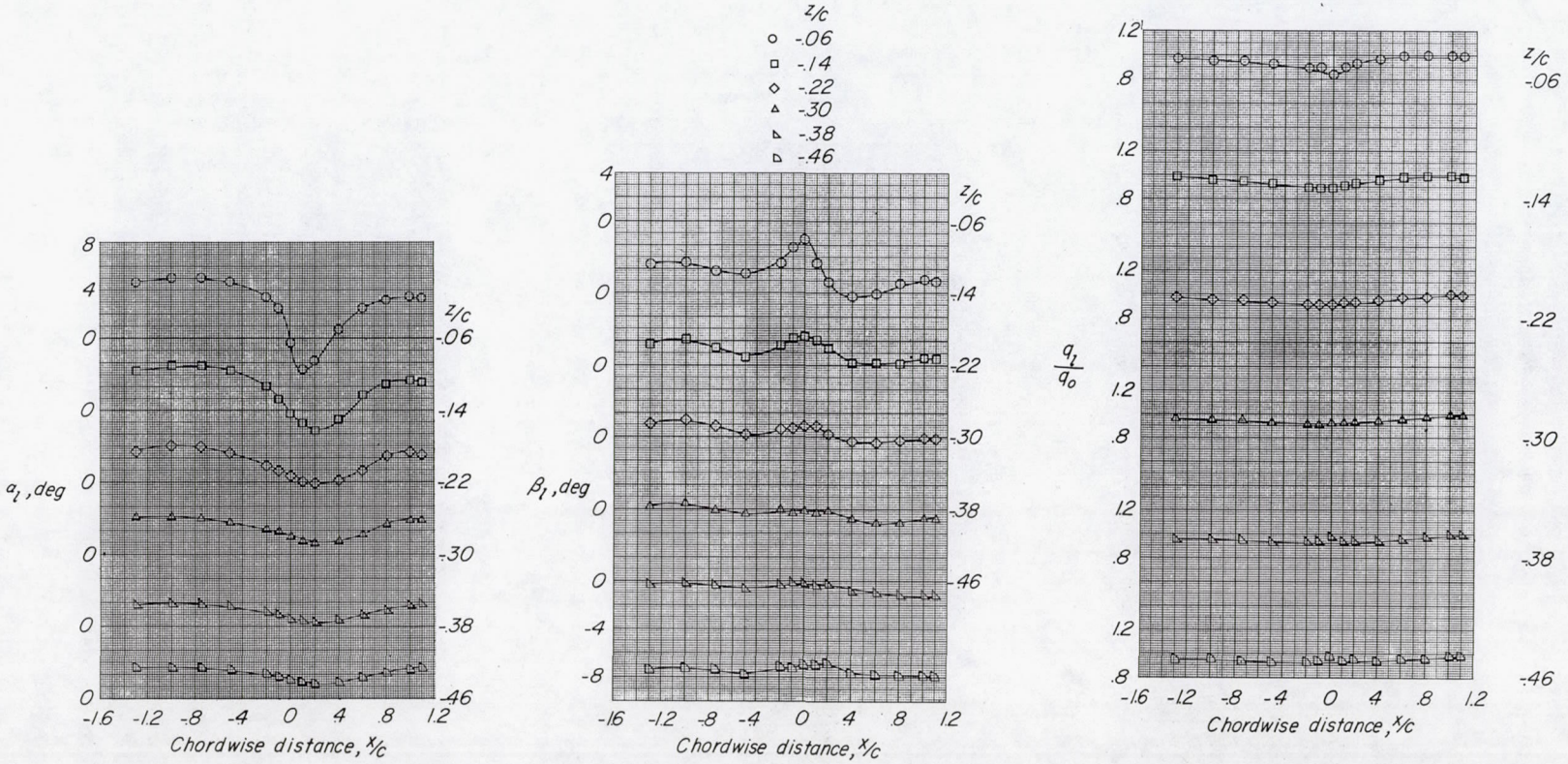

(c) $\alpha = -0.2^\circ$; $\beta = 8^\circ$.

Figure 8.- Continued.



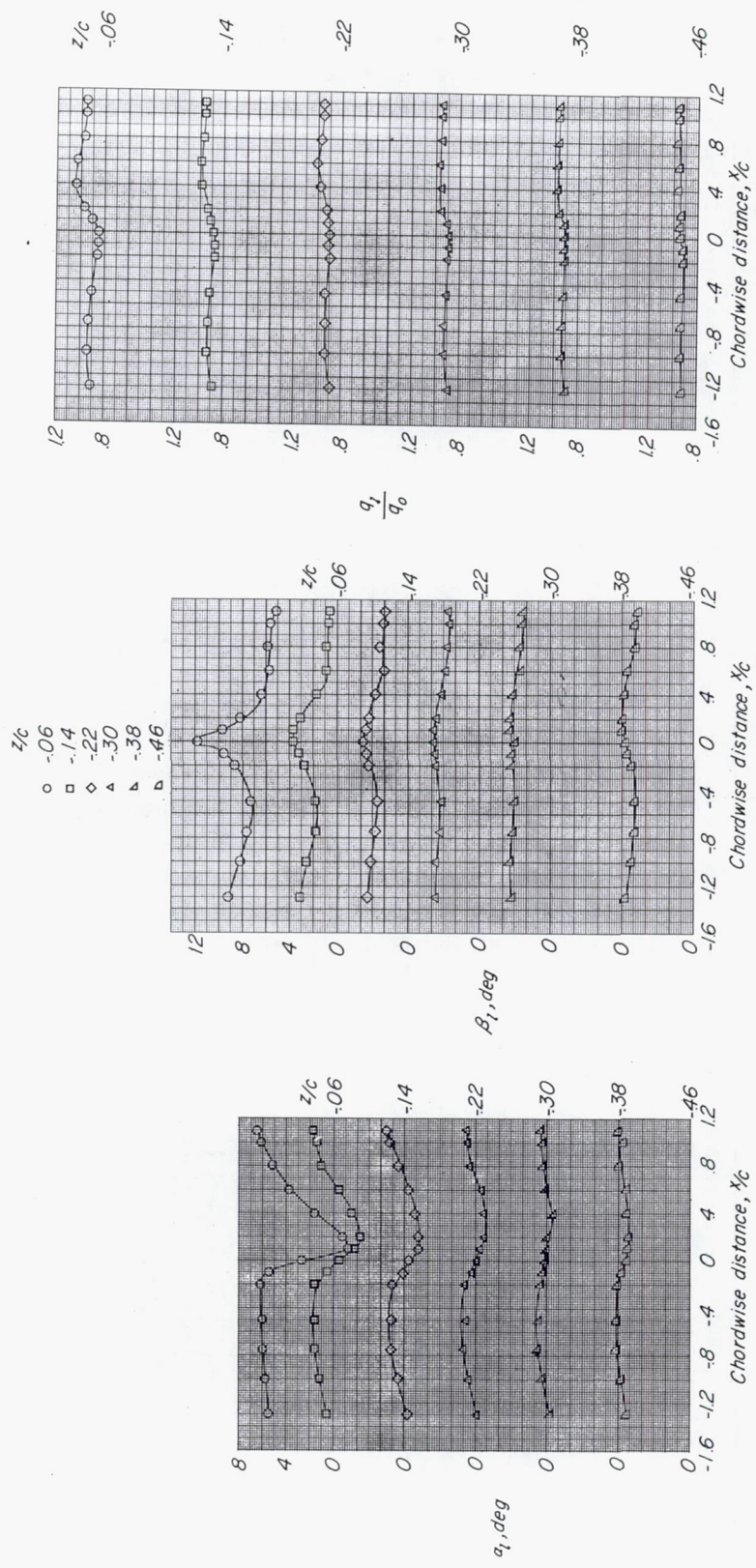

(d) $\alpha = 3.8^{\circ}$; $\beta = 0^{\circ}$.

Figure 8.- Continued.



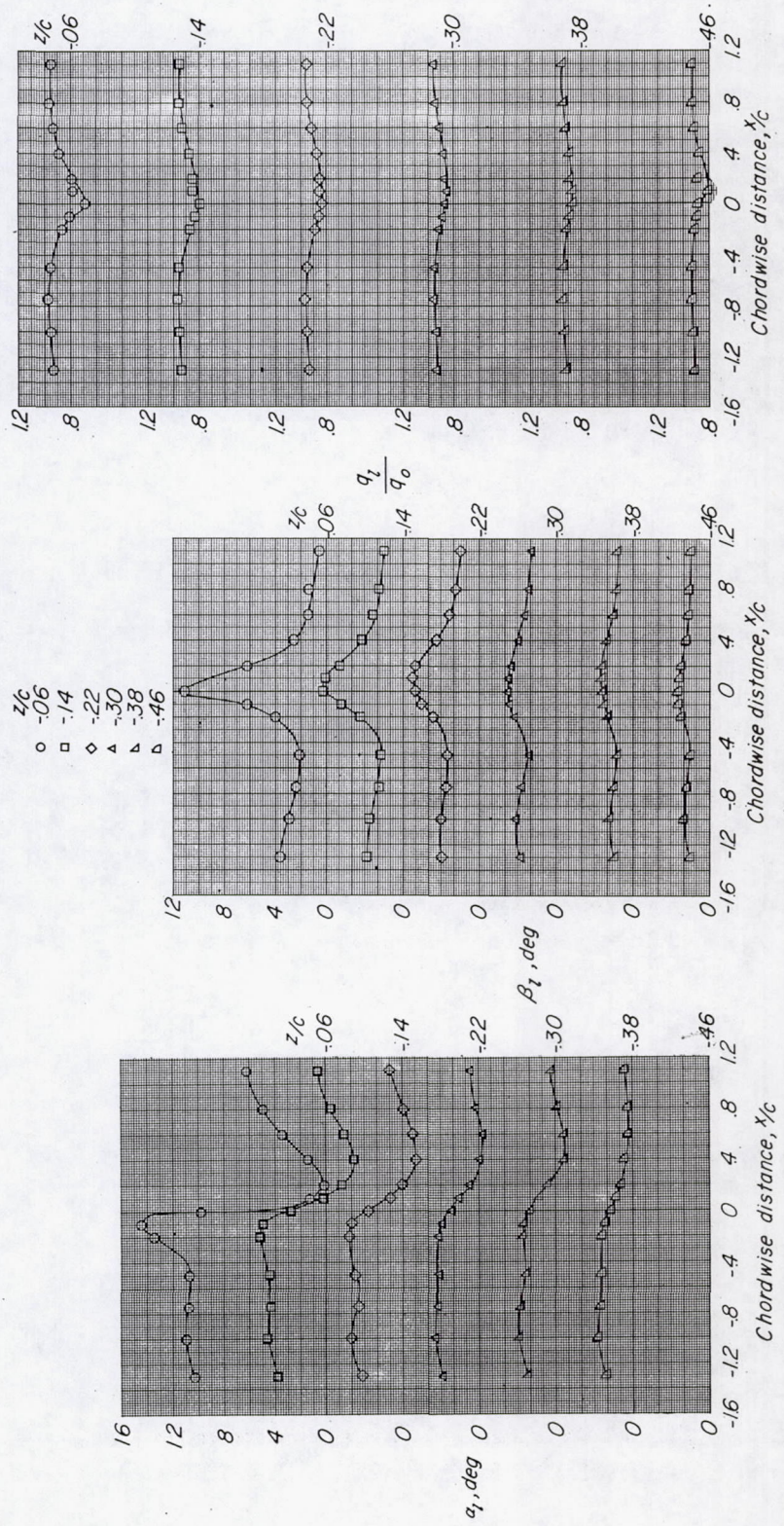

(e) $\alpha = 3.8^\circ$; $\beta = -8^\circ$.

Figure 8.- Continued.



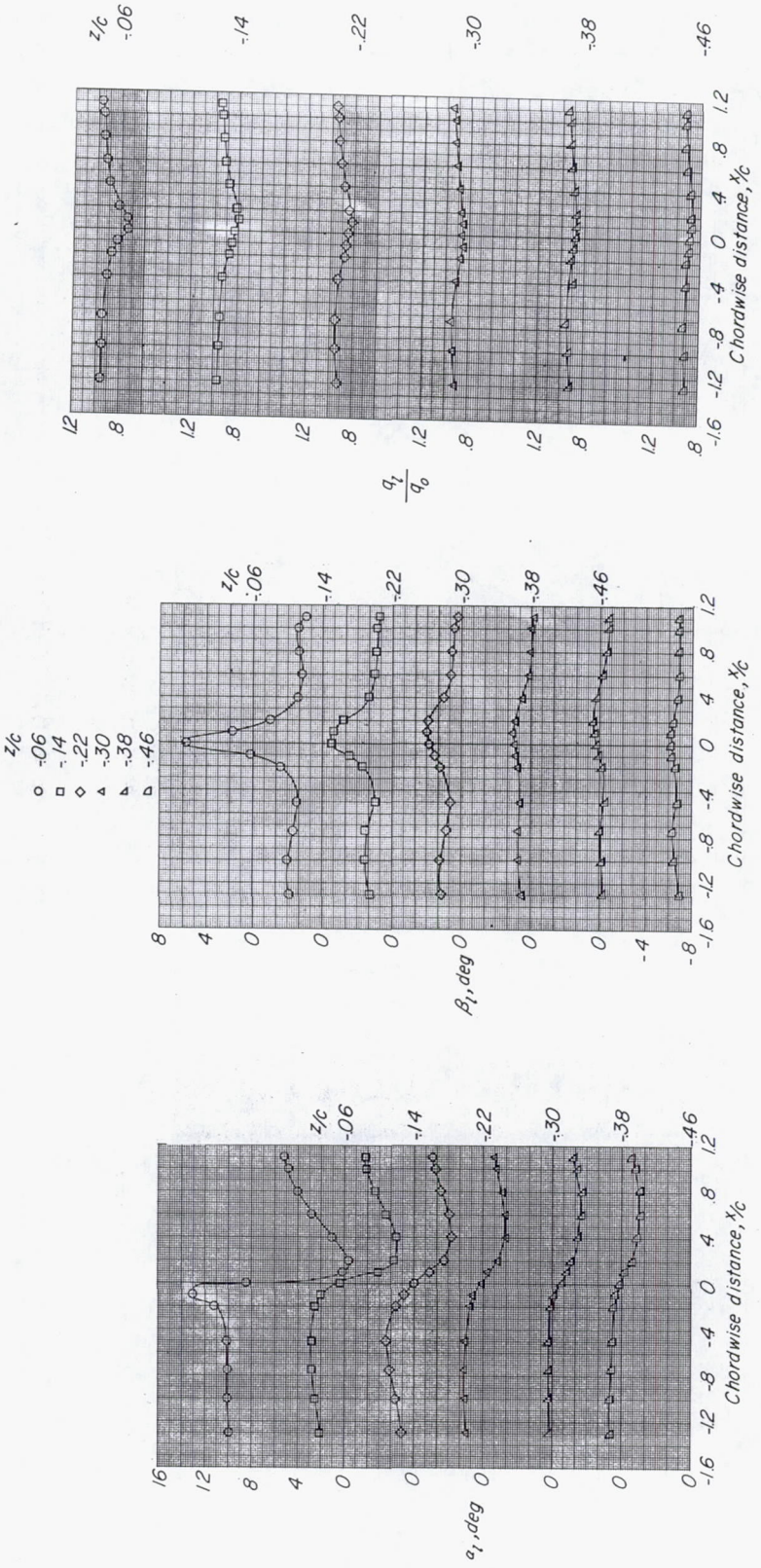

(f) $\alpha = 3.8^{\circ}$; $\beta = 8^{\circ}$.

Figure 8.- Continued.



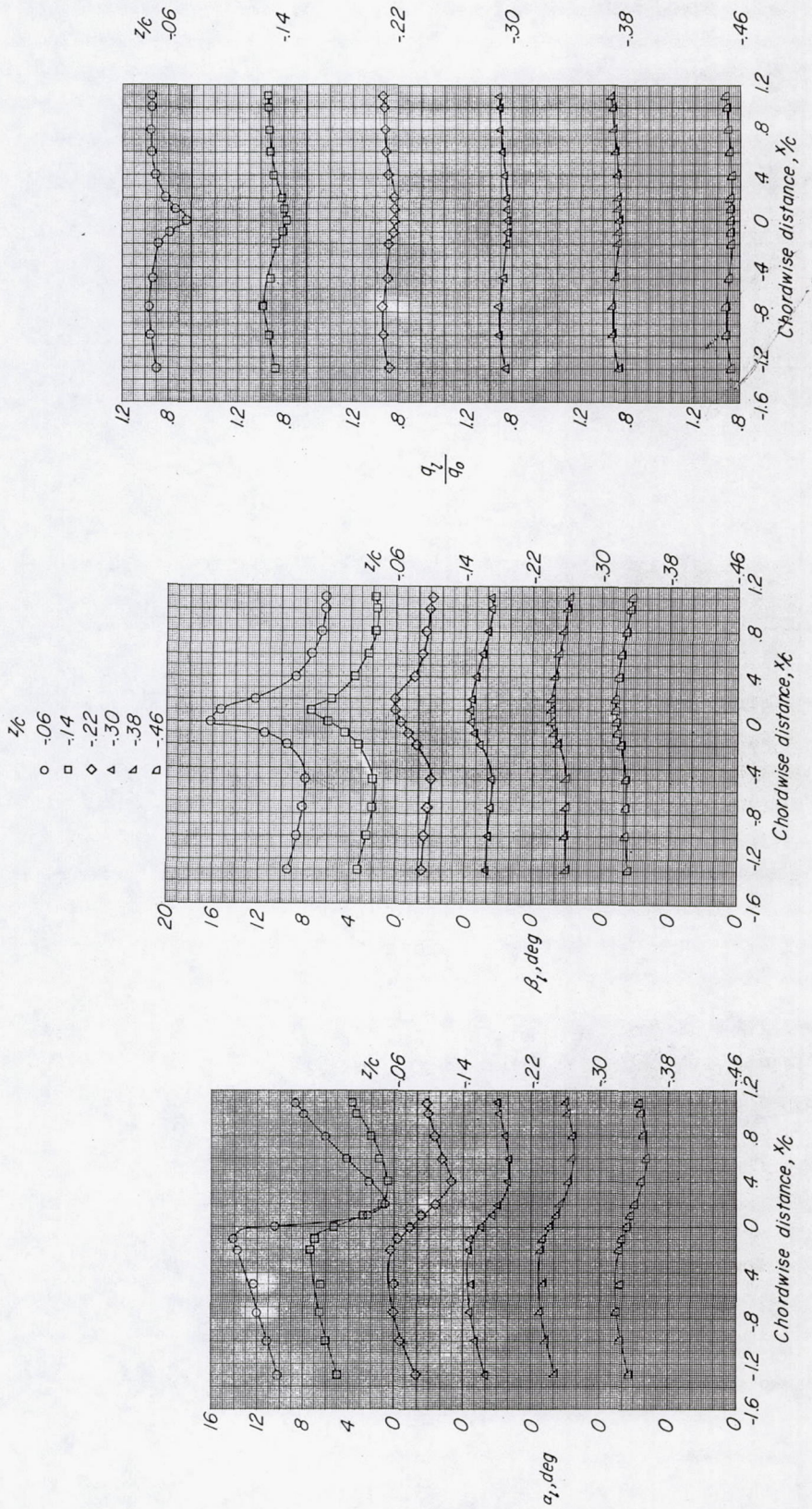

(g) $\alpha = 8.2^{\circ}$; $\beta = 0^{\circ}$.

Figure 8.- Continued.



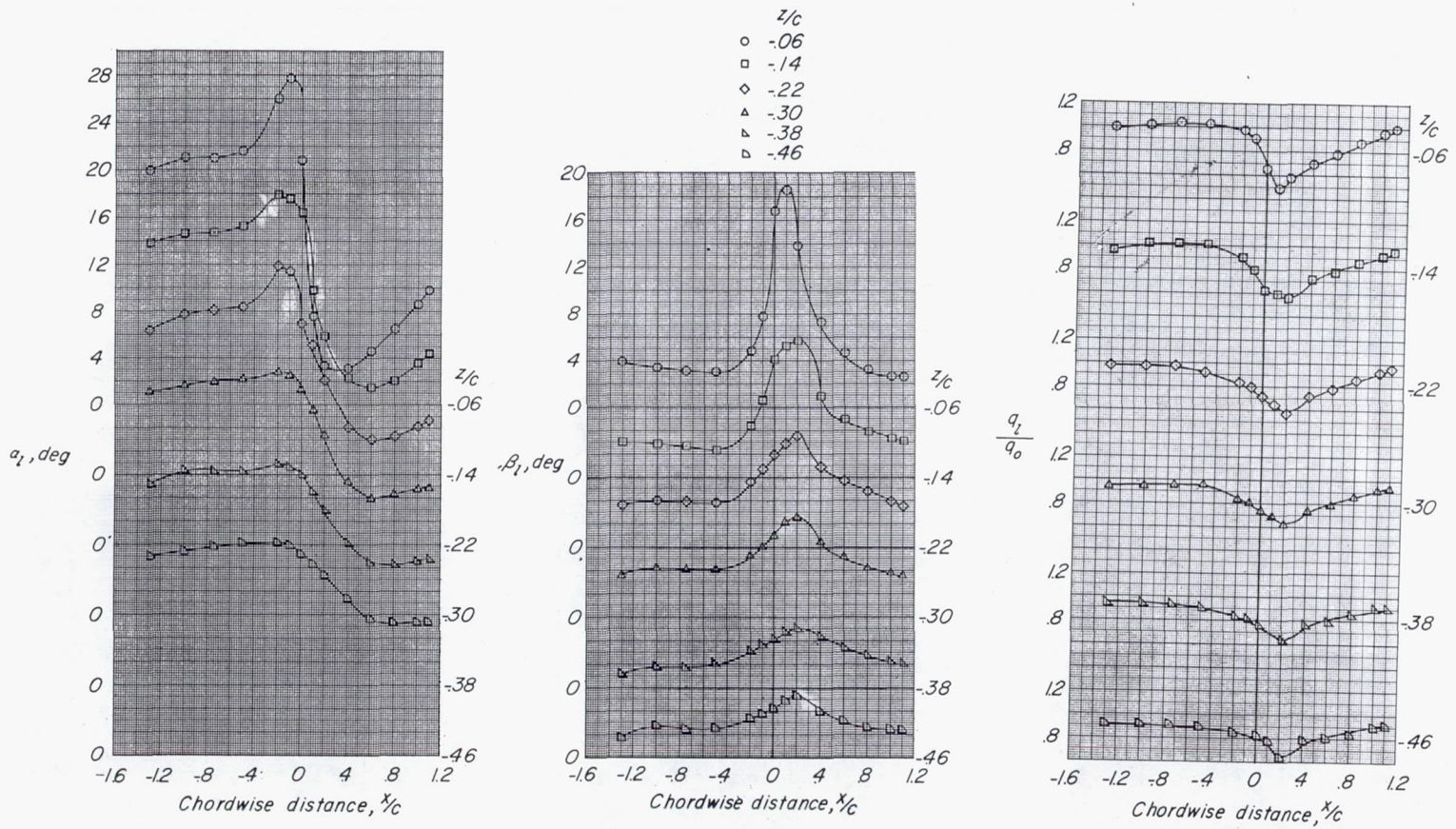

(h) $\alpha = 8.2^{\circ}$; $\beta = -8^{\circ}$.

Figure 8.- Continued.



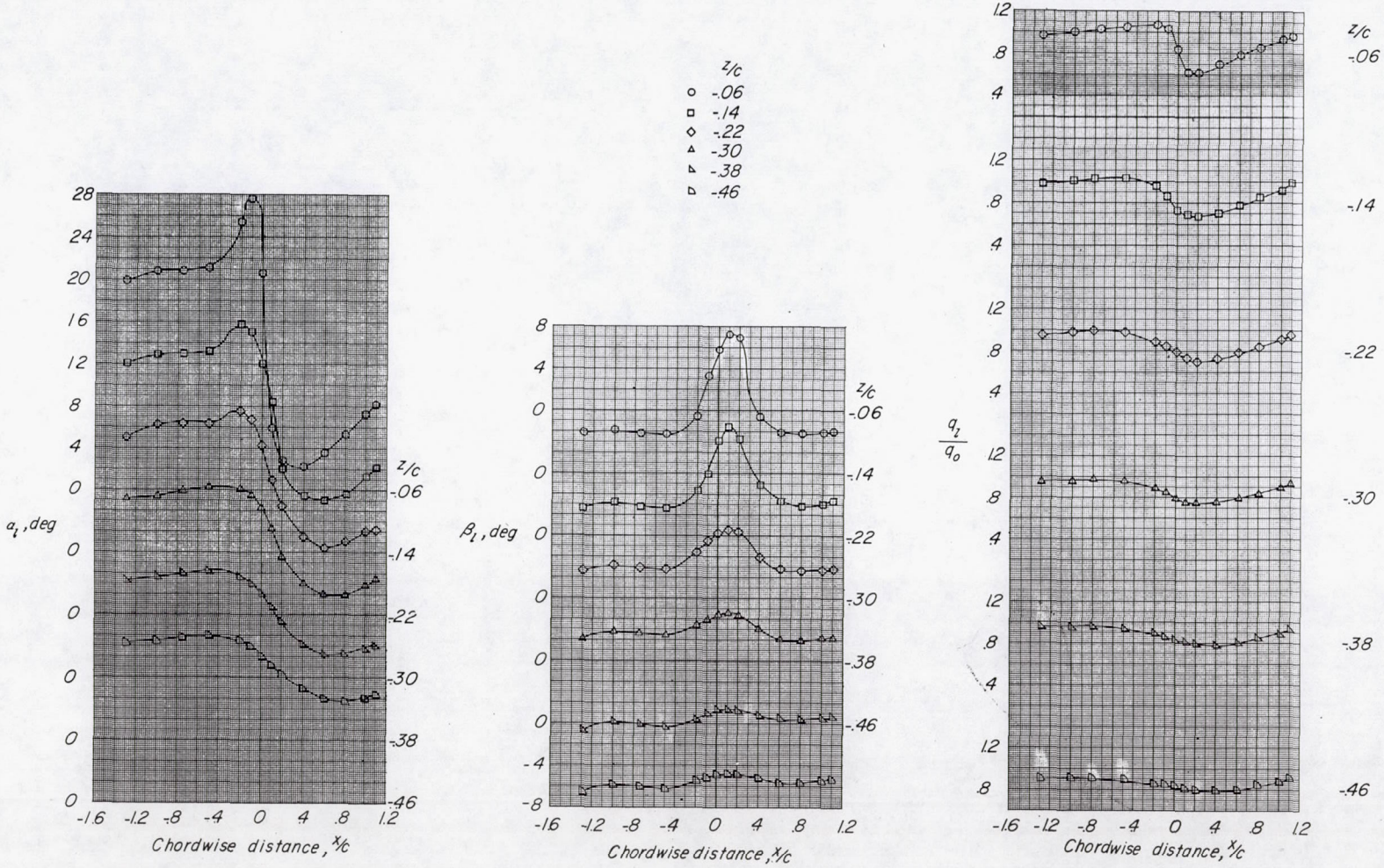

(i) $\alpha = 8.2^{\circ}$; $\beta = 8^{\circ}$.

Figure 8.- Continued.



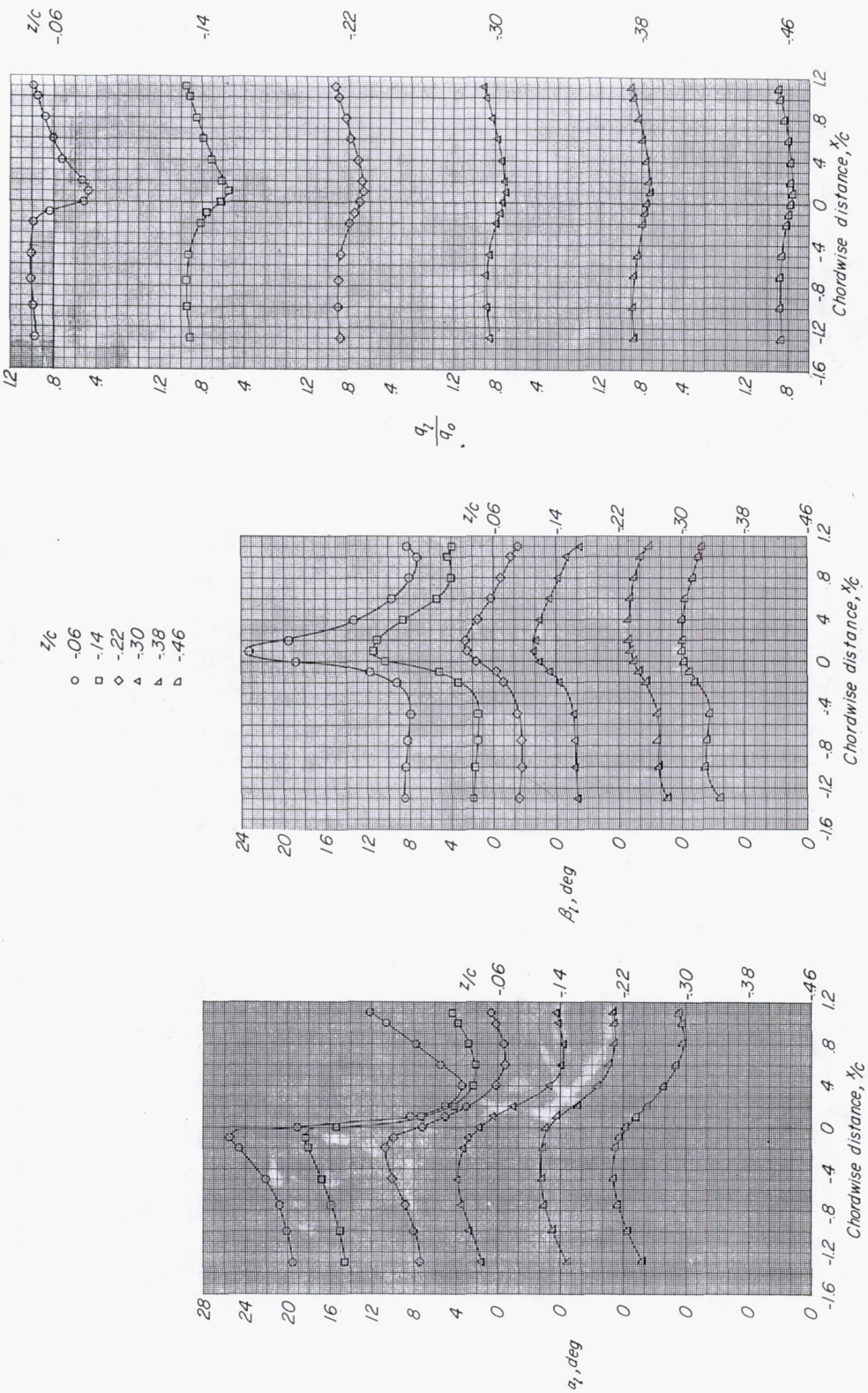

(j) $\alpha = 16.4^{\circ}$; $\beta = 0^{\circ}$.

Figure 8.- Continued.



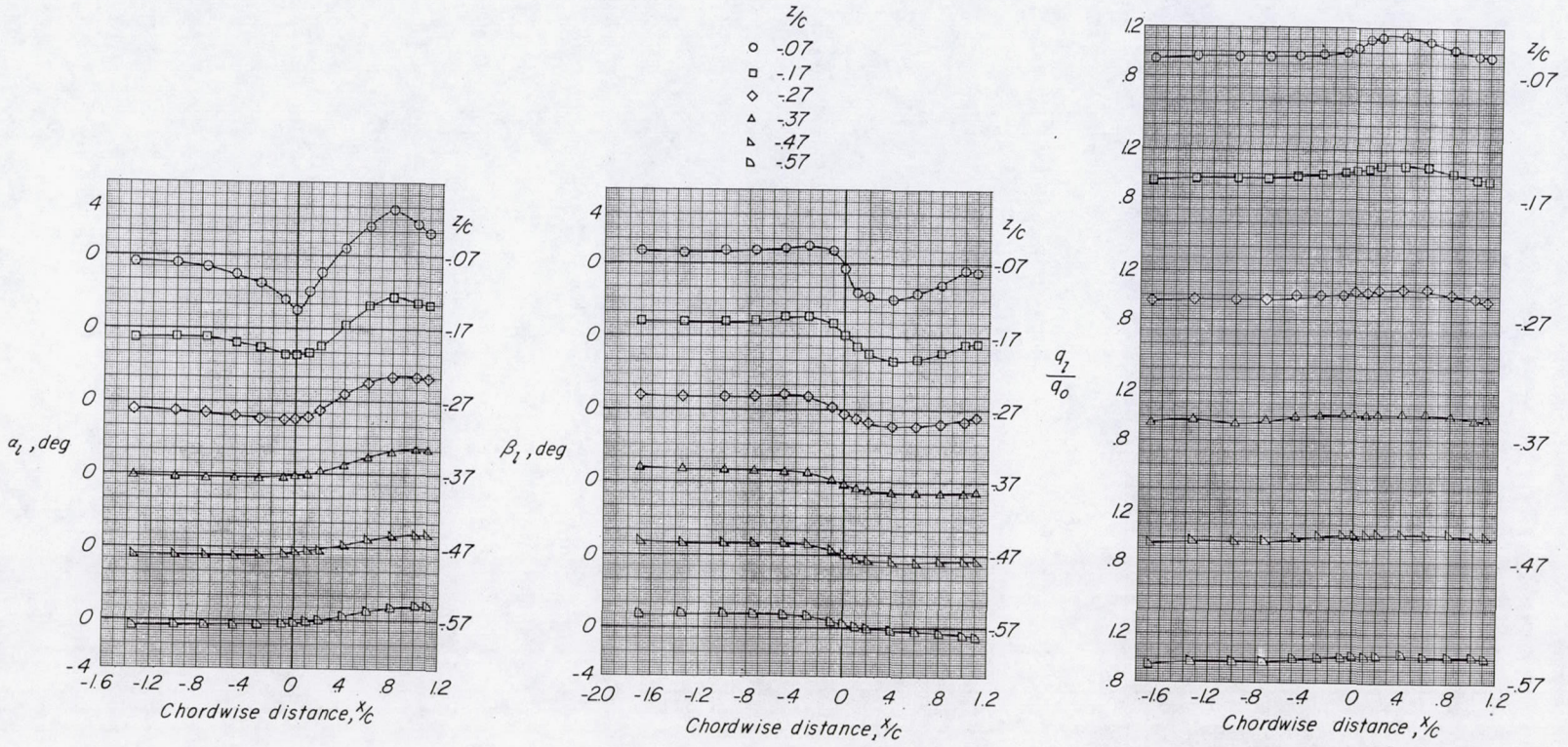

(k) $\alpha = 16.4^\circ$; $\beta = -8^\circ$.

Figure 8.- Continued.



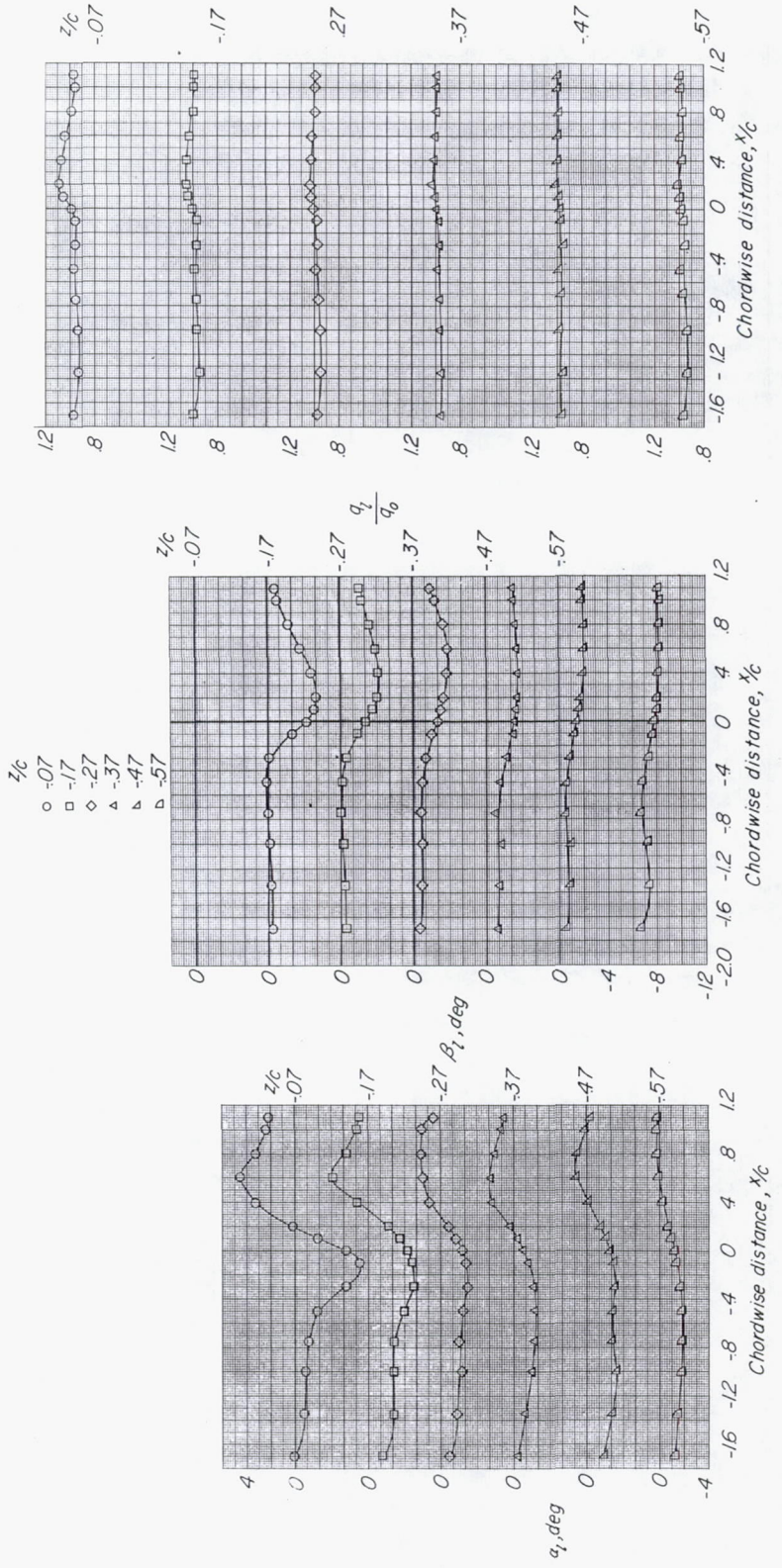

(l) $\alpha = 16.4^{\circ}$; $\beta = 8^{\circ}$.

Figure 8.- Concluded.



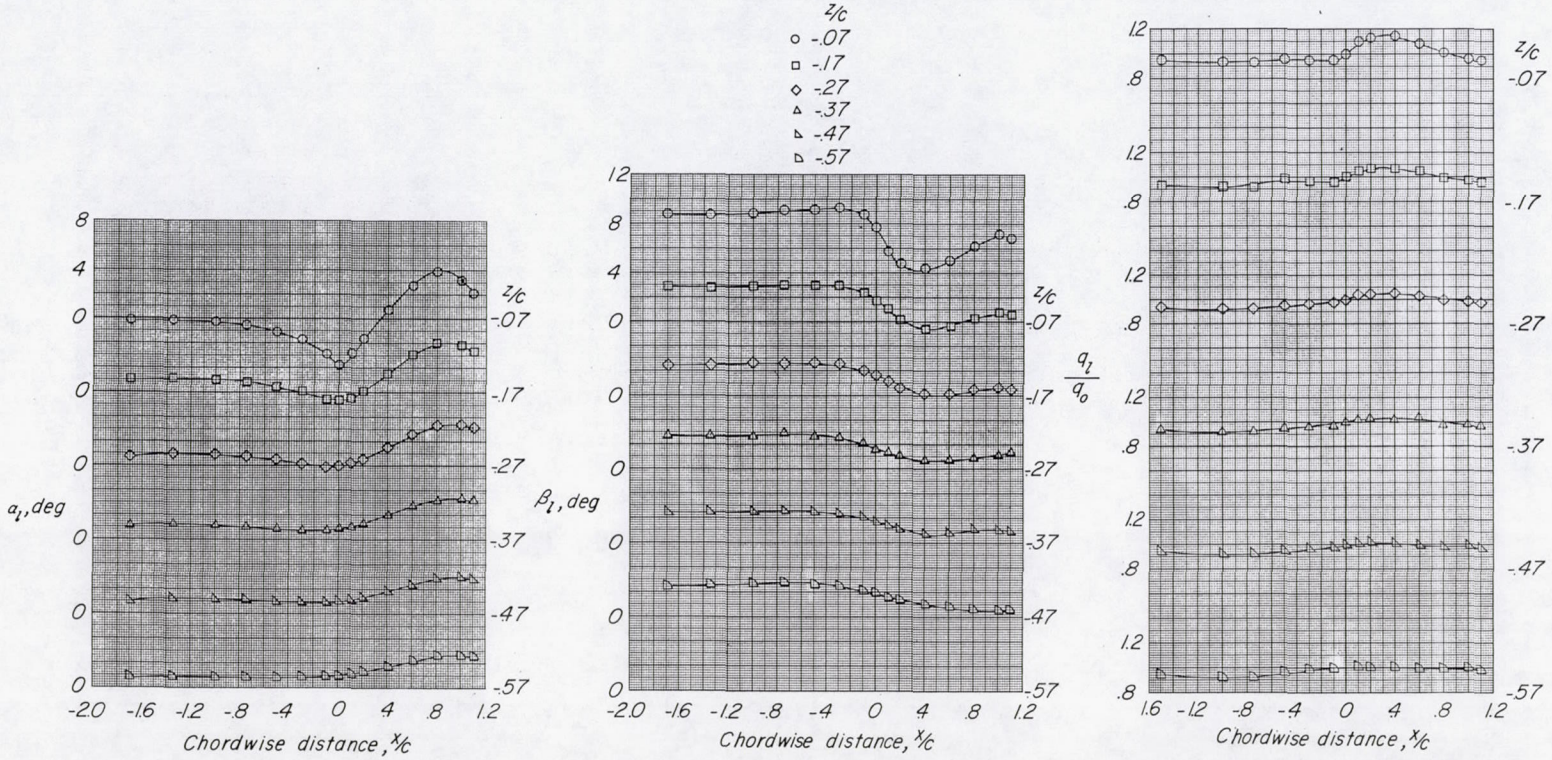

(a) $\alpha = -0.2^\circ$; $\beta = 0^\circ$.

Figure 9.- Flow-field characteristics of swept-wing—fuselage combination at $y/\frac{b}{2} = -0.50$.



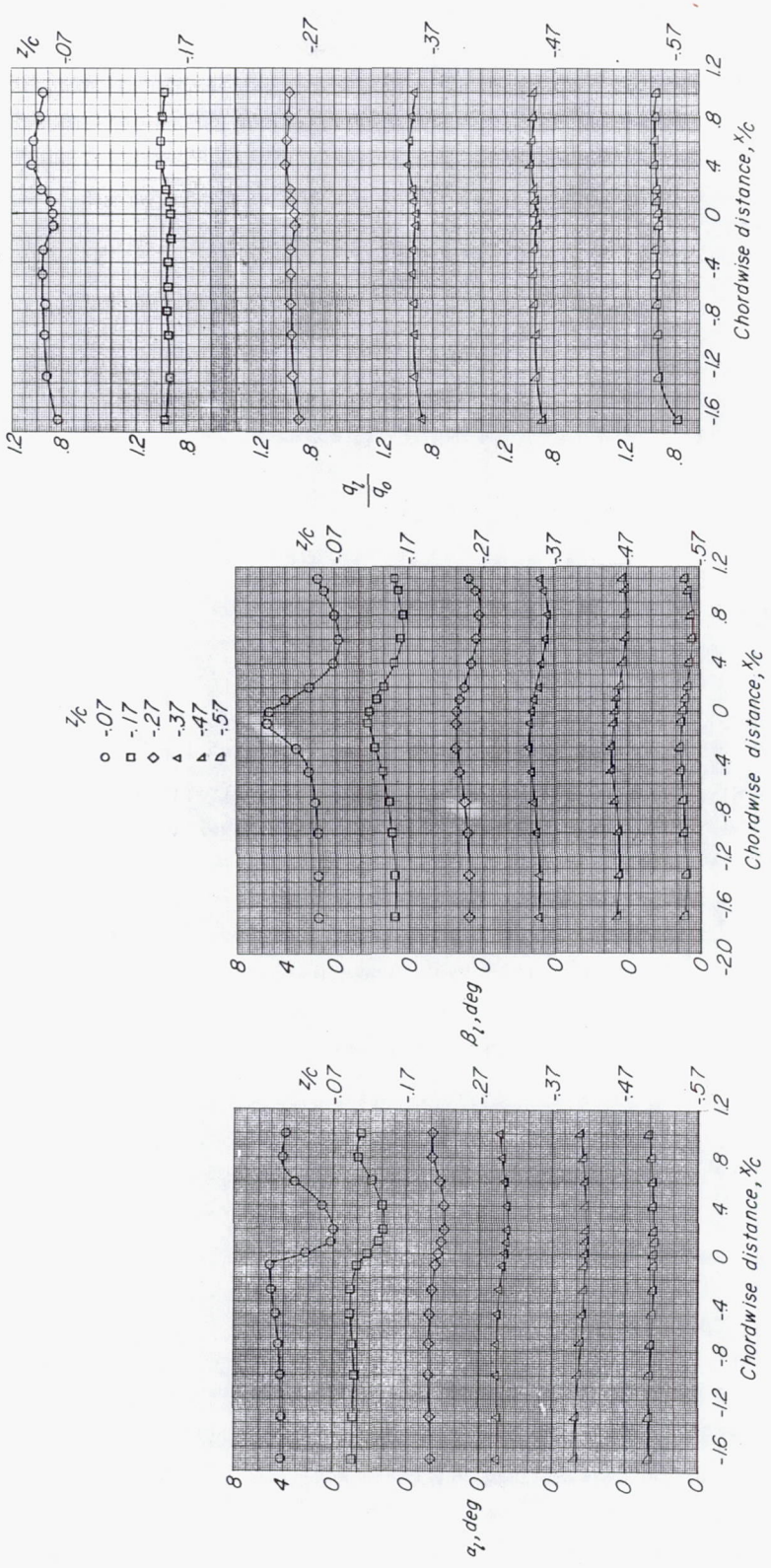

(b) $\alpha = -0.2^{\circ}$; $\beta = -8^{\circ}$.

Figure 9.- Continued.



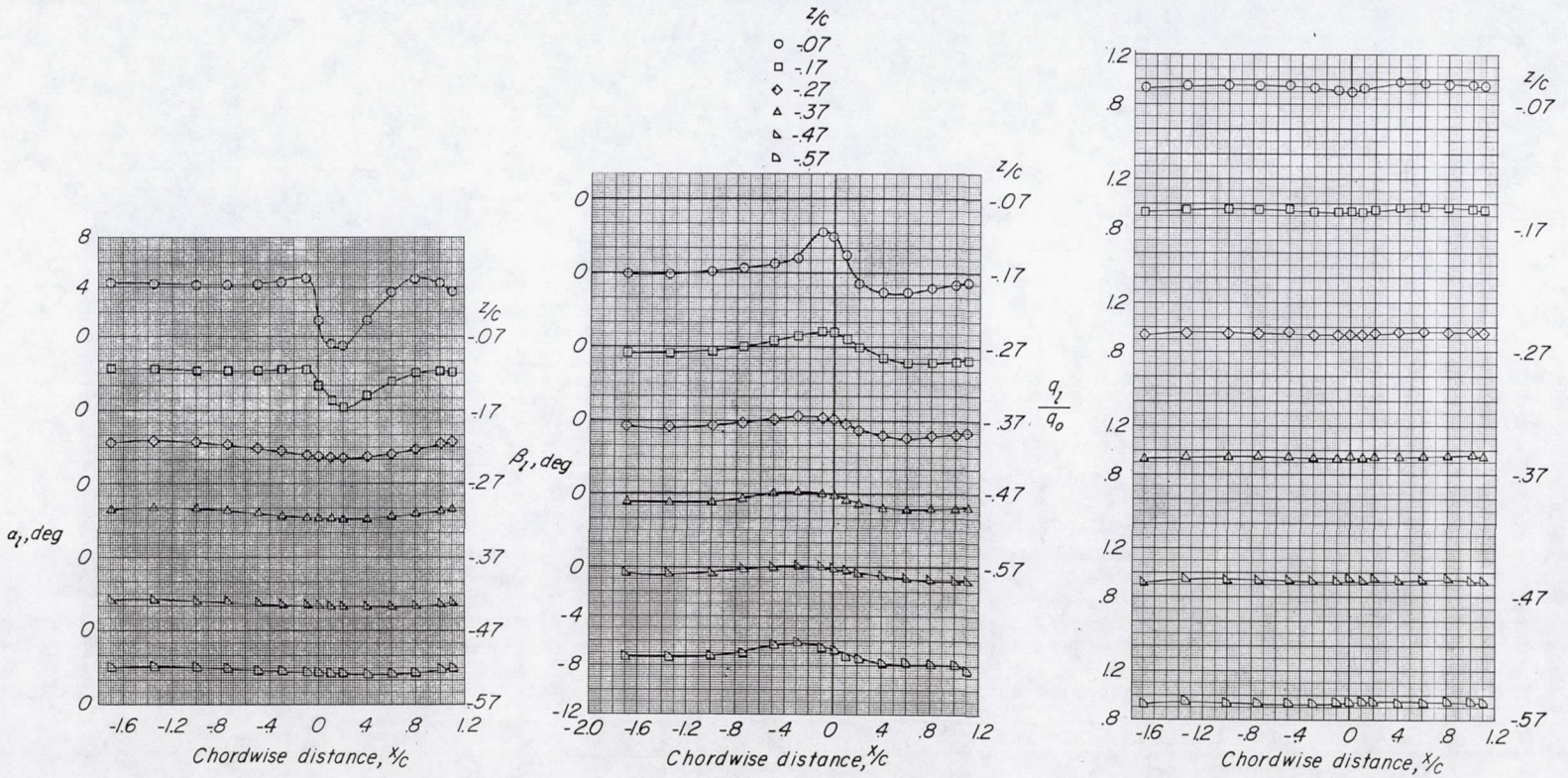

(c) $\alpha = -0.2^{\circ}$; $\beta = 8^{\circ}$.

Figure 9.- Continued.



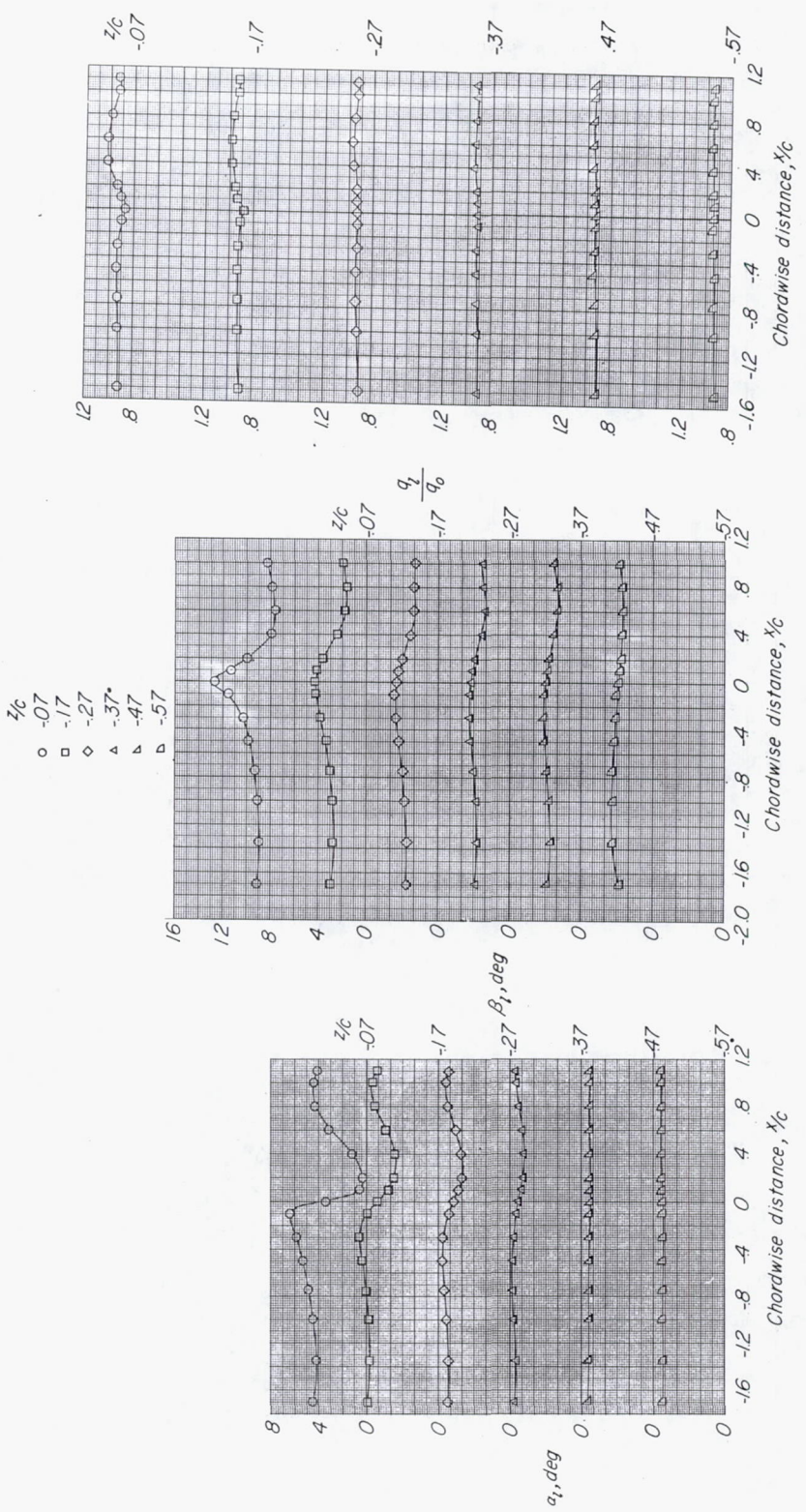

(d) $\alpha = 3.8^{\circ}$; $\beta = 0^{\circ}$.

Figure 9.- Continued.



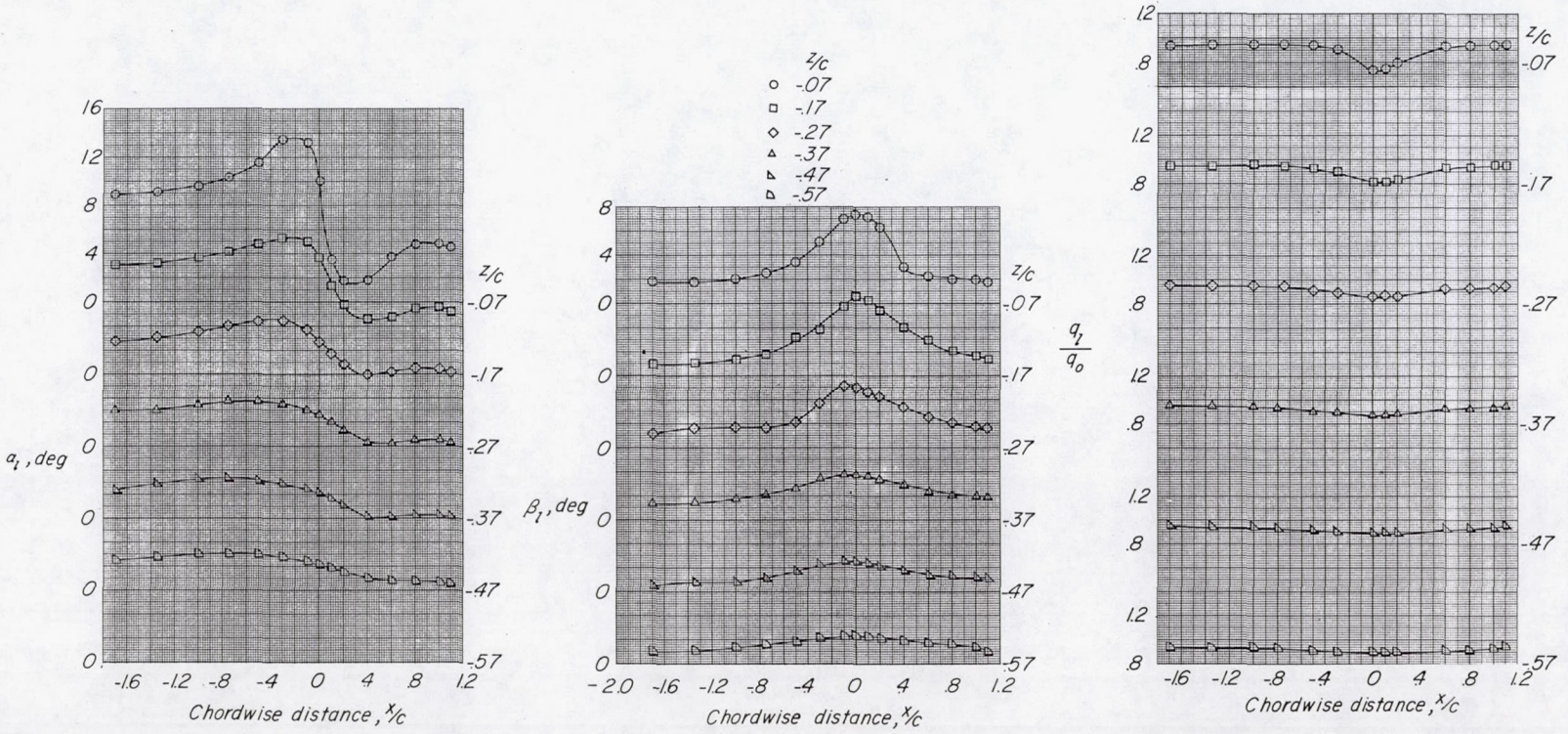

(e) $\alpha = 3.8^{\circ}$; $\beta = -8^{\circ}$.

Figure 9.- Continued.



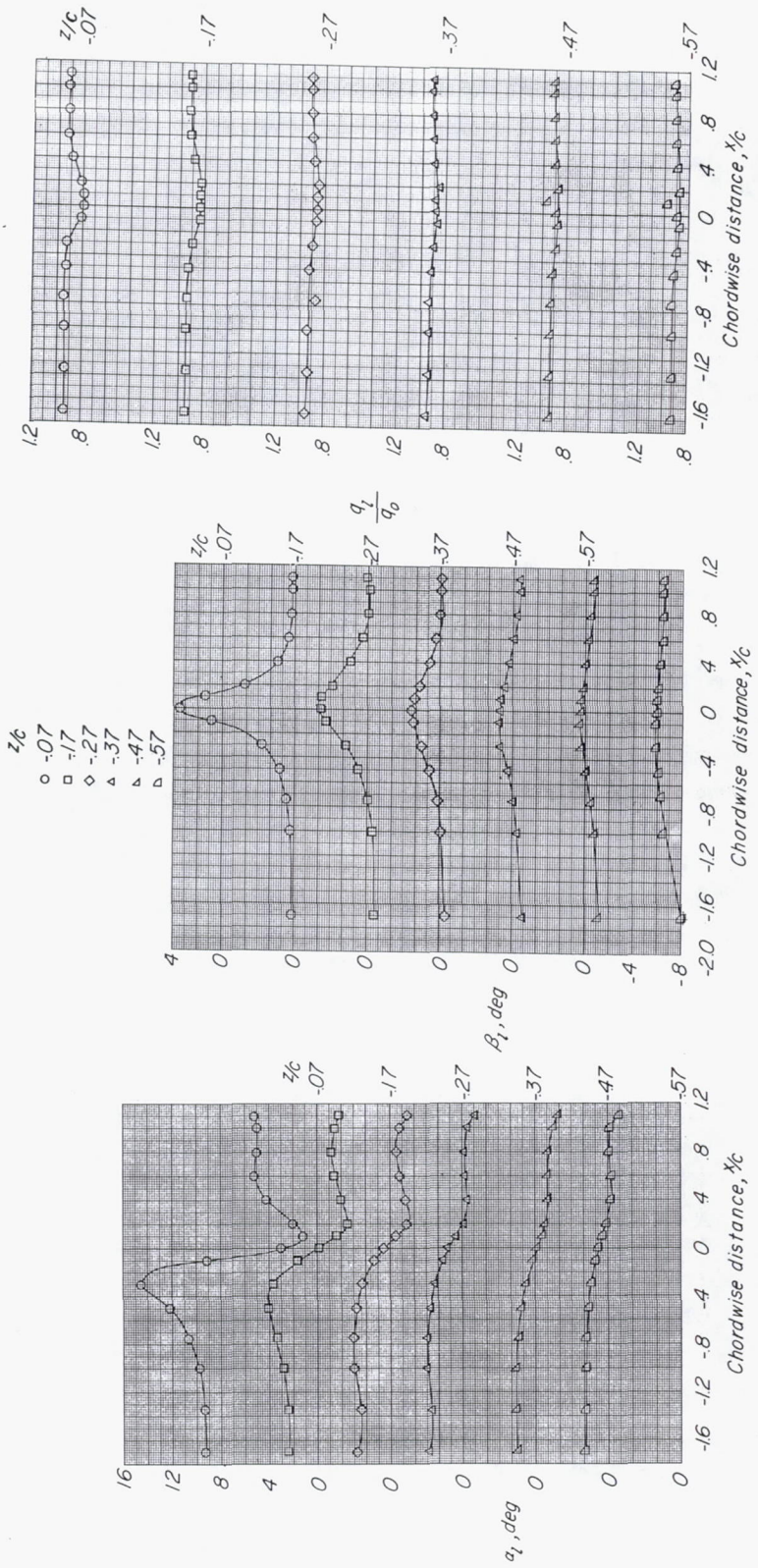

(f) $\alpha = 3.8^{\circ}$; $\beta = 8^{\circ}$.

Figure 9.- Continued.



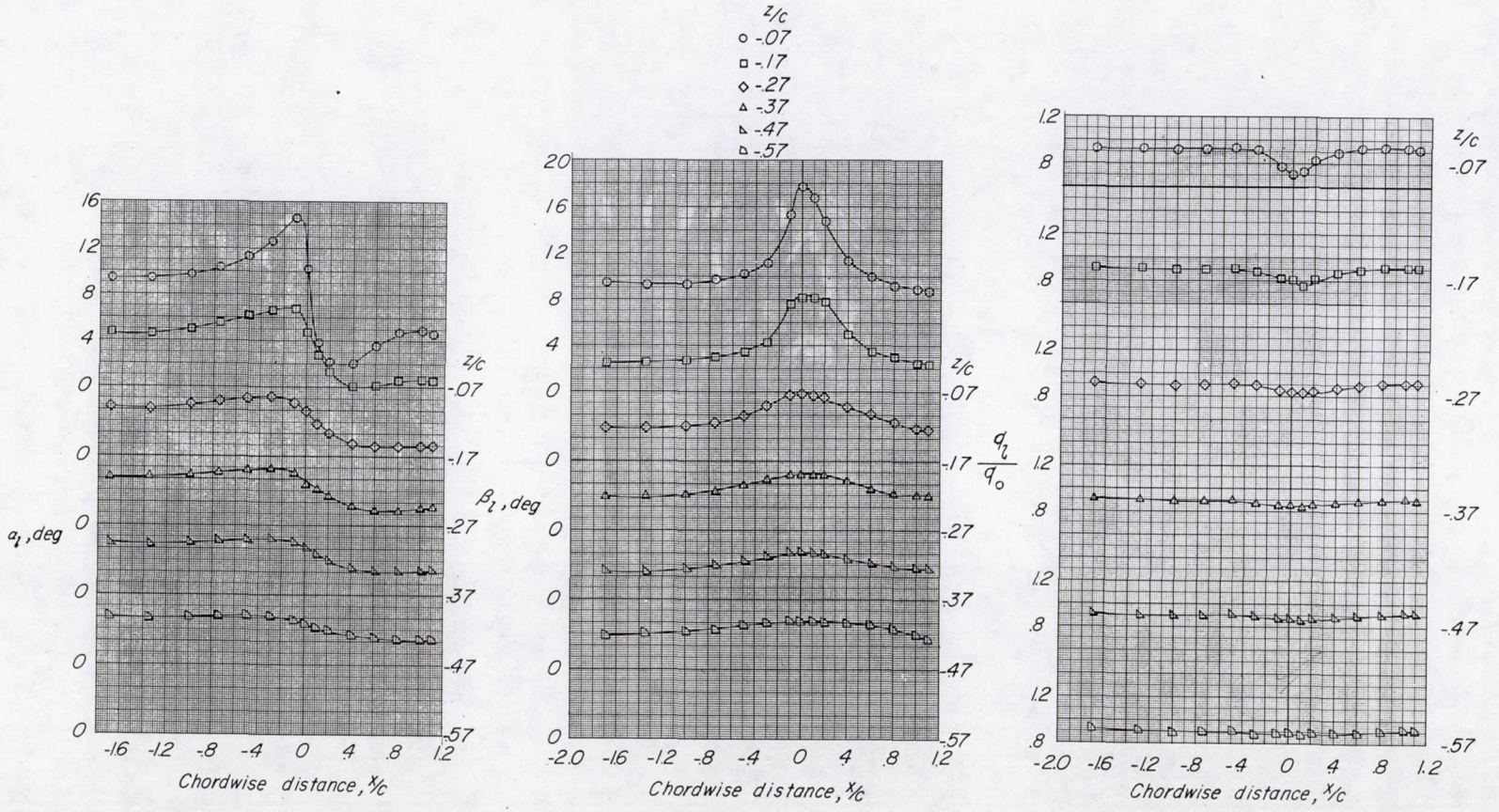

(g) $\alpha = 8.2^{\circ}$; $\beta = 0^{\circ}$.

Figure 9.- Continued.



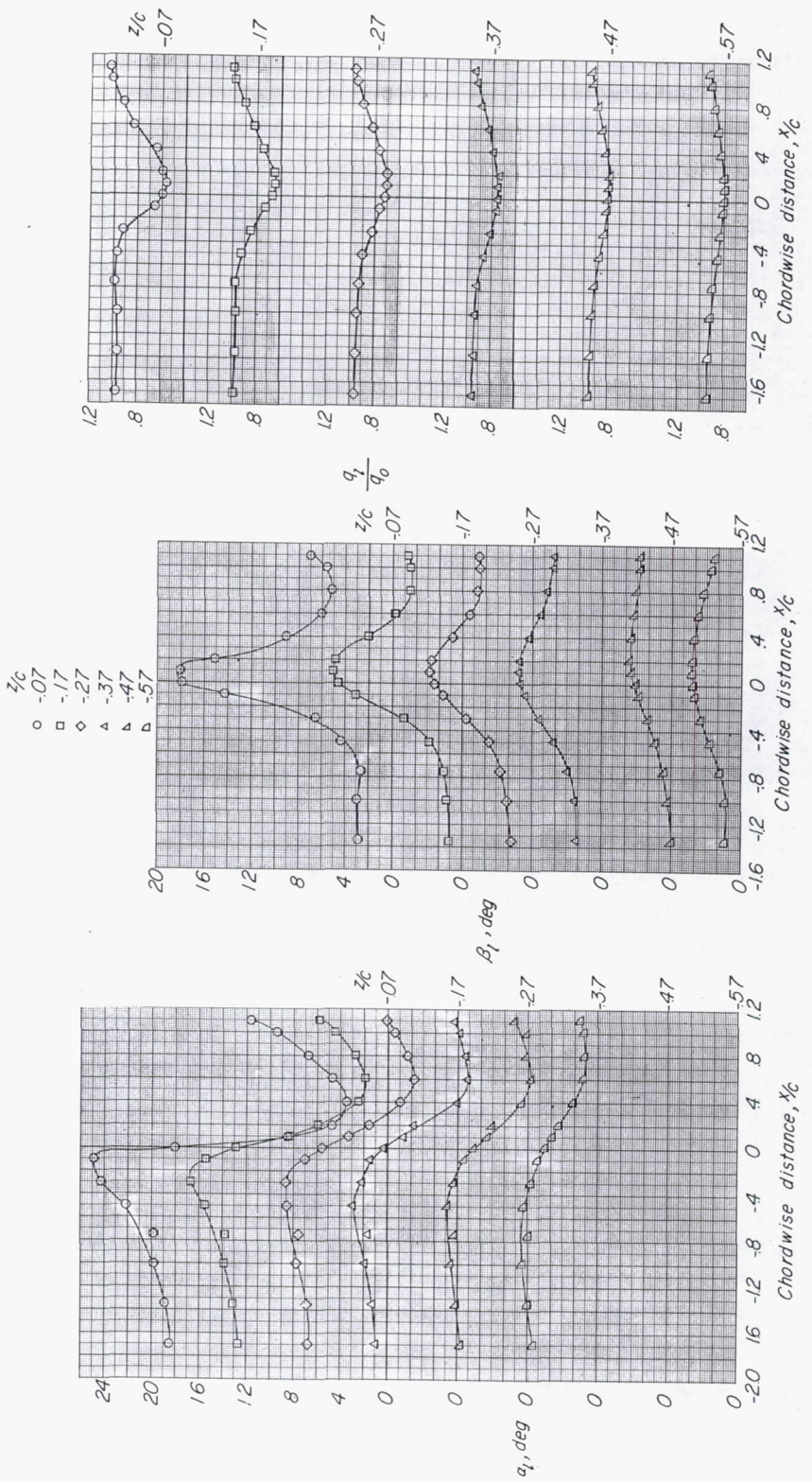

(h) $\alpha = 8.2^{\circ}$; $\beta = -8^{\circ}$.

Figure 9.- Continued.



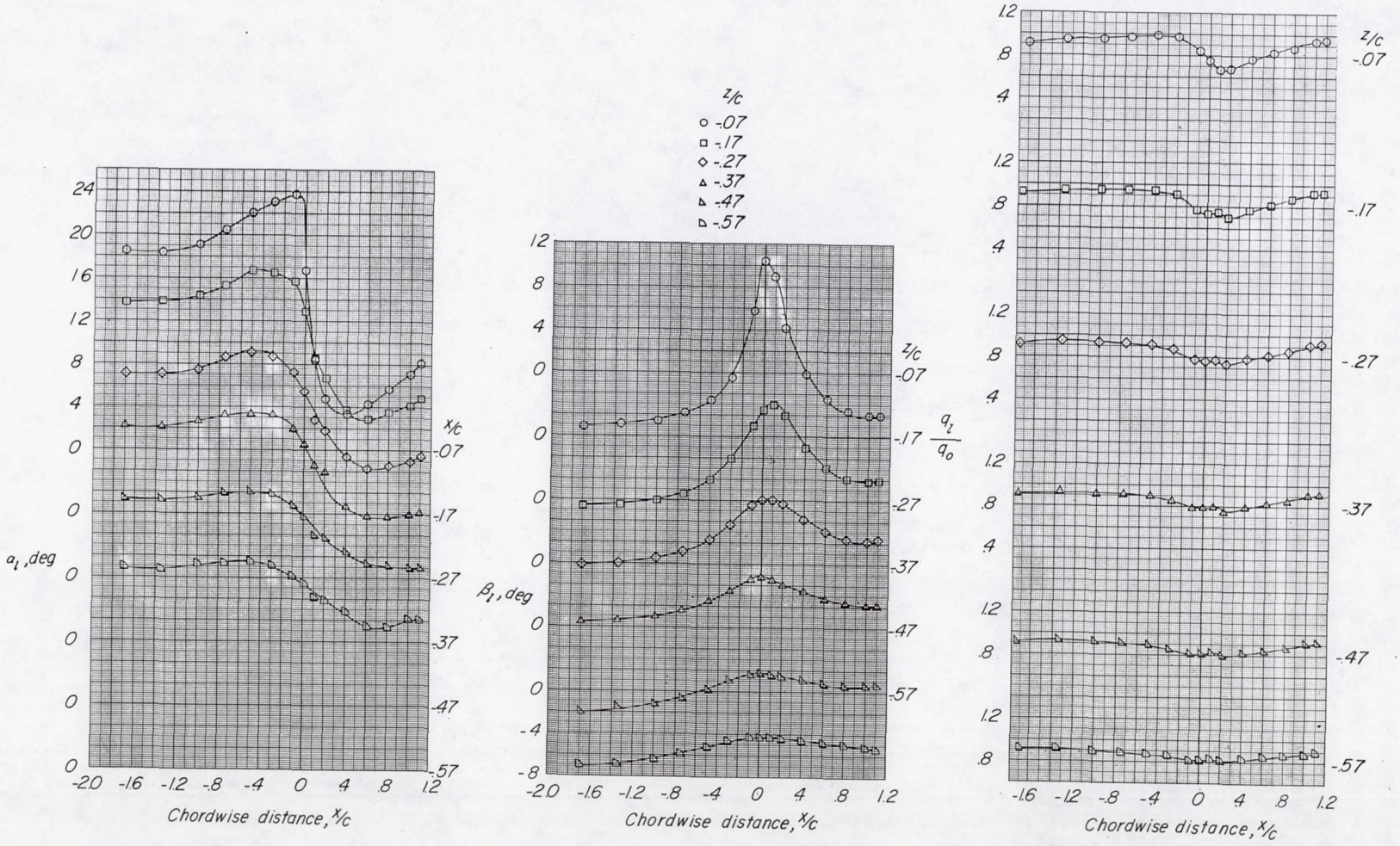

(i) $\alpha = 8.2^{\circ}$; $\beta = 8^{\circ}$.

Figure 9.- Continued.



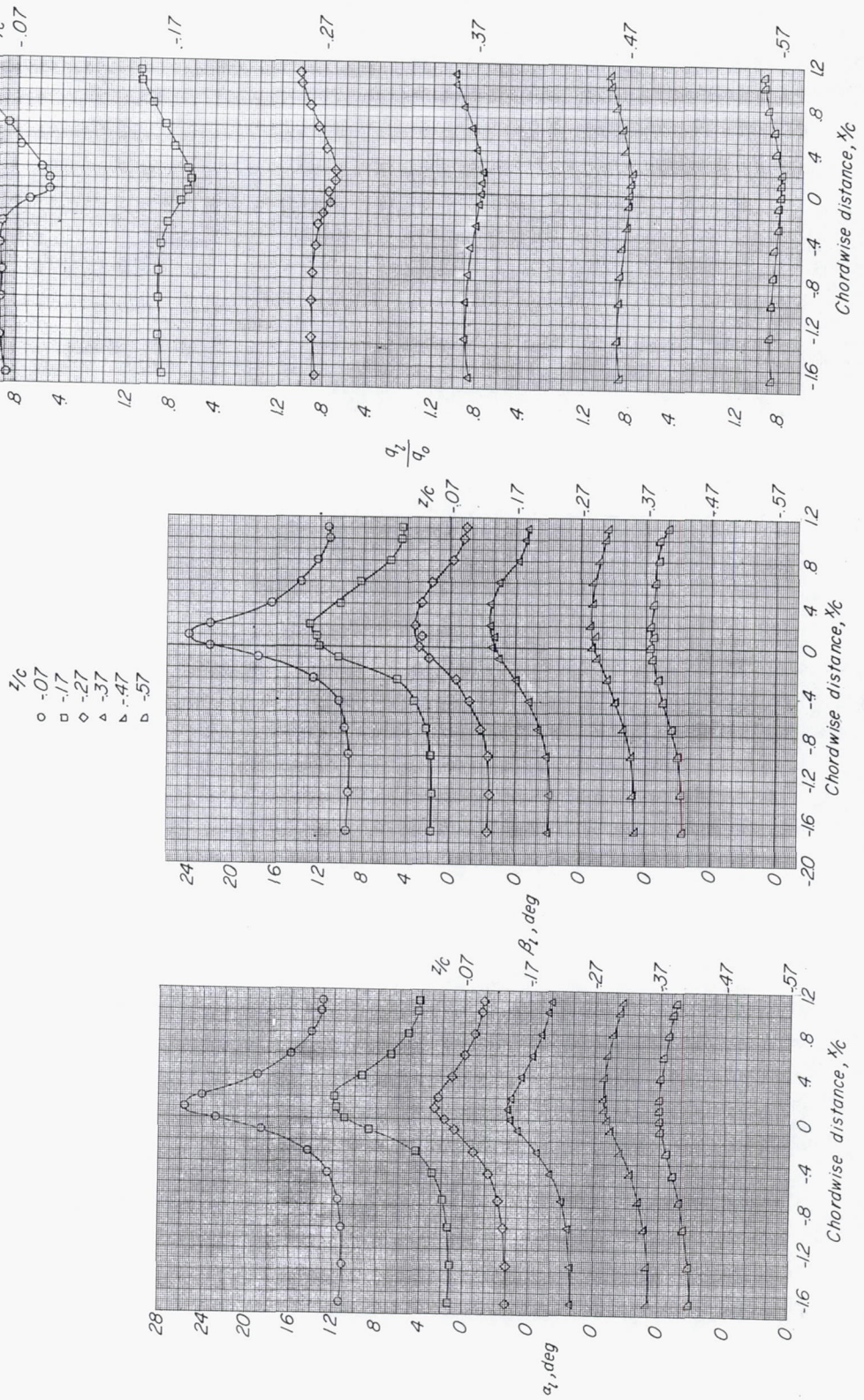

(j) $\alpha = 16.4^{\circ}$; $\beta = 0^{\circ}$.

Figure 9.- Continued.



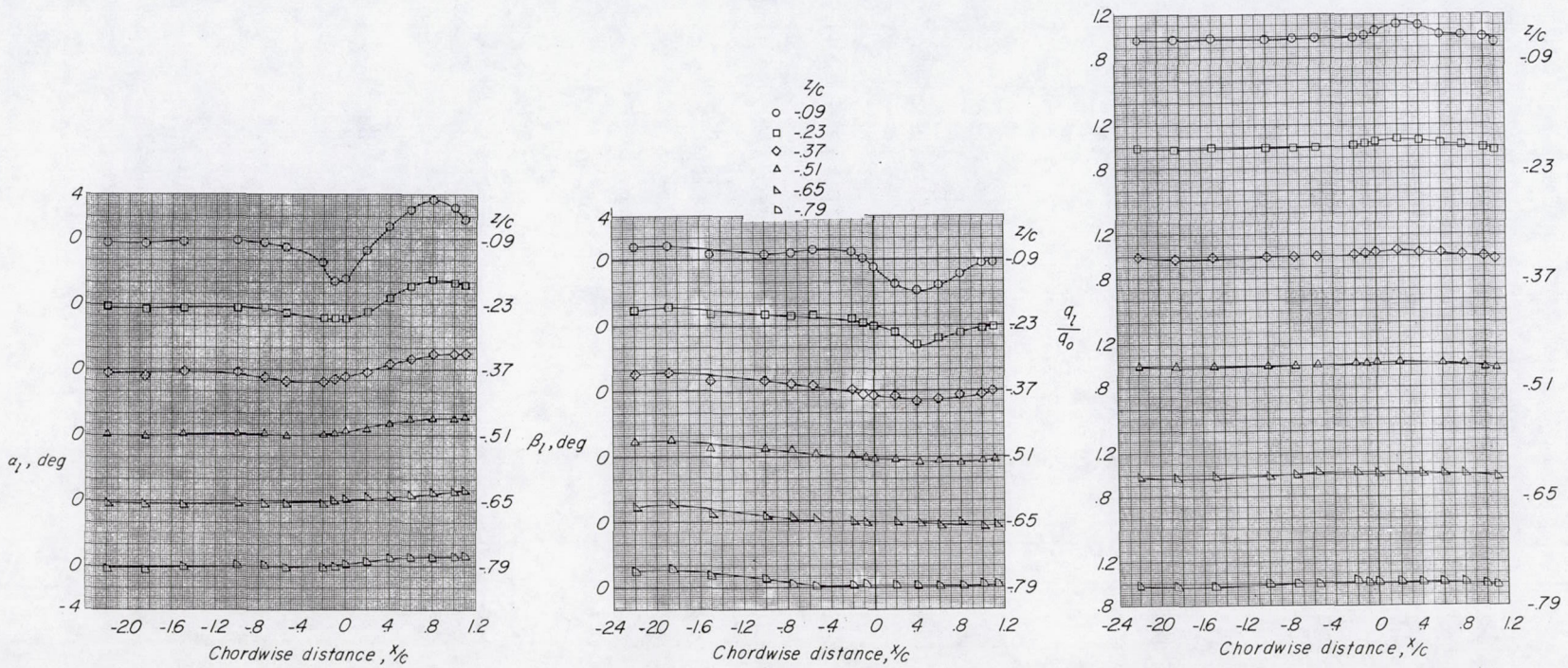

(k) $\alpha = 16.4^\circ$; $\beta = -8^\circ$.

Figure 9.- Continued.



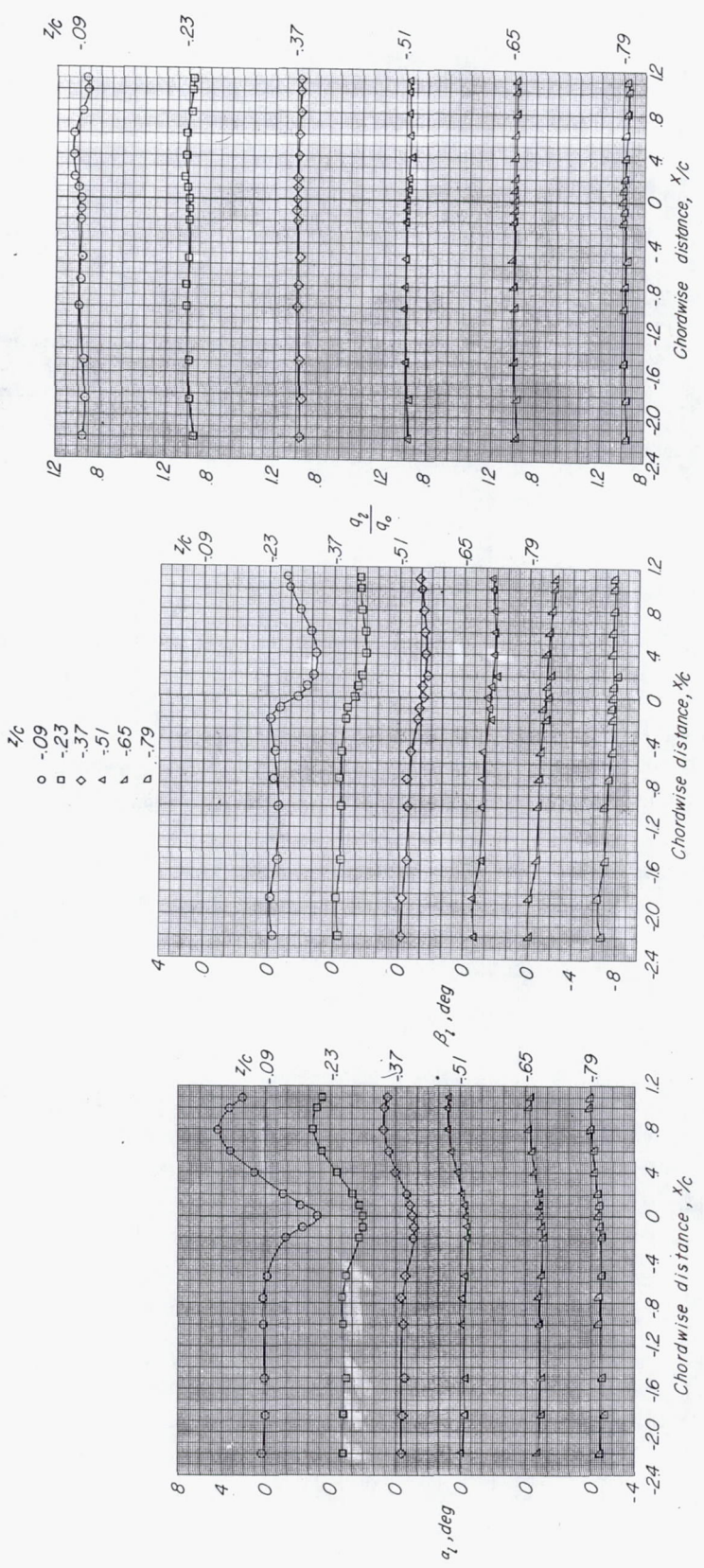

(l) $\alpha = 16.4°$; $\beta = 8°$.

Figure 9.- Concluded.



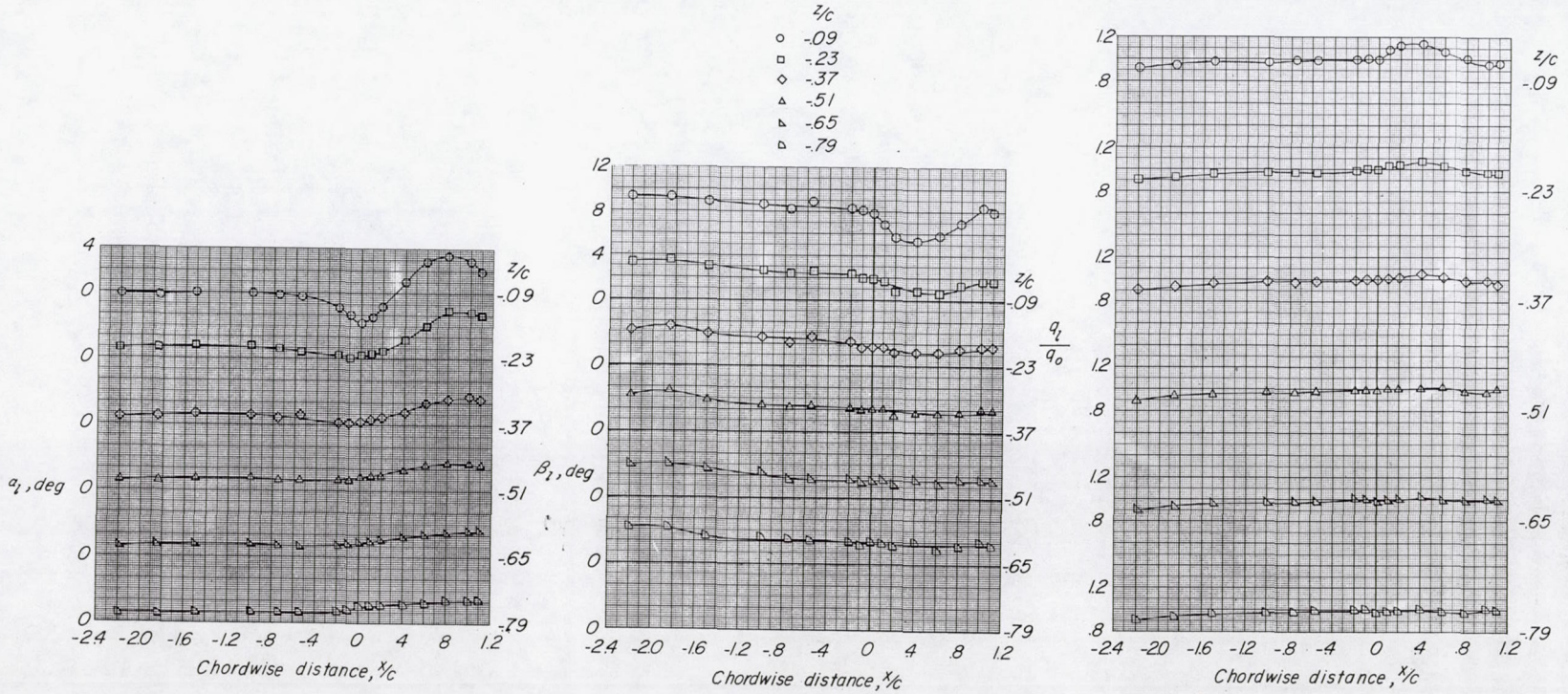

(a) $\alpha = -0.2^{\circ}$; $\beta = 0^{\circ}$.

Figure 10.- Flow-field characteristics of the swept-wing—fuselage combination at $y/\frac{b}{2} = -0.75$.




(b) $\alpha = -0.2^{\circ}$; $\beta = -8^{\circ}$.

Figure 10.- Continued.

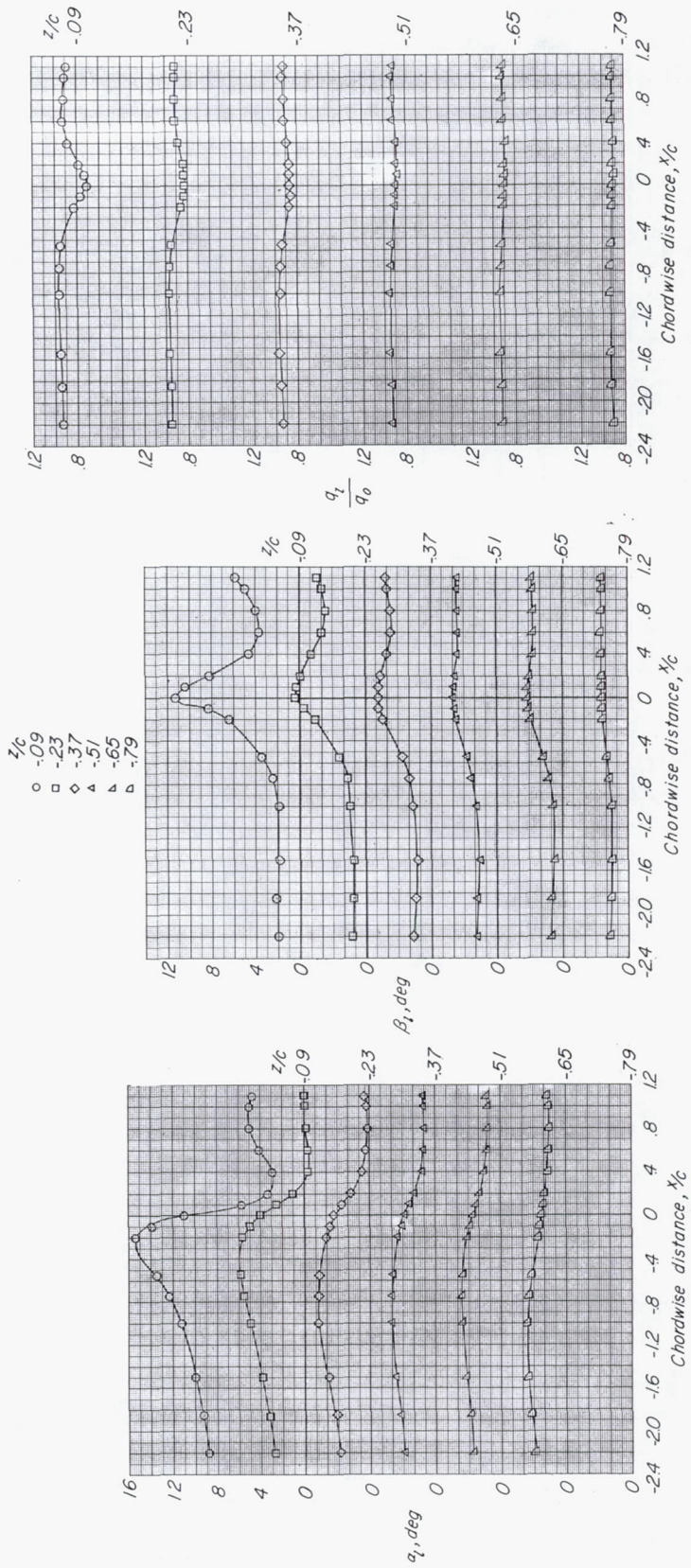



(c) $\alpha = -0.2^{\circ}$; $\beta = 8^{\circ}$.

Figure 10.- Continued.

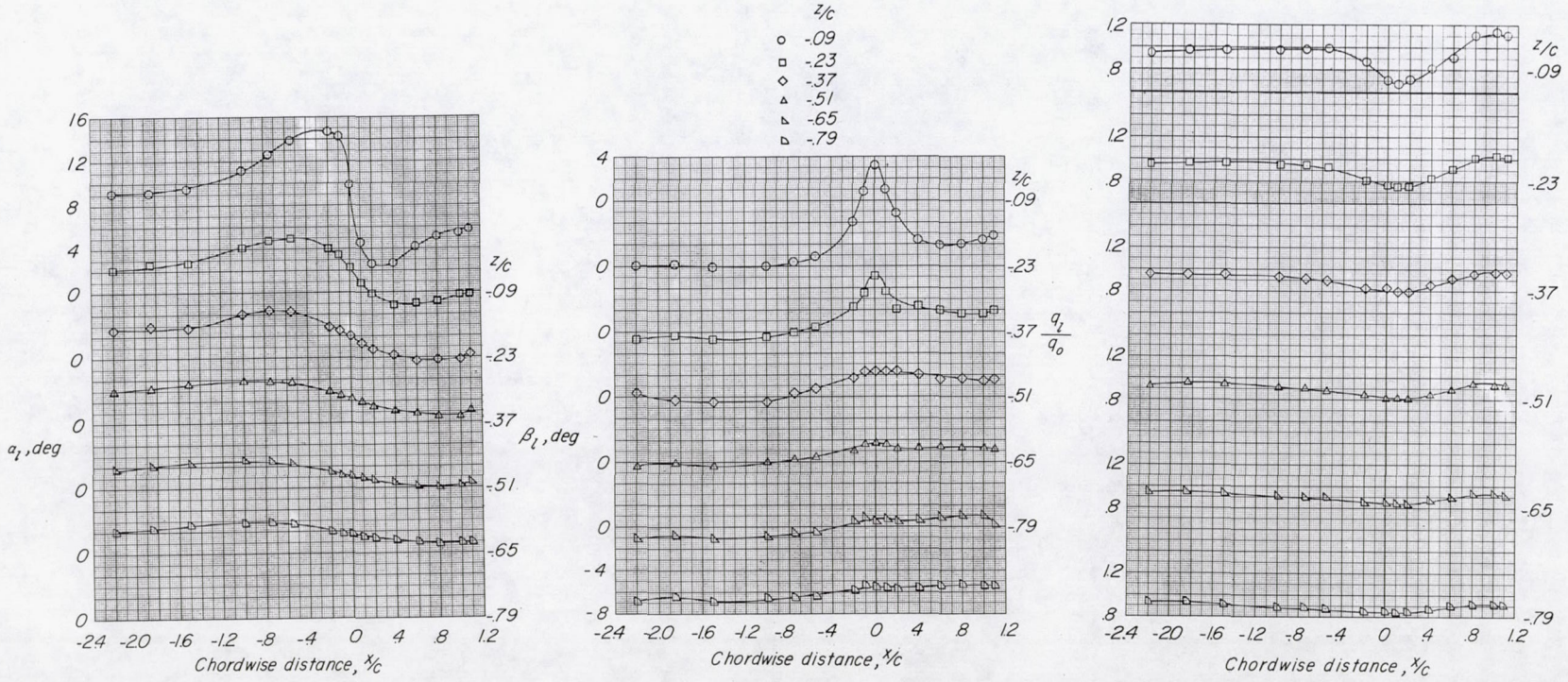


CONFIDENTIAL



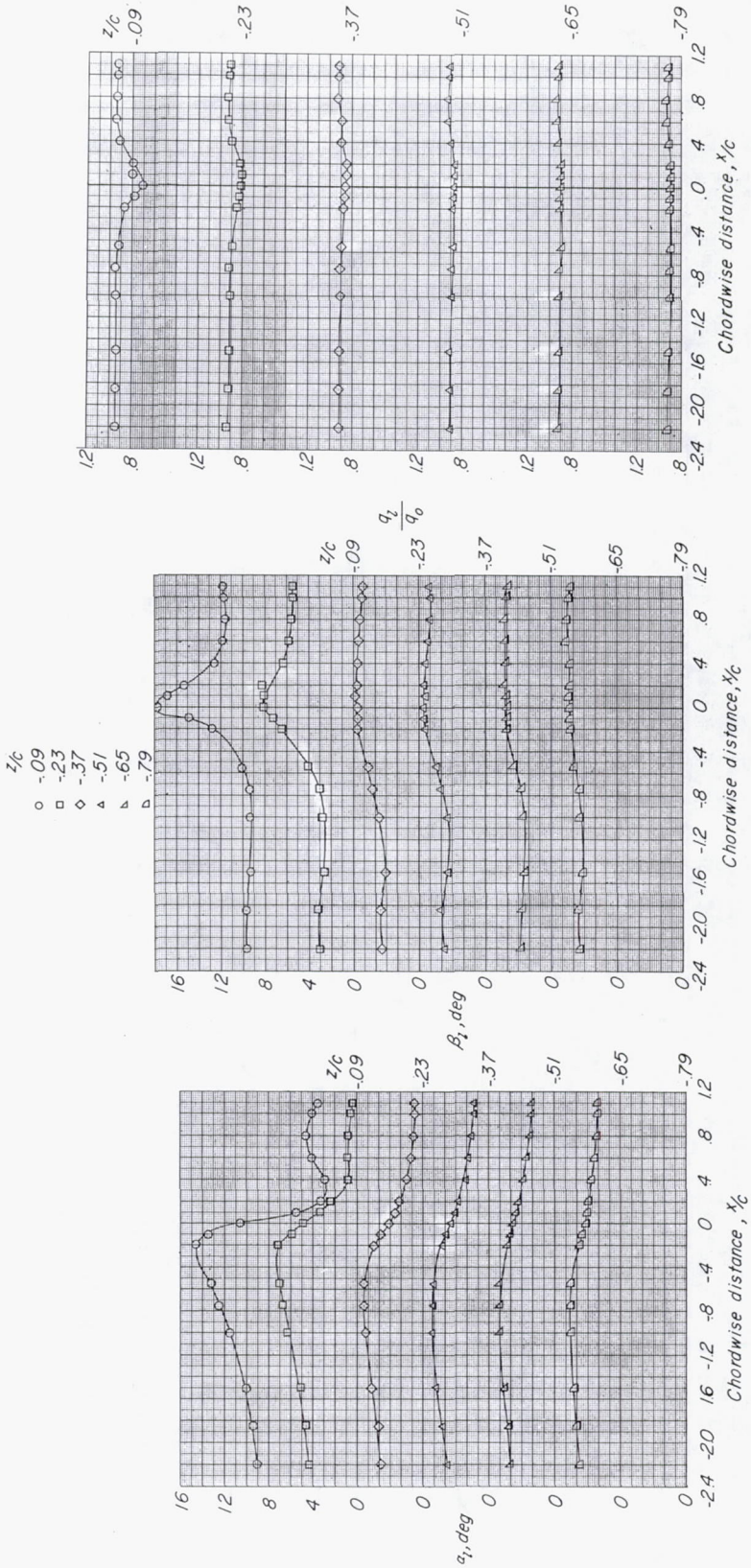

(d) $\alpha = 8.2^{\circ}$; $\beta = 0^{\circ}$.

Figure 10.- Continued.



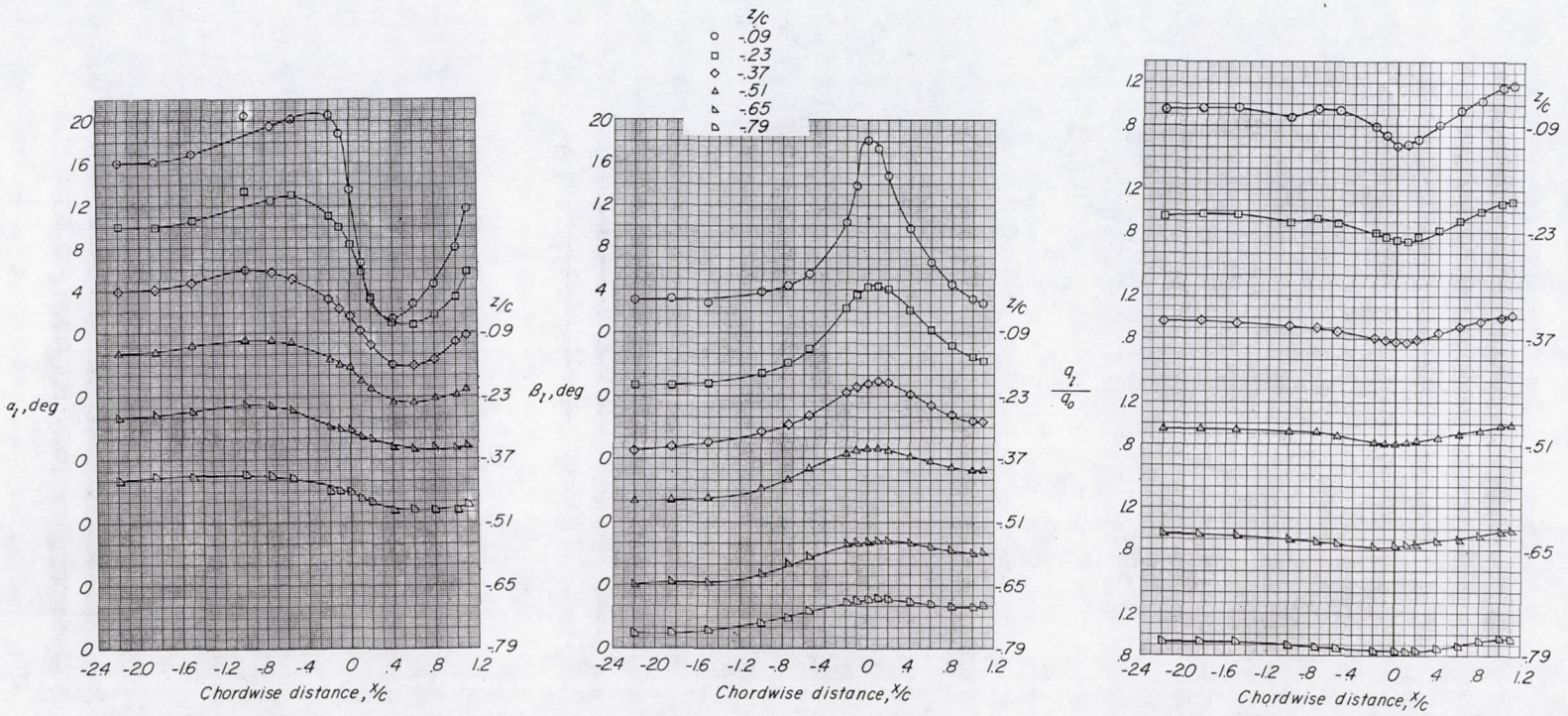

(e) $\alpha = 8.2^\circ$; $\beta = -8^\circ$.

Figure 10.- Continued.



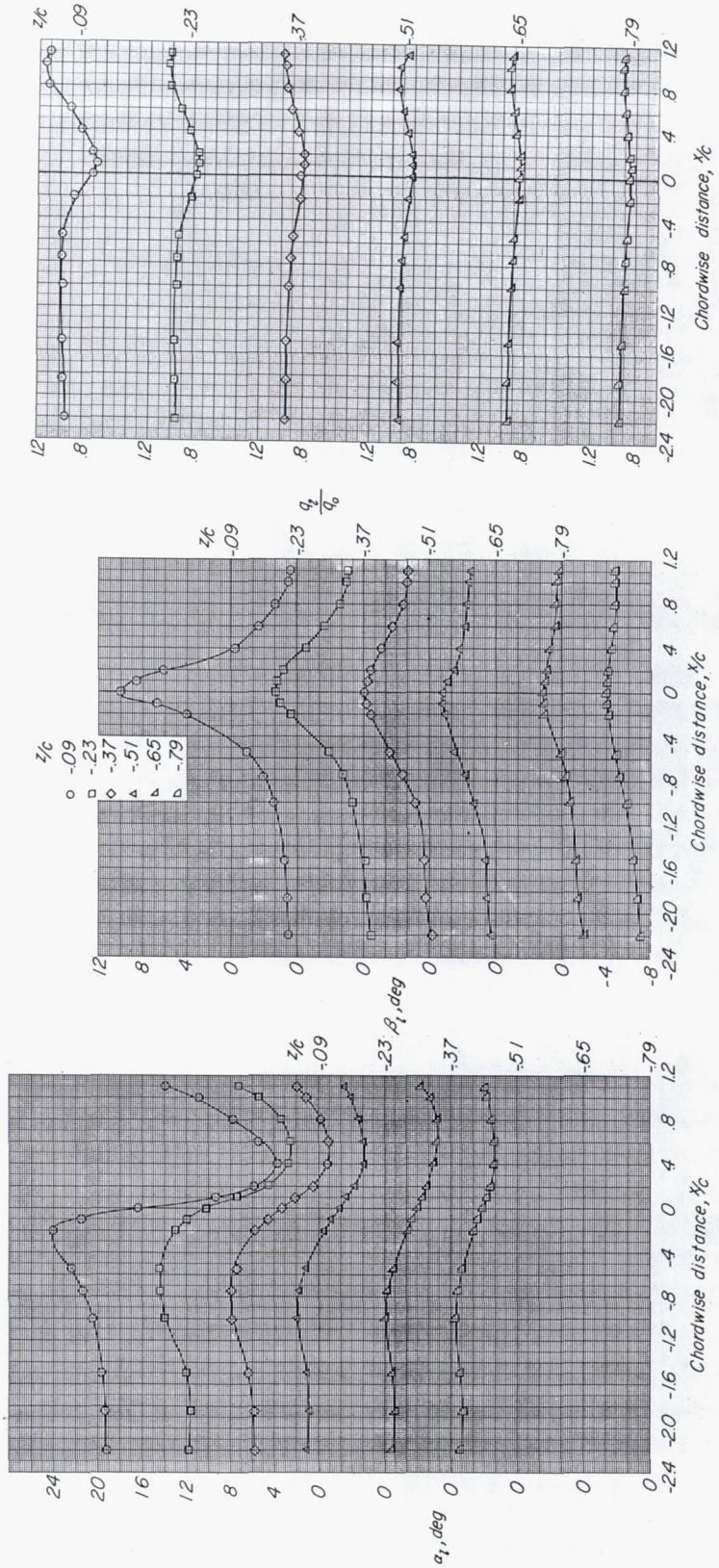

(f) $\alpha = 8.2^{\circ}$; $\beta = 8^{\circ}$.

Figure 10.- Continued.



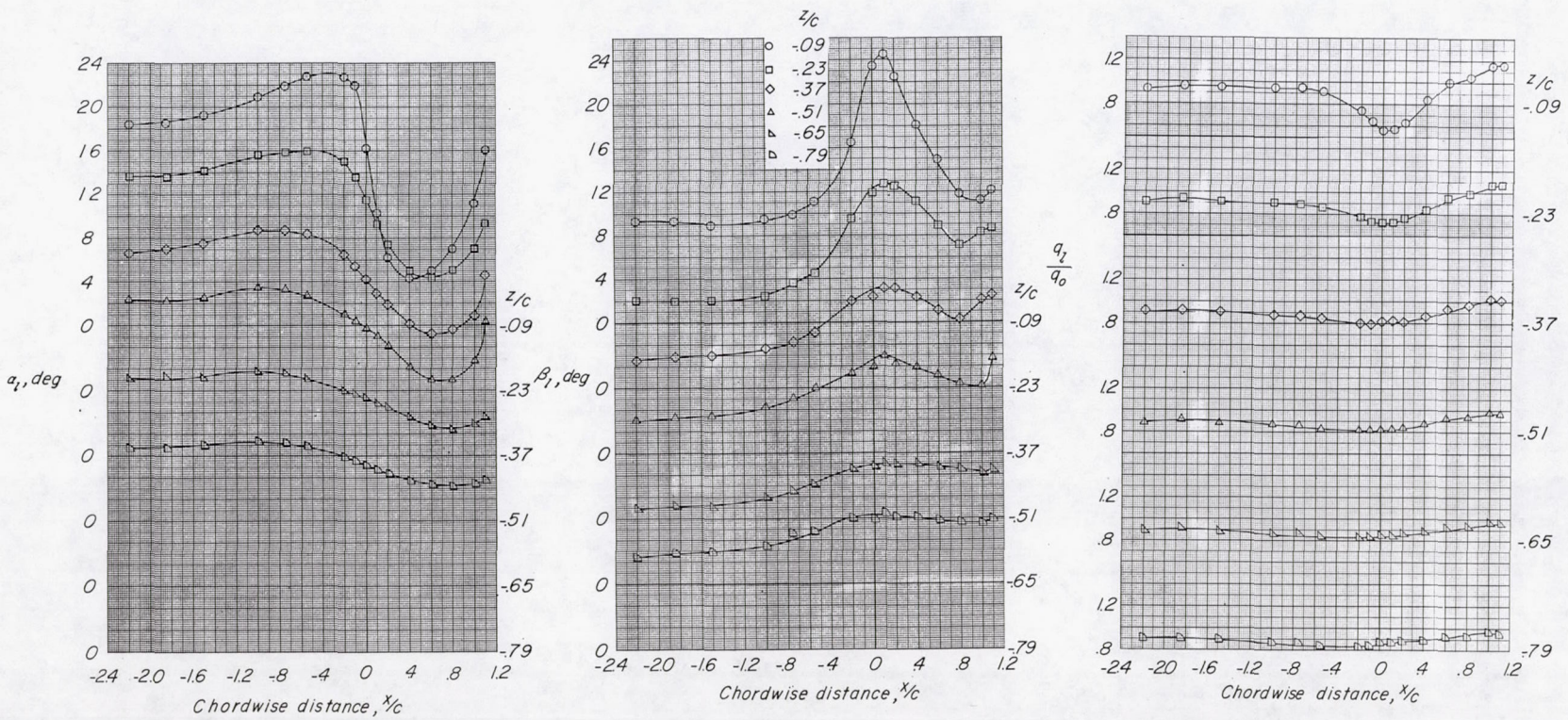

(g) $\alpha = 16.4^{\circ}$; $\beta = 0^{\circ}$.

Figure 10.- Continued.



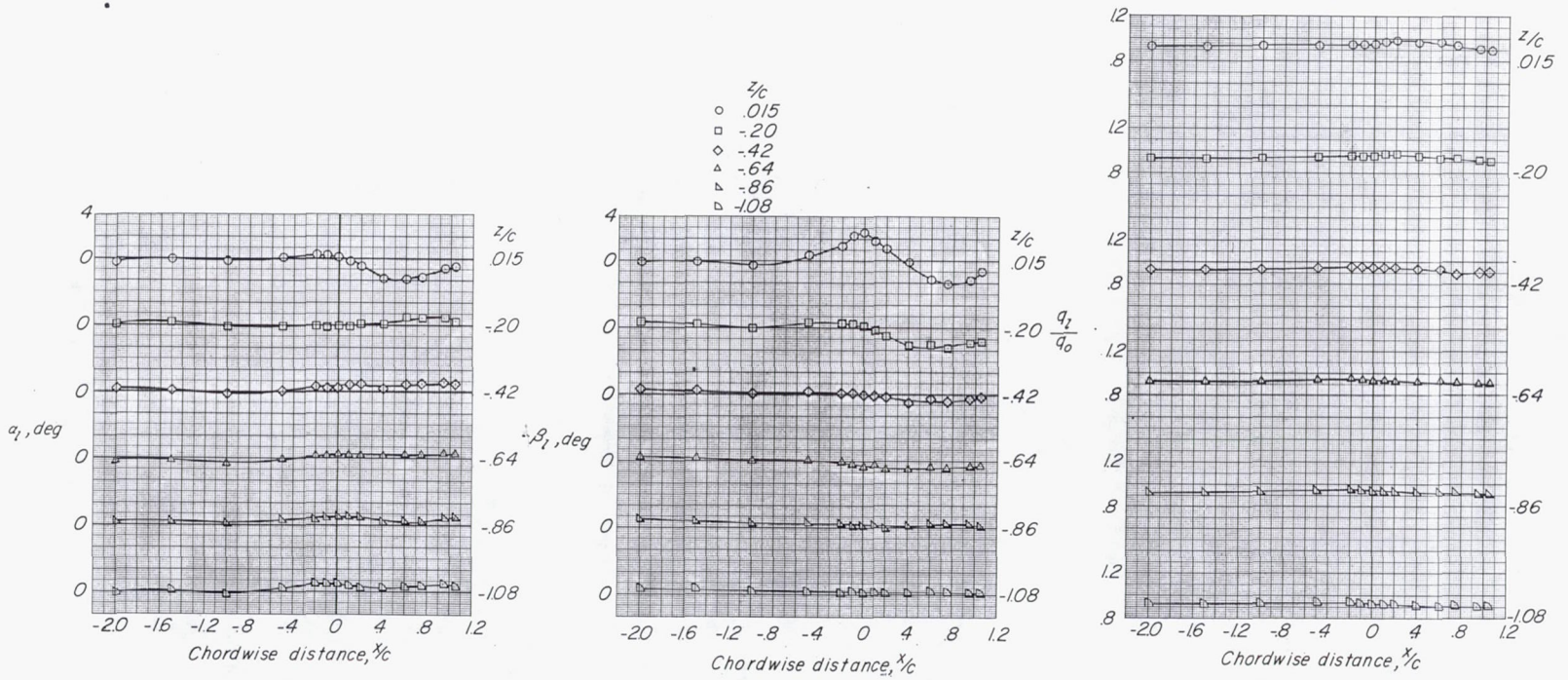

(h) $\alpha = 16.4^{\circ}$; $\beta = -8^{\circ}$.

Figure 10.- Continued.



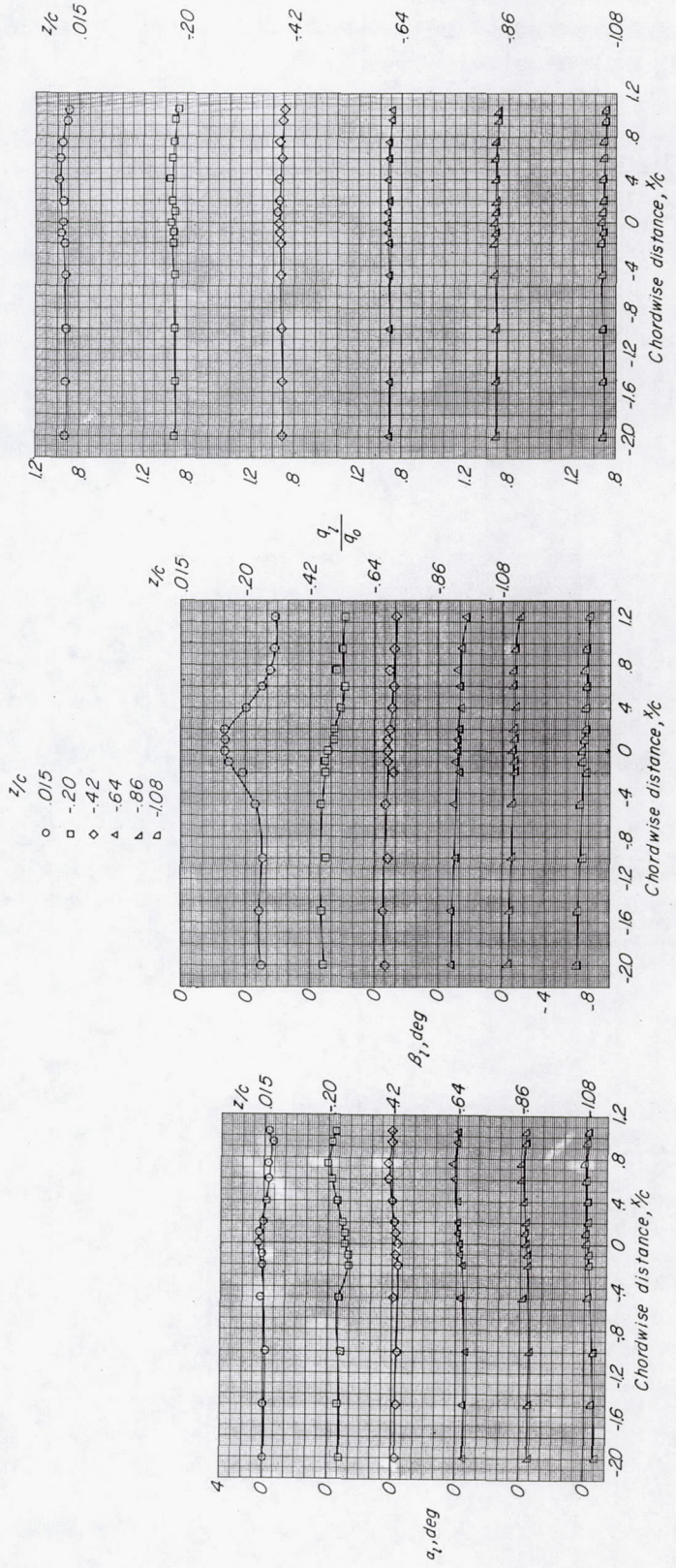

(i) $\alpha = 16.4^{\circ}$; $\beta = 8^{\circ}$.

Figure 10.- Concluded.



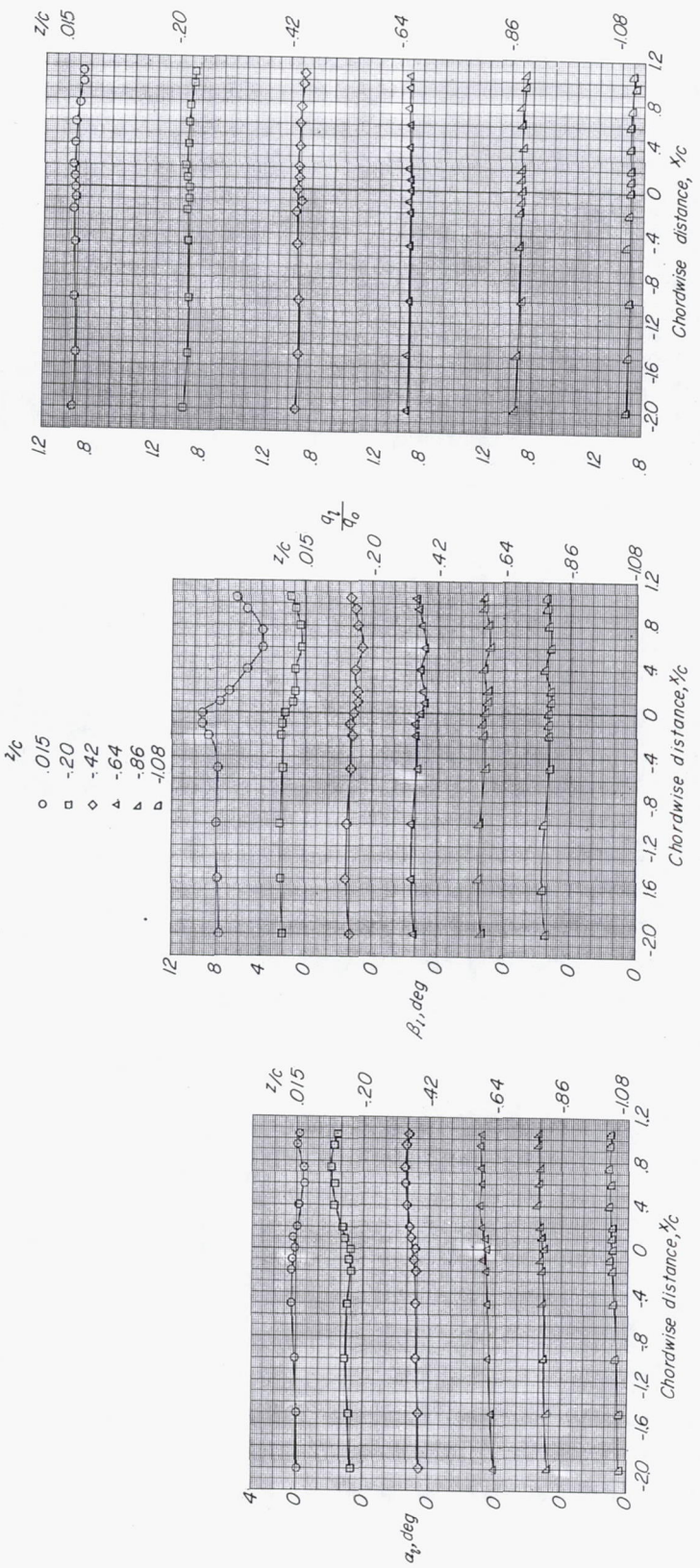

(a) $\alpha = -0.2^{\circ}$; $\beta = 0^{\circ}$.

Figure 11.- Flow-field characteristics of the swept-wing—fuselage combination at $y/\frac{b}{2} = -1.01$.



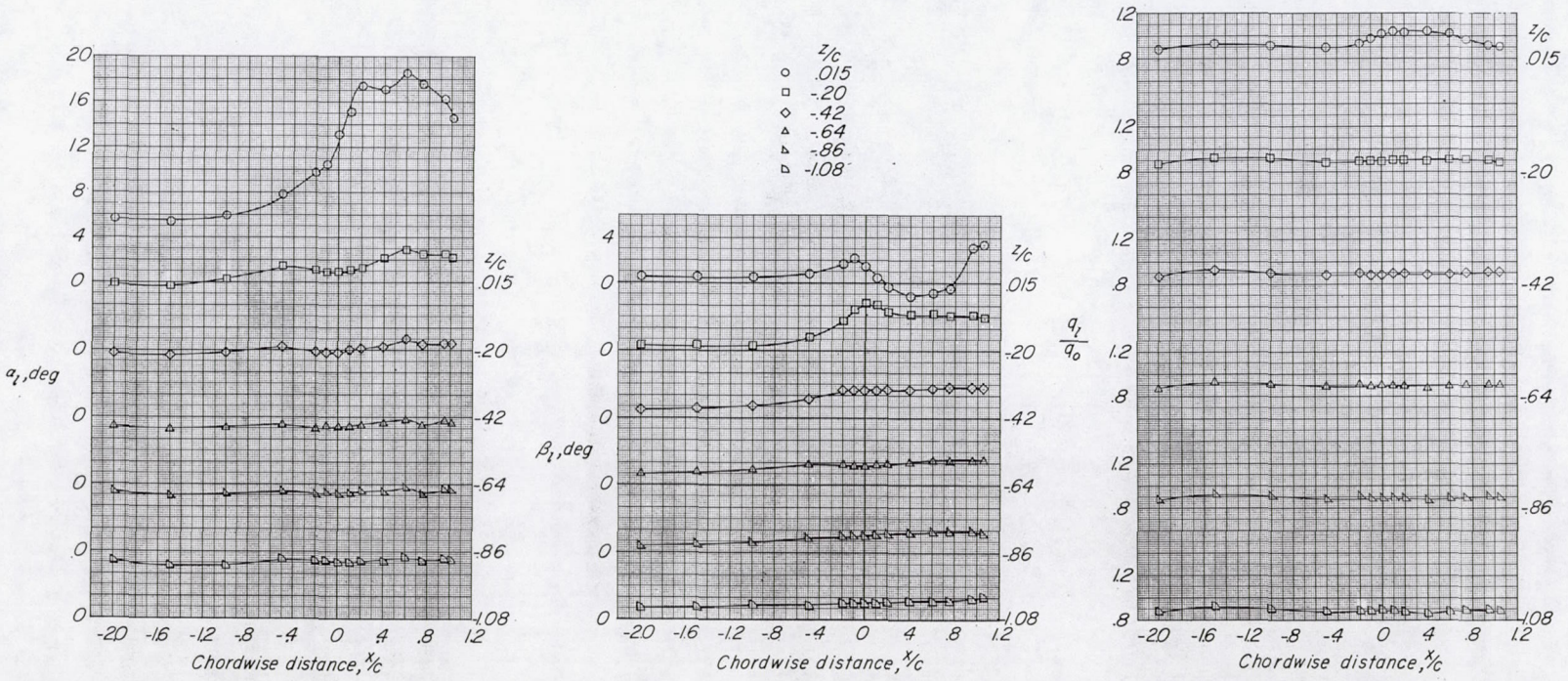

(b) $\alpha = -0.2^{\circ}$; $\beta = -8^{\circ}$.

Figure 11.- Continued.



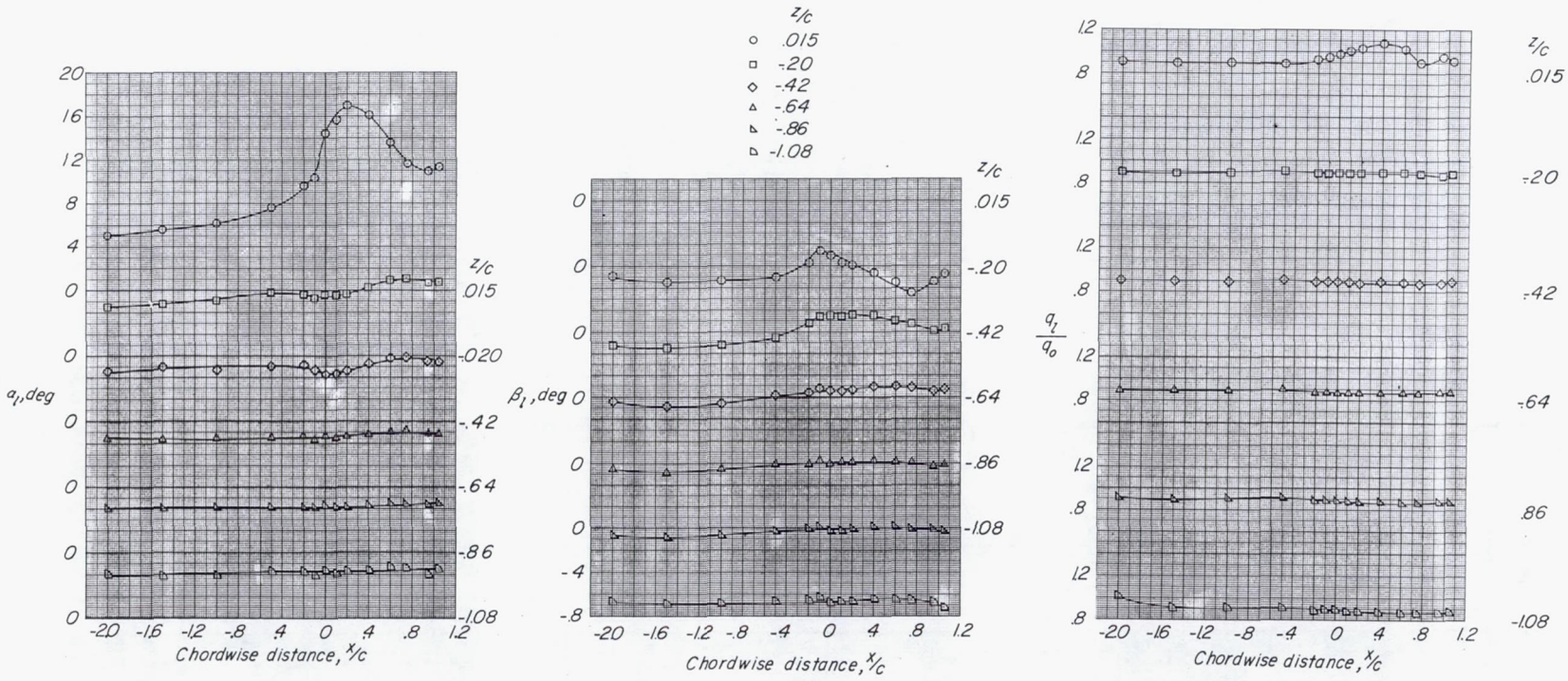

(c) $\alpha = -0.2^{\circ}$; $\beta = 8^{\circ}$.

Figure 11.- Continued.



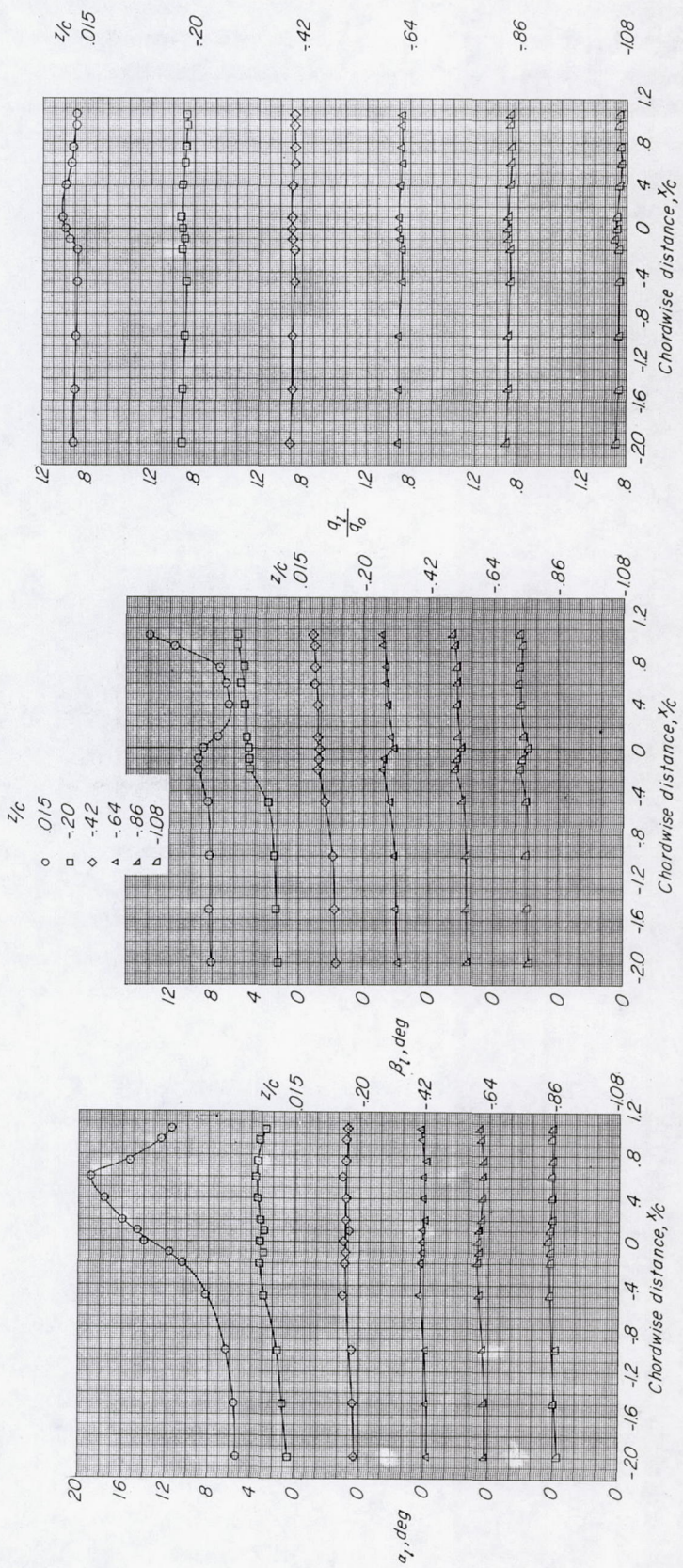

(d) $\alpha = 3.8^\circ$; $\beta = 0^\circ$.

Figure 11.- Continued.



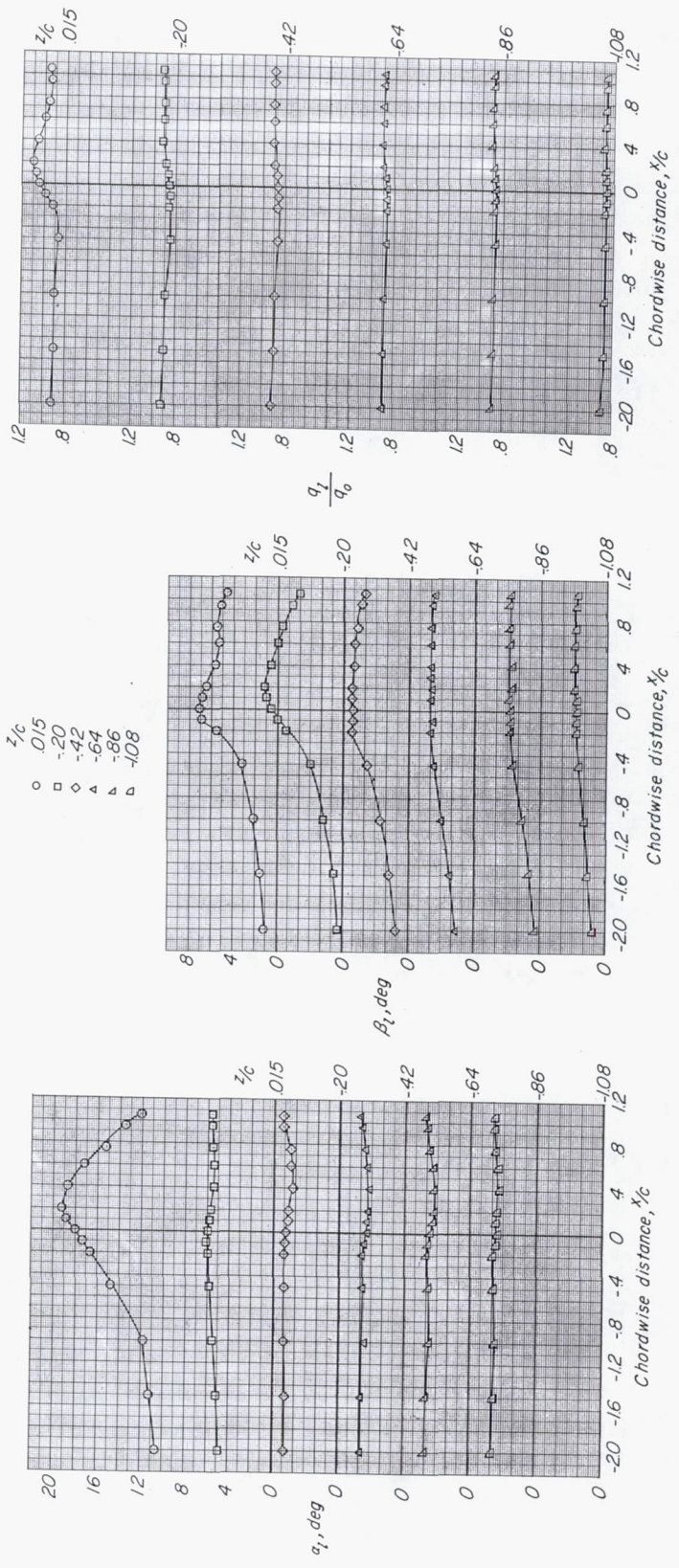

(e) $\alpha = 3.8^{\circ}$; $\beta = -8^{\circ}$.

Figure 11.- Continued.



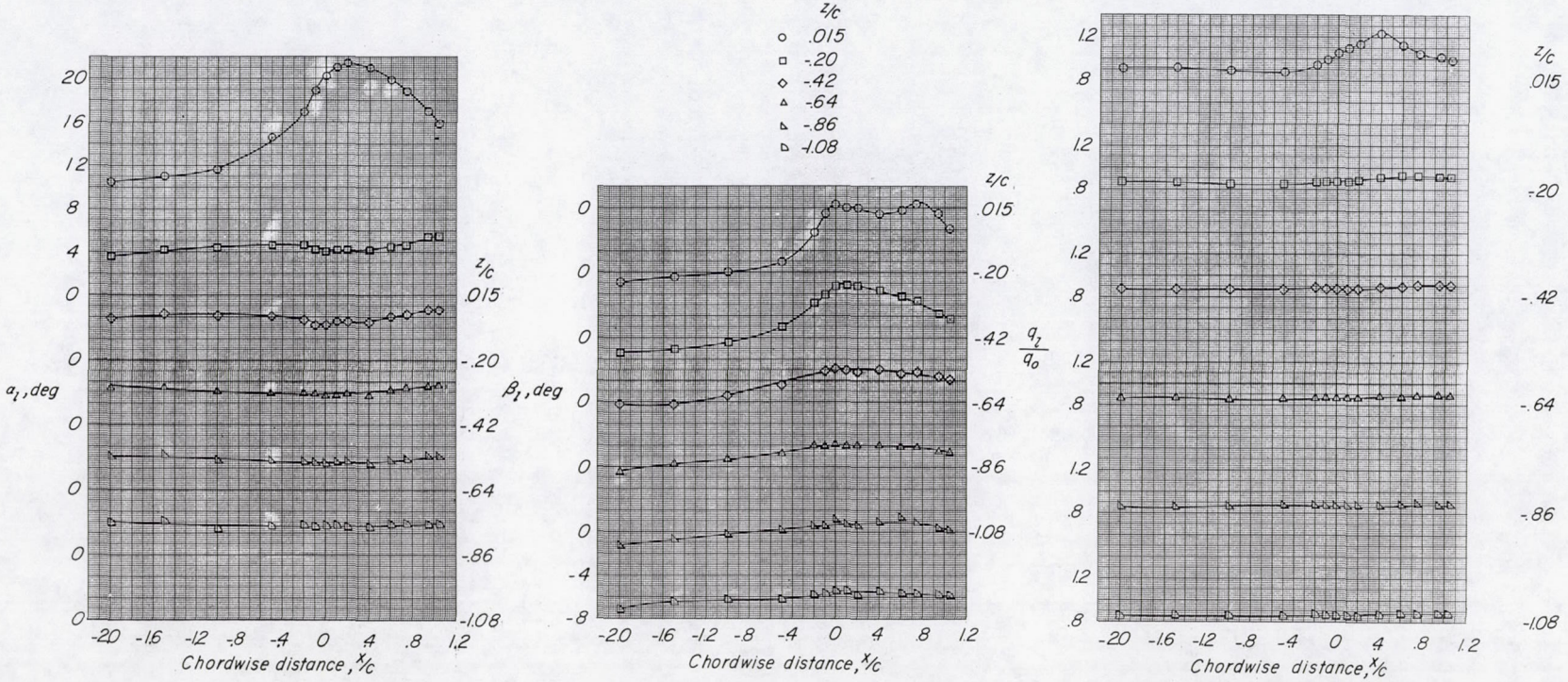

(f) $\alpha = 3.8°$; $\beta = 8°$.

Figure 11.- Continued.




(g) $\alpha = 8.2^{\circ}$; $\beta = 0^{\circ}$.

Figure 11.- Continued.

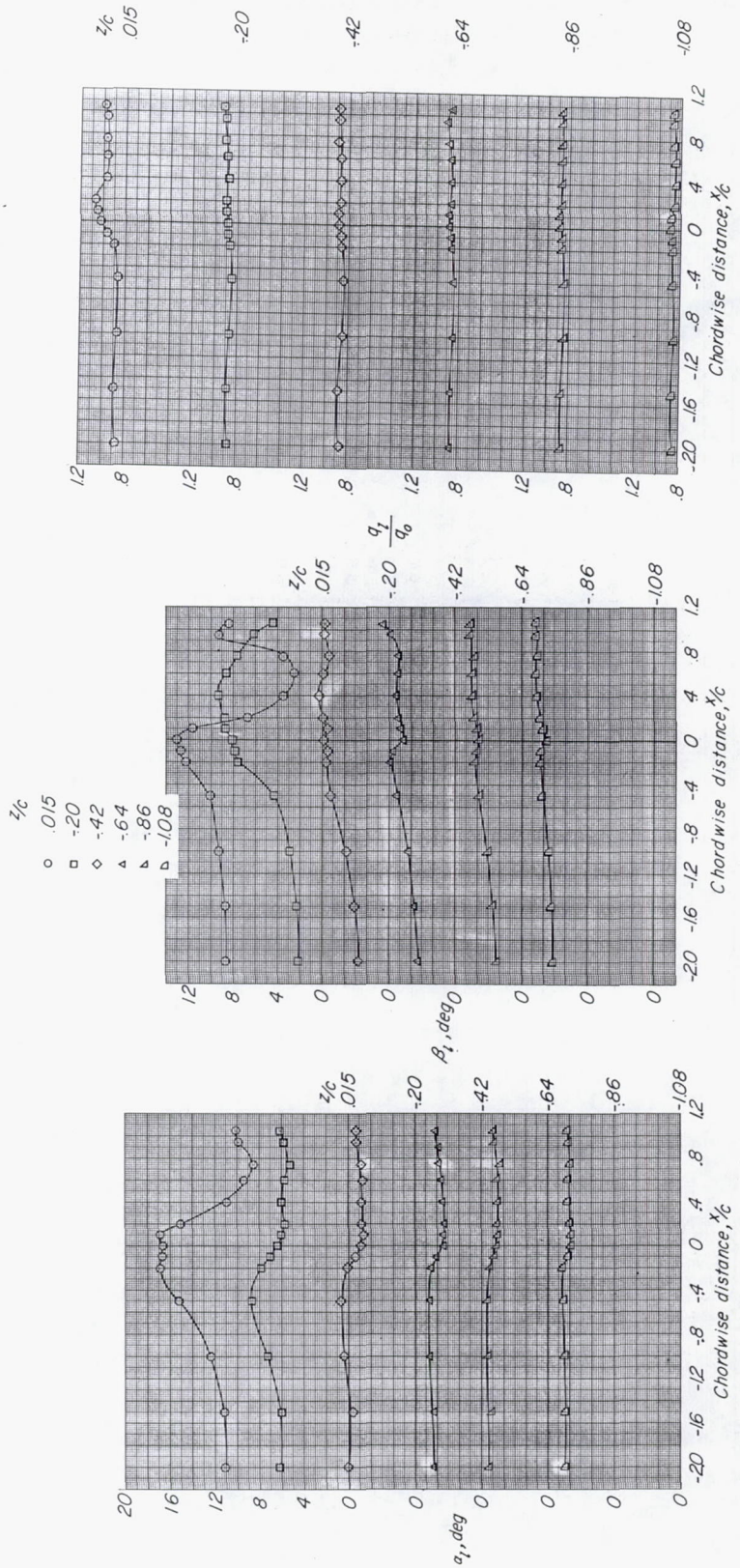



(h) $\alpha = 8.2^{\circ}$; $\beta = -8^{\circ}$.

Figure 11.- Continued.

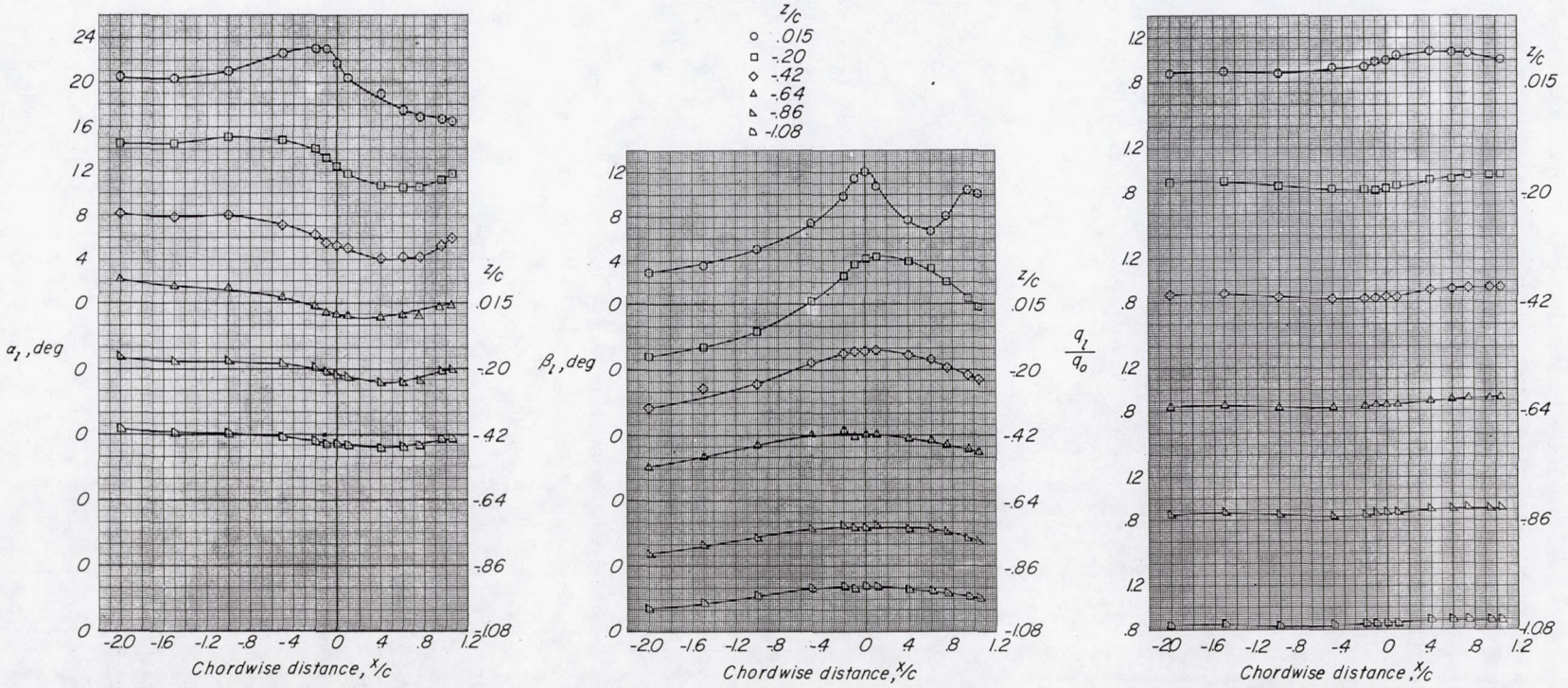


CONFIDENTIAL




(i) $\alpha = 8.2^{\circ}$; $\beta = 8^{\circ}$.

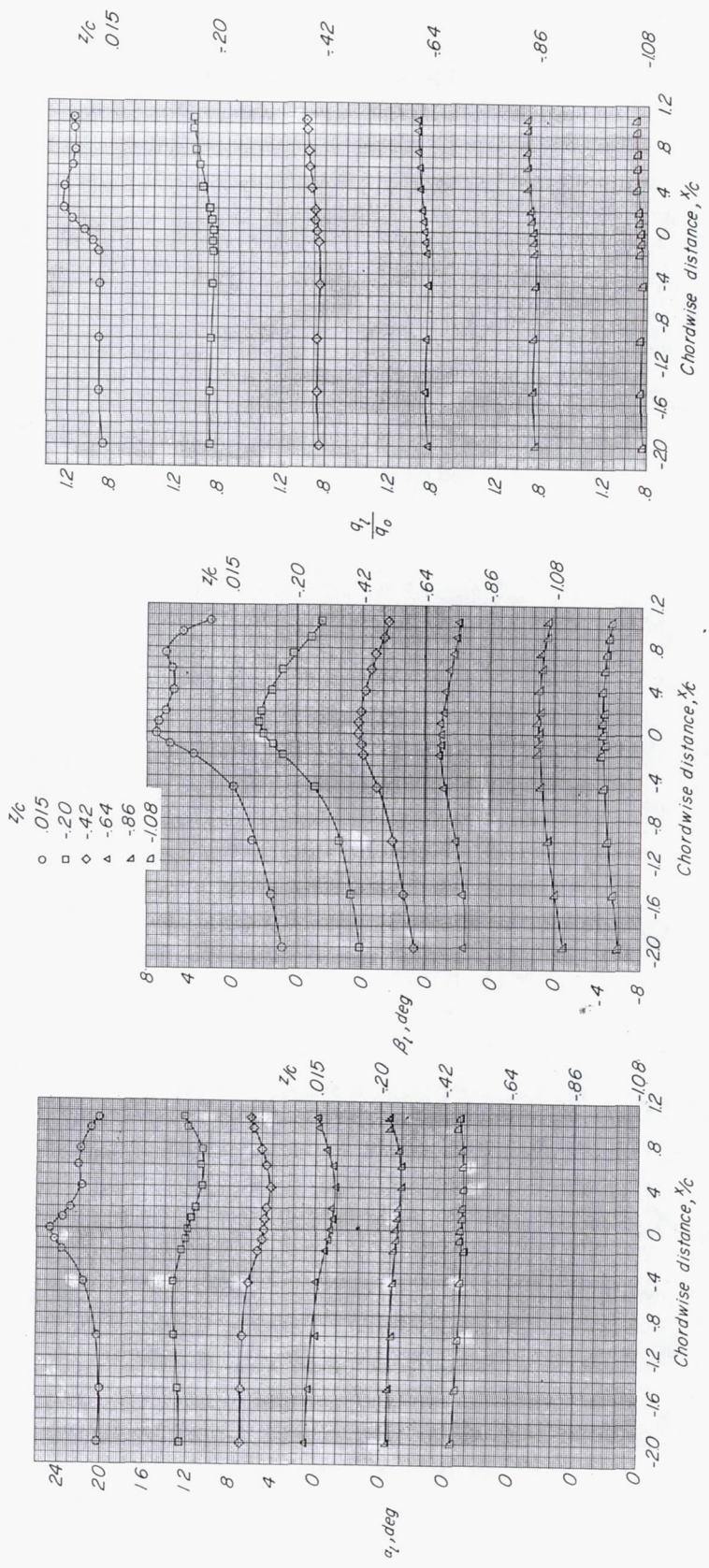
Figure 11.- Continued.




(j) $\alpha = 16.4^\circ$; $\beta = 0^\circ$.

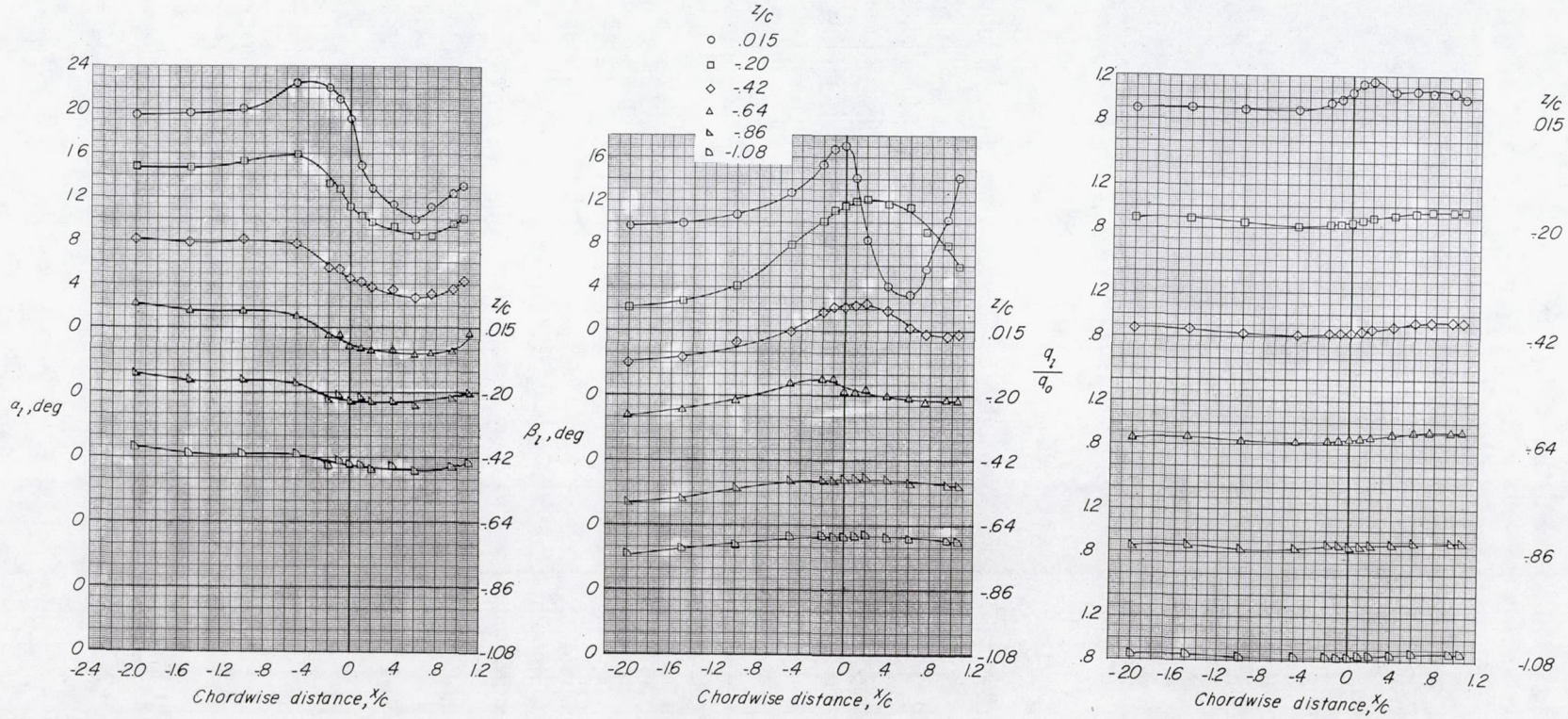
Figure 11.- Continued.

CONFIDENTIAL



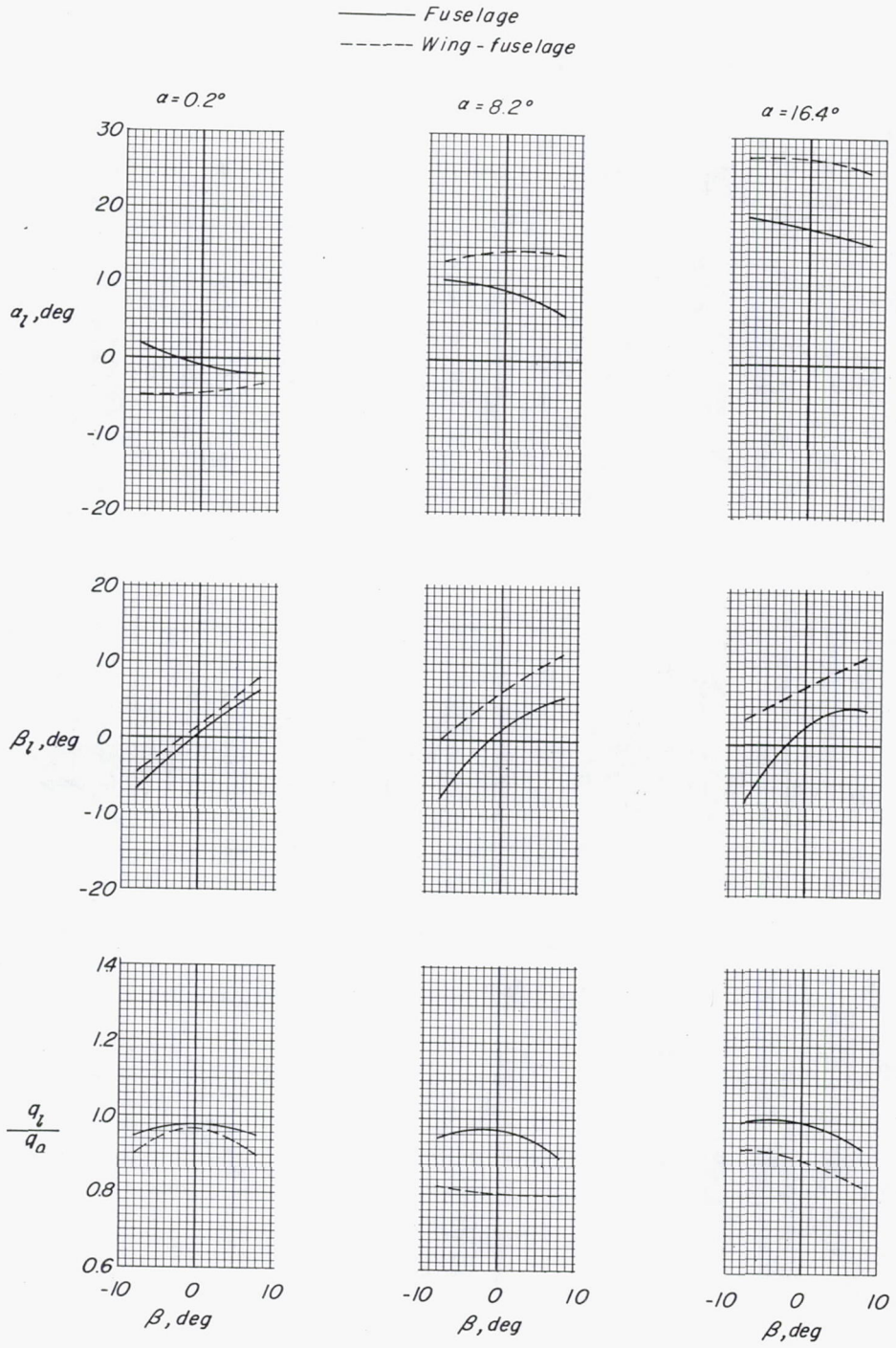

(k) $\alpha = 16.4^{\circ}$; $\beta = -8^{\circ}$.

Figure 11.- Continued.



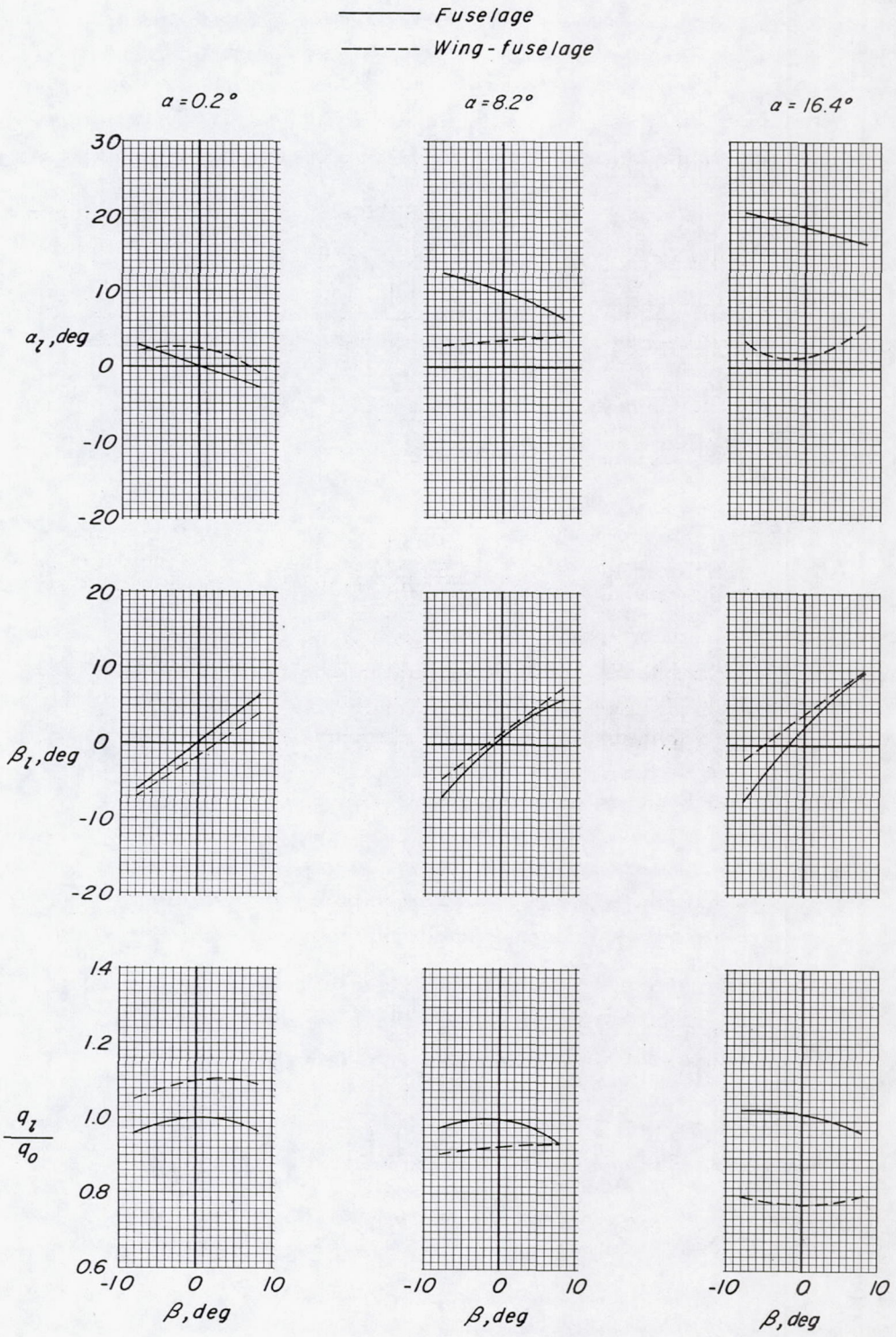

(l) $\alpha = 16.4^\circ$; $\beta = 8^\circ$.

Figure 11.- Concluded.



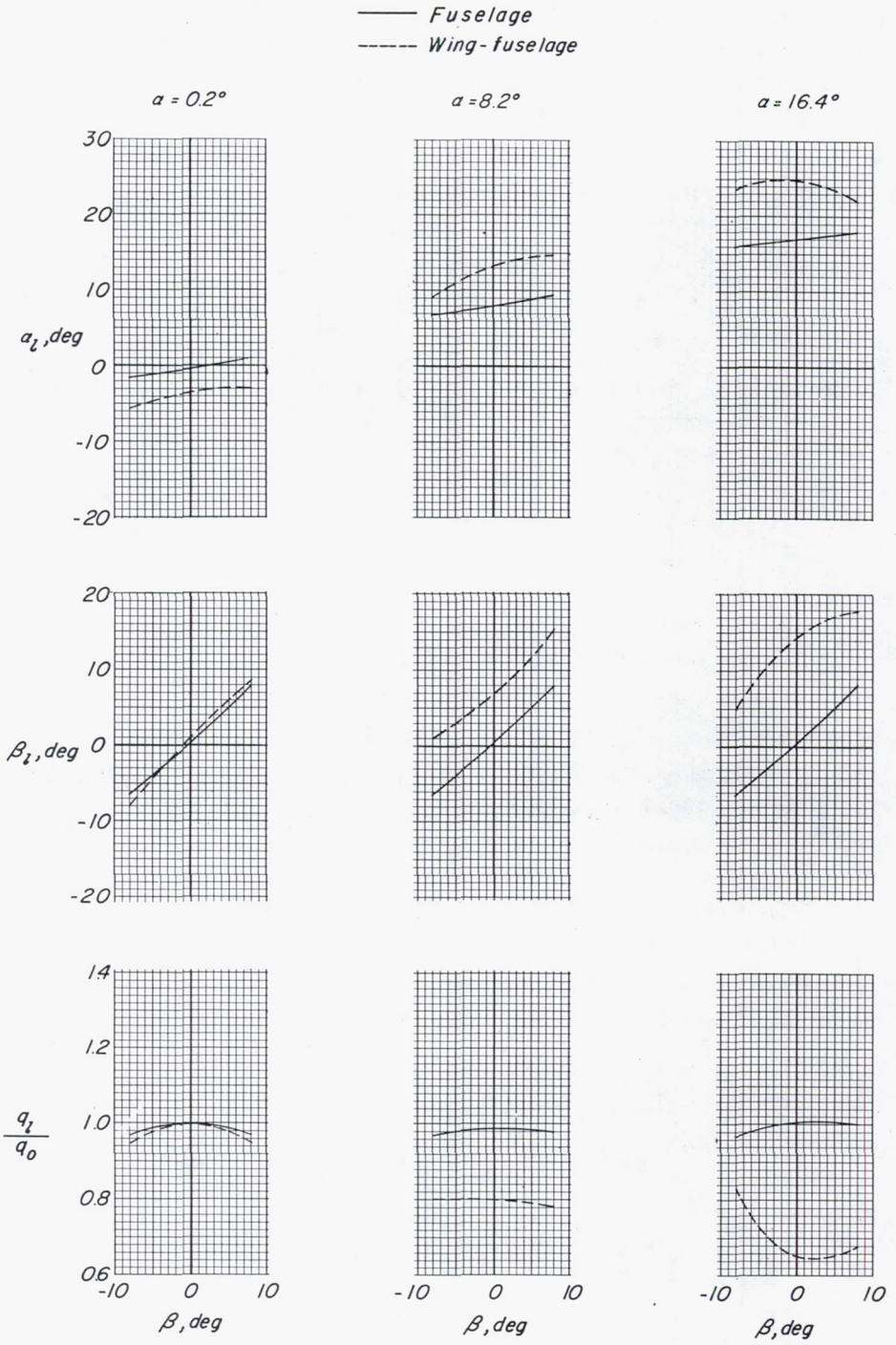

(a) x/c = -0.10.

Figure 12.- Comparison of flow fields of fuselage with swept-wing—fuselage combination at one-quarter semispan location. $z/\frac{b}{2} = -0.085$.



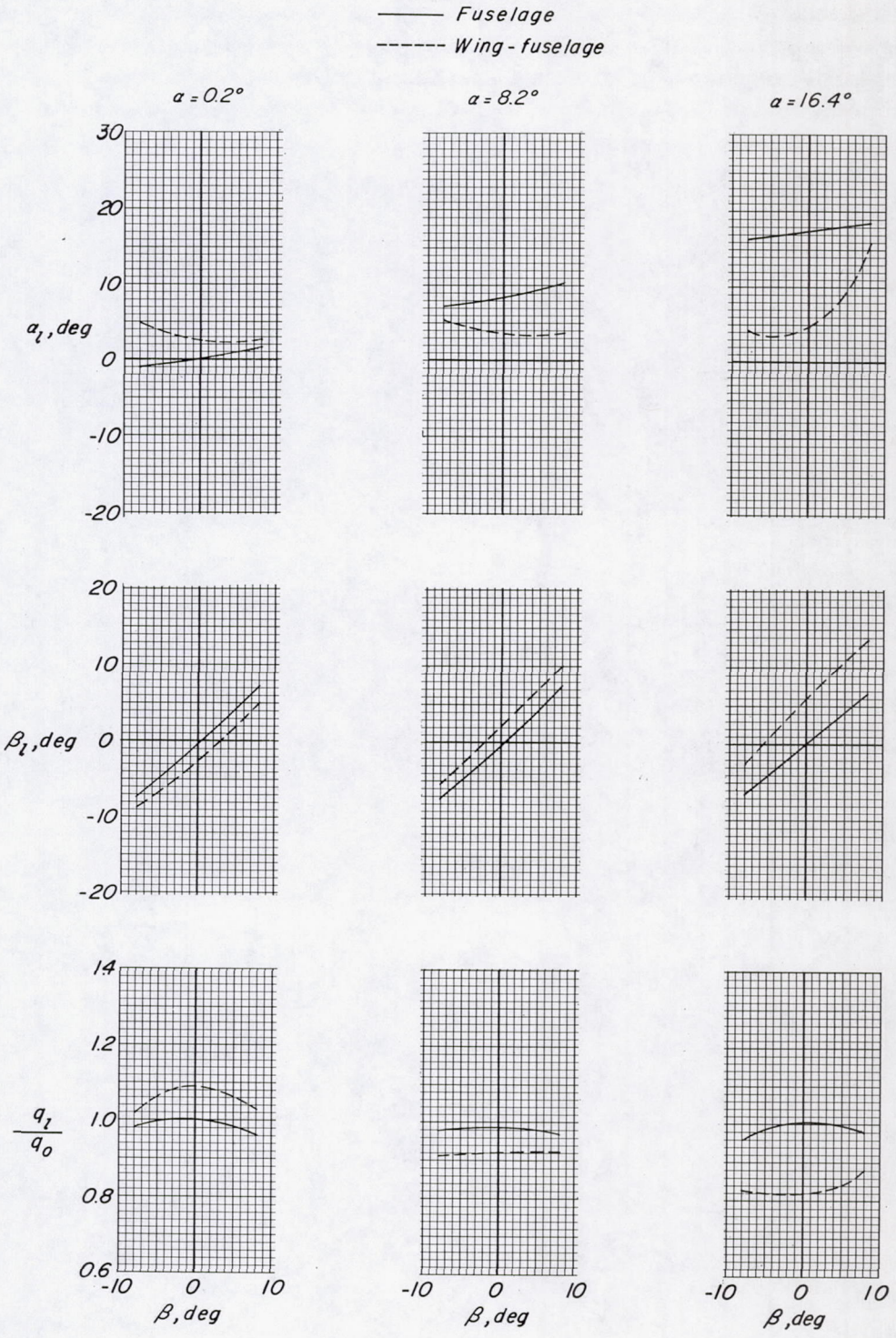

(b) x/c = 0.60.

Figure 12.- Concluded.



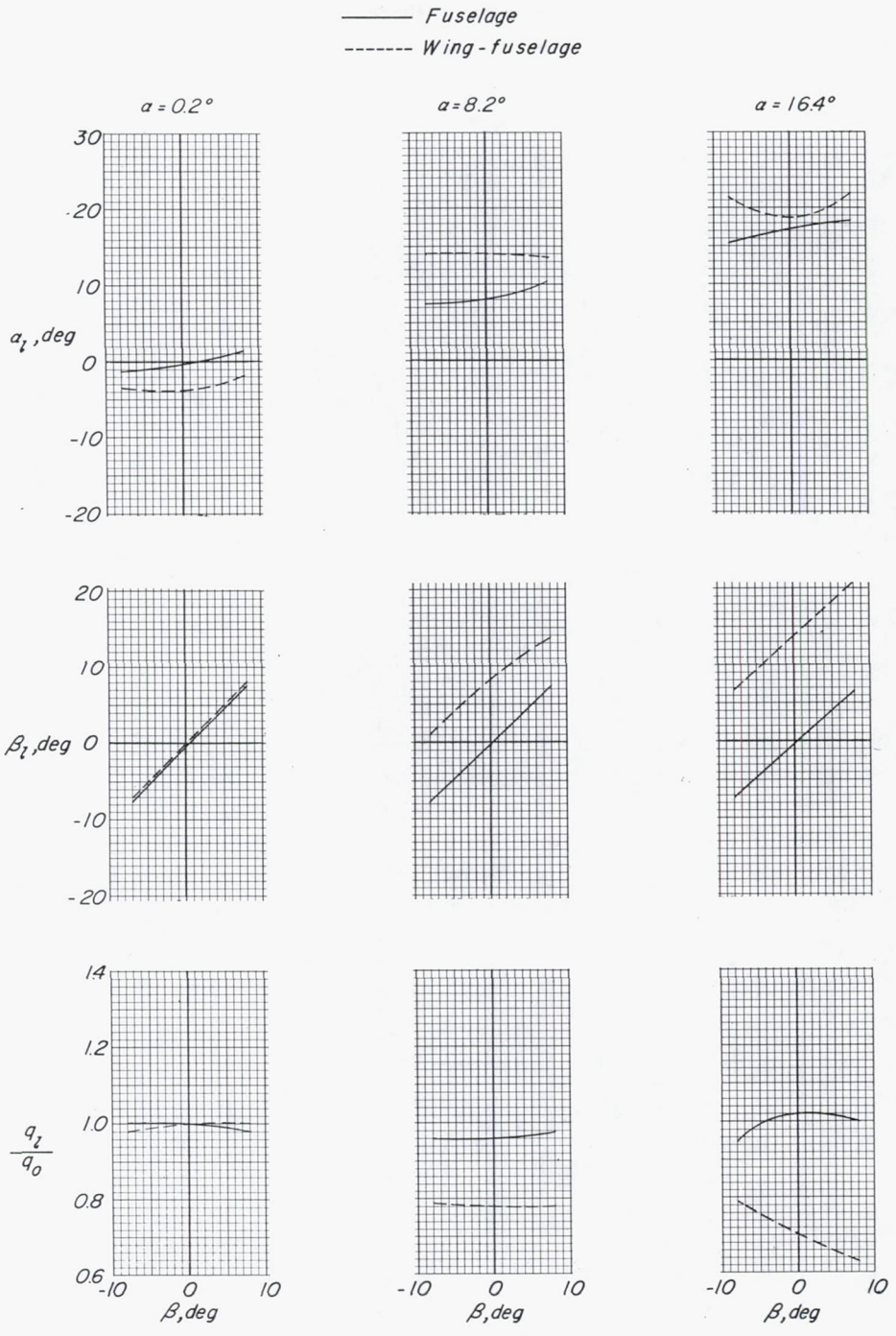

(a) x/c = -0.10.

Figure 13.- Comparison of flow fields of fuselage alone and swept-wing—fuselage combination at one-half semispan location. $z/\frac{b}{2} = -0.085$.



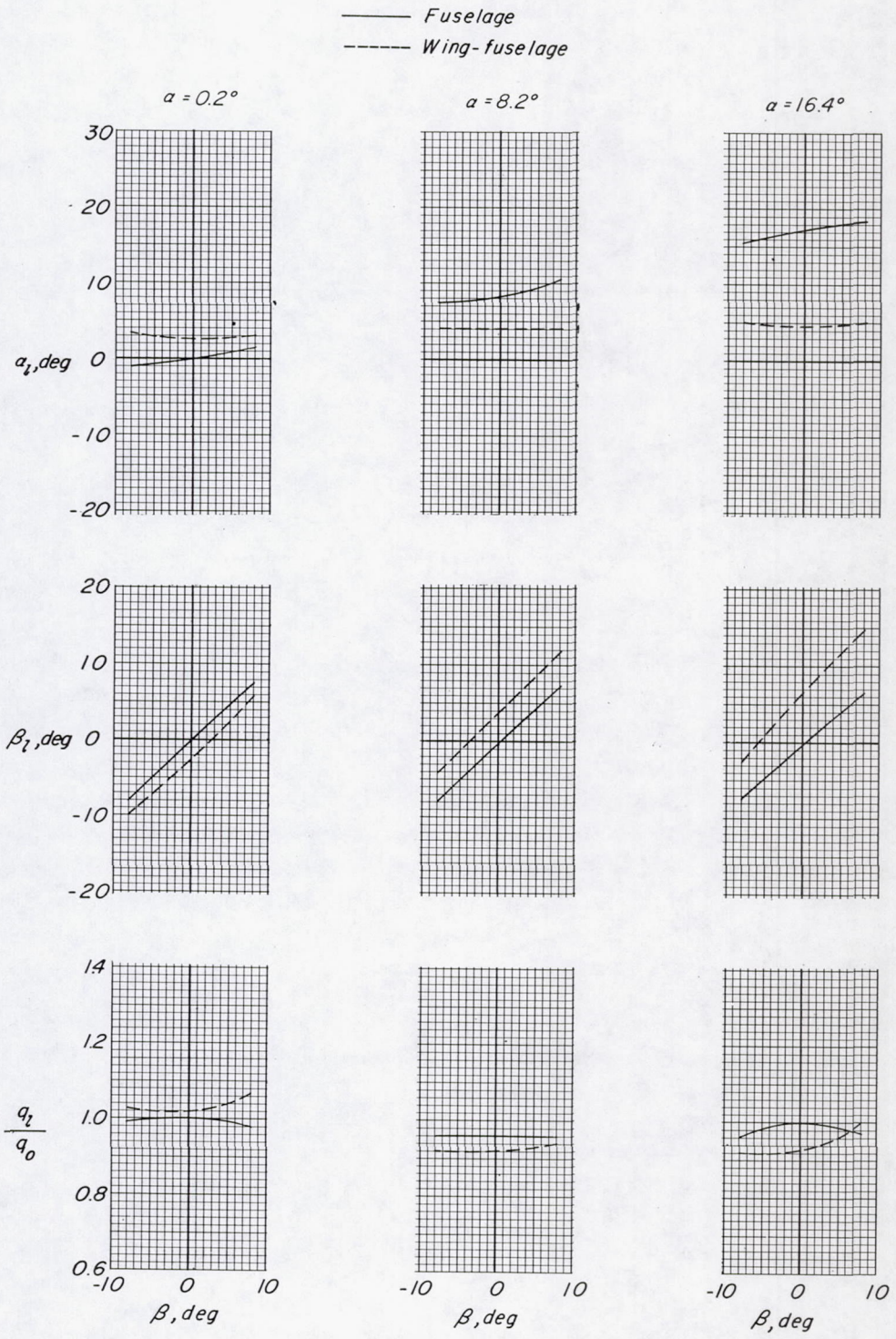

(b) x/c = 0.60.

Figure 13.- Concluded.



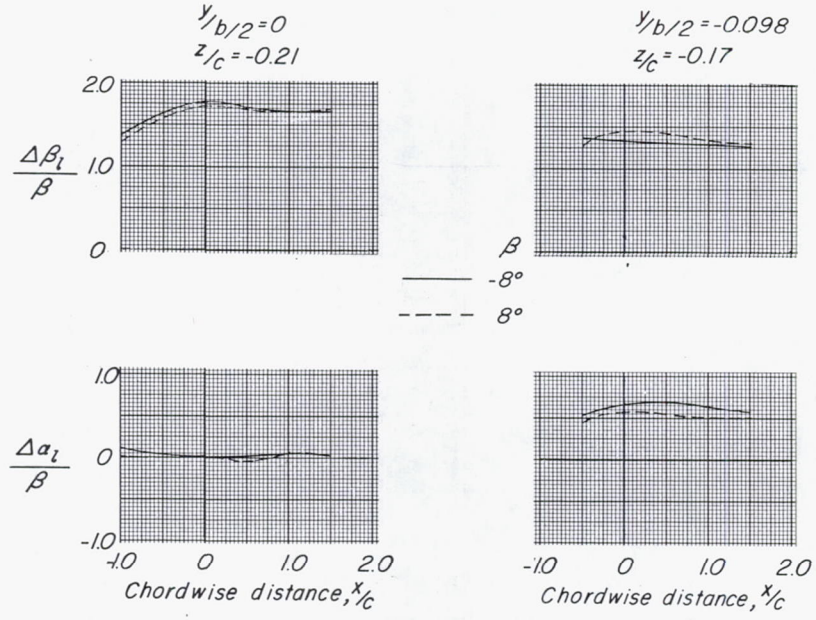

(a) x/c = -0.10.

Figure 14.- Comparison of flow fields of fuselage alone and swept-wing—fuselage combination at three-quarter semispan location. $z/\frac{b}{2} = -0.085$.

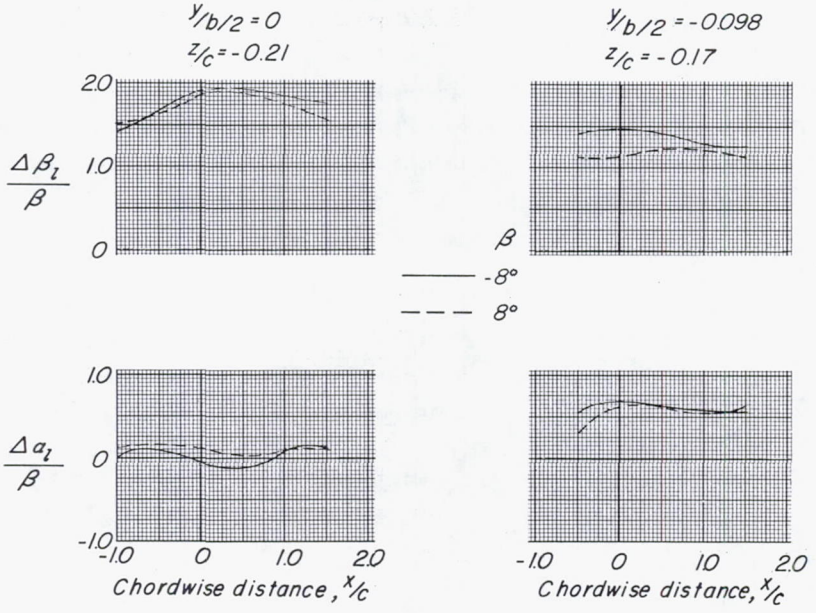



(b) x/c = 0.60.

Figure 14.- Concluded.




(a) $\alpha = -0.2$.




(b) $\alpha = 8.2$.

Figure 15.- Effect of variation in sideslip angle on the local-flow angularities near the fuselage of the sweptback-wing—fuselage combination.